Research Partnership to Secure Energy for America

FINAL REPORT

New Safety Barrier Testing Methods

RPSEA Document Number: TBD
RPSEA Contract Number: 08121-2101-02
SwRI® Project Number: 18.15490

Prepared by:

Shane P. Siebenaler
Rebecca A. Owston, Ph.D.
Steven T. Green
Angel M. Wileman
Jessica M. Brysch
Darin L. George, Ph.D.

Southwest Research Institute®
6220 Culebra Road
San Antonio, TX 78238

Release Date: April 19, 2012

SOUTHWEST RESEARCH INSTITUTE®

SAN ANTONIO
DETROIT
HOUSTON
WASHINGTON, DC

LEGAL NOTICE

This report was prepared by Southwest Research Institute as an account of work sponsored by the Research Partnership to Secure Energy for America, RPSEA. Neither RPSEA members of RPSEA, the National Energy Technology Laboratory, the U.S. Department of Energy, nor any person acting on behalf of any of the entities:

a) Makes any warranty or representation, express or implied, with respect to accuracy, completeness, or usefulness of the information contained in this document, or that the use of any information, apparatus, method, or process disclosed in this document may not infringe privately-owned rights, or

b) Assumes any liability with respect to the use of, or for any and all damages resulting from the use of, any information, apparatus, method, or process disclosed in this document.

THIS IS A FINAL REPORT. THE DATA, CALCULATIONS, INFORMATION, CONCLUSIONS, AND/OR RECOMMENDATIONS REPORTED HEREIN ARE THE PROPERTY OF THE U.S. DEPARTMENT OF ENERGY.

ABSTRACT

Testing of safety valves after installation is a critical task for ensuring safe offshore oil production. These valves cannot be directly tested using conventional measurement methodologies. Instead, pressure monitoring is used. This approach is costly and can result in extended shutdown periods.

A project was undertaken to determine an alternate means of conducting this testing. A number of technologies were identified and subsequently ranked. Due to the large number of existing wells with the need for testing, it was decided to largely steer clear of technologies that required retrofitting of existing infrastructure, particularly for surface-controlled subsurface safety valves (SCSSVs). The resulting tradeoff study picked well-specific modeling as the candidate technology. This approach is able to capture thermal and other environmental effects.

A numerical model was developed that allows for determination of leakage rates, as well as the required test duration. The model is computationally-inexpensive and allows for the operator to conduct simple trending of results. The sensitivity of various criteria was also explored. One significant finding of this work is that thermal effects of the well must be accounted for in order to properly interpret pressure results. Utilization of this model can reduce overall tests times and give operators a sense of the level of uncertainty in interpreting measured pressure changes. A similar modeling approach was also used for pressure buildup testing of wellhead valves, such as primary master valves and underwater safety valves.

REPORT APPROVAL

This report has been approved by the following Southwest Research Institute management on April 19, 2012:

J. Christopher Buckingham, Program Director
Fluid Dynamics and Multiphase Flow

This Page Left Intentionally Blank

TABLE OF CONTENTS

Section **Page**

TABLE OF CONTENTS vi
LIST OF FIGURES viii
LIST OF TABLES ix
EXECUTIVE SUMMARY x
VALUE TO MEMBERS xii
1. INTRODUCTION 1-1
1.1 Background 1-1
1.2 Project Approach 1-2
1.3 Report Organization 1-2
2. TRADEOFF STUDY 2-1
2.1 Brainstormed Ideas 2-1
2.2 Evaluation Criteria 2-3
2.2.1 Technology Evaluation 2-5
2.3 Transition in Focus to Subsurface Valves 2-6
3. PROOF OF CONCEPT 3-1
3.1 Current Industry Testing Procedures and Project Objectives 3-1
3.1.1 Regulatory Context 3-3
3.1.2 Prior Efforts 3-3
3.1.3 Path Forward 3-3
3.2 Computational Fluid Dynamics Modeling 3-3
3.2.1 Modeling Progression Map 3-3
3.2.2 CFD Code Inputs and Setup Configuration 3-4
3.2.3 CFD Conclusions 3-6
3.3 Analytical Model 3-6
3.3.1 Assumptions 3-7
3.3.2 Rock Thermal Profile 3-8
3.3.3 Material Properties 3-9
3.3.4 Model Description 3-10
3.3.5 Liquid Density 3-11
3.3.6 Gas Volume 3-11
3.3.7 Model Equations 3-11
3.3.8 Nomenclature 3-11
3.3.9 Liquid Volume 3-13
3.3.10 Heat Transfer 3-13
3.3.11 Thermal Capacity 3-14
3.3.12 Model Summary 3-14

TABLE OF CONTENTS (cont'd)

Section **Page**

3.4 Analytical Results 3-15
3.4.1 Zero-Leakage Behavior 3-15
3.4.2 Leakage Cases 3-17
3.4.3 Wellbore Characteristics 3-21
3.5 Real Gas Effects 3-26
3.6 Phase Separation 3-27
3.7 Revisiting of PMV 3-35
3.7.1 Overview 3-35
3.7.2 Numerical Model 3-36
3.7.3 Analytical Model 3-37
3.7.4 Non-Choked Flow 3-40
3.7.5 Model Comparison 3-41
3.8 Proof-of-Concept Conclusion 3-43
4. CONCLUSIONS 4-1
5. REFERENCES 5-1
APPENDIX A – Technology Evaluation Results A-1
APPENDIX B – Technology Descriptions B-1
APPENDIX C – Computational Fluid Dynamics (CFD) C-1
APPENDIX D – CFD Modeling – Early Efforts D-1

LIST OF FIGURES

Section		Page
Figure 1.1.	Project Progression Flowchart	1-2
Figure 2.1.	Process for Tradeoff Study	2-1
Figure 3.1.	Heat Transfer and Mass Flow Mechanisms Influencing Shut-in Pressure	3-2
Figure 3.2.	CFD Modeling Roadmap	3-4
Figure 3.3.	Shut-in Wellbore Schematic of Example Case	3-5
Figure 3.4.	Heat Loads for Shut-in Conditions for SCSSVs	3-7
Figure 3.5.	Steady Well and Formation Temperature for Flowing Well	3-9
Figure 3.6.	Model Subvolumes	3-10
Figure 3.7.	Change in Gas Cap Pressure With and Without Accommodation for Changes in Liquid Column (No Thermal Contraction, β)	3-15
Figure 3.8.	Gas Cap Decay Rate for Non-Leak Case of Various Gas Cap Percentages	3-16
Figure 3.9.	Percent Difference in Models That Include and Do Not Include Shrinkage of Liquid Column	3-16
Figure 3.10.	Pressure Profile for Various Leak Rates	3-17
Figure 3.11.	Difference in Pressure Decay for Various Leak Rates in Comparison with Zero-Leakage Case	3-18
Figure 3.12.	Difference in Zero-Leakage versus 400-cc/min Leak for Various GVFs	3-18
Figure 3.13.	Pressure Decay for Various Starting Tubing Pressures	3-19
Figure 3.14.	Deviation of Pressure Curves for Leak Cases When Compared to Zero-Leakage Cases	3-20
Figure 3.15.	Decay Curves for Zero-Leakage and 400-cc/min Leak Cases With 1% Uncertainty Bands	3-20
Figure 3.16.	Required Time to a Detect Leak as a Function of System Uncertainty	3-21
Figure 3.17.	Pressure Response for Various Fluid Temperatures with 20% Gas Cap and No Leakage	3-22
Figure 3.18.	Decay Curves for Varied Rock Profile Temperatures with 30% Gas Cap Percentage and Zero Leakage	3-22
Figure 3.19.	Decay Curves for Varied Overall Heat Transfer Coefficients with Zero Leakage	3-23
Figure 3.20	Difference in Pressure Decay for Various Overall Heat Transfer Coefficients Normalized to 3.819 watt/m2·K	3-24
Figure 3.21.	Pressure Decay Comparing 400 cc/min Leak and Zero Leakage with Tubing Inside Diameters of 6.184 inches and 5.0 inches	3-24
Figure 3.22.	Deviation of Pressure Curves for Various Well Lengths and Leak Cases when Compared to the 500-m Depth Model	3-25
Figure 3.23.	Comparison of the Ideal Gas and Non-Ideal Gas Forms of the Thermal Model for the Baseline Case	3-27
Figure 3.24.	The Effects of the M and Eo on the Terminal Velocity of a Bubble	3-30
Figure 3.25.	Flow Patterns in Vertical Flowing Pipes	3-31
Figure 3.26.	Total Separation Time in Minutes as a Function of Well Depth at Four Viscosities	3-34

LIST OF FIGURES (cont'd)

Section **Page**

Figure 3.27. Comparison of Numerical and Analytical Model for No Heat Transfer 3-41
Figure 3.28. Comparison of Numerical and Analytical Model When Heat Transfer is Introduced 3-42
Figure 3.29. Comparison Between Models for Large Volume 3-42
Figure 3.30. Pressure and Flow Curve for Choked Flow Transition 3-43

LIST OF TABLES

Section **Page**

Table 1.1. Outline of Report Content 1-2
Table 2.1. New Technologies Considered 2-2
Table 2.2. Means of Supplementing Existing Procedures 2-3
Table 2.3. Grading Criteria.....2-3
Table 2.4. Guidance Utilized for Assessing Grades for Each Criterion 2-4
Table 2.5. Scoring Summary 2-6
Table 3.1. Solid Material Properties.....3-6
Table 3.2. Rise Velocity and Time for a Single Bubble to Travel from 500 m Below the Gas Cap to the Bottom of the Final Gas Cap 3-33
Table 3.3. Rise Velocity and Time for a Single Bubble to Travel 500 m Upward, Based on its Location in the Well 3-33
Table 3.4 Rise Velocity and Time for a Single Bubble to Travel 500 m to the Gas Cap, Based on the Tubing Inner Diameter 3-35
Table 3.5. Calculated Time to Reach Non-Choked Flow.....3-38

EXECUTIVE SUMMARY

Safety barriers play an important role in offshore oil and gas production, particularly in deepwater applications. The ability for the barriers to perform reliably and the ability to test their performance are key factors to safe production operations. The production master valve (PMV) and surface-controlled subsurface safety valve (SCSSV) are two barriers that play such a role in deepwater applications.

The focus of the work on this project was to determine the current state-of-the-art in performing in-situ leak testing of safety barriers for wells with subsea trees. This testing is typically performed by sealing off volumes in the flow line downstream of each valve and monitoring pressure buildup downstream of the sealing mechanism of the barriers. This approach requires that the production be stopped for several hours until testing can be completed, particularly if more than one barrier is tested. Such a shutdown has economic implications due to cessation of production. Additionally, this downtime results in flow assurance and other technical challenges that are introduced by such static lines over long periods of time in cold temperatures where methane may be present. Overcoming some of these obstacles would be a large benefit to operators of deepwater installations.

As part of this project, alternate means of conducting this testing were identified and subsequently ranked regarding their suitability for this application. Due to the large number of existing wells with the need for testing, it was decided to largely avoid technologies that required retrofitting of existing infrastructure, particularly for surface-controlled subsurface safety valves. The resulting tradeoff study picked well-specific modeling as the candidate technology. This approach utilizes a model to capture thermal and other environmental effects. Based on guidance from the project oversight committee, the primary focus for the proof-of-concept work on this project was for SCSSVs.

Computational fluid dynamics (CFD) modeling was executed as a means of comparing field data for a specific well across a family of similar wells. Unfortunately, the CFD models proved to be computationally-expensive and did not provide reliable results. Thus, it was concluded that CFD is not an ideal candidate for this application.

A numerical model was developed that allows for determination of leakage rates while taking into consideration a number of complex well transients. The model is computationally-inexpensive and allows for the operator to conduct simple trending of results. The sensitivity of various criteria was also explored. One significant finding of this work is that thermal effects of the well must be accounted for in order to properly interpret pressure results. Utilization of this model can reduce overall tests times and give operators a sense of the level of uncertainty in interpreting measured pressure changes. A similar modeling approach was also used for pressure buildup testing of wellhead valves, such as primary master valves and underwater safety valves.

Although this model works well for the applications considered, future efforts may be warranted to expand the application of such modeling. For example, the model could be extended in regards to the treatment of real gas behavior and accommodation of additional thermal effects, such as convection.

VALUE TO MEMBERS

This report documents work that shines a light on current approaches for testing of various safety barriers on wells with subsea trees. The results of this project include a numerical model that can be used by operators to interpret pressure buildup testing data. Additionally, even capturing the observations from the models will allow operators to determine the parameters of importance when conducting such testing. This model will help operators determine the operational envelope of their testing. Additionally, this report also gives an evaluation of other technologies that might aid operators of specific wells determine if additional technologies should be employed.

1. INTRODUCTION

1.1 Background

Safety barriers play an important role in offshore oil and gas production, particularly in deepwater applications. The ability for the barriers to perform reliably and the ability to test their performance are key factors to safe production operations. The production master valve (PMV) and surface-controlled subsurface safety valve (SCSSV) are two barriers that play such a role in deepwater applications.

The focus of the work on this project was to determine the current state-of-the-art in performing in-situ leak testing of PMVs and SCSSVs. This testing is typically performed by sealing off volumes in the flow line downstream of each valve and monitoring pressure buildup downstream of the sealing mechanism of the barriers. This approach requires that the production be stopped for several hours until testing can be completed, particularly if more than one barrier is tested. Such a shutdown has economic implications due to cessation of production. Additionally, this downtime results in flow assurance and other technical challenges that are introduced by such static lines over long periods of time in cold temperatures where methane may be present. Overcoming some of these obstacles would be a large benefit to operators of deepwater installations.

Two of the advantages of the current approach are that minimal instrumentation is needed and no specialized equipment is required. Also, there are well-established procedures for such testing. The current approach does, however, have some drawbacks:

- While the flow is shut-in, the volume of trapped fluid will begin to cool. This cooling can affect pressure monitoring, as the fluid properties can change dramatically when the line is cooled. This scenario is amplified in two-phase applications.
- The cooling during shut-in can also introduce flow assurance issues; for example, hydrate formation can come into play during long shut-in periods.
- Many deepwater wells are producing a flow with multiple phases. As the shut-in period evolves, separation of these phases must be accounted for when checking for leaks. Most current approaches only consider leakage of one phase.
- Pressure buildup requires that other valves used for downstream sealing are themselves not leaking or that the operator can enter into an elongated cycle of troubleshooting during the testing interval.
- In a pressure buildup test, direct measurement of leakage rate is not possible. Instead, an equivalent leak rate must be inferred by the change in pressure in the isolated section.

New technology or methods are required in order to drive down the time elapsed during testing and to minimize uncertainty introduced though such scenarios as fluid cooling or secondary valve leaks. A new approach to safety barrier testing should have at least one of three features:

- The ability to reduce test time.
- The ability to directly quantify leak rate.
- The ability to work in multiphase conditions.

Advances in at least one of the three areas would represent an improvement over current methods for testing, provided that the cost to implement new technology is not too high. The

direct impact of implementing new technology for testing safety barriers is an economic savings related to reduced production loss and costs associated with hydrate remediation or other flow assurance issues.

1.2 Project Approach

Figure 1.1 provides an overview of the progression utilized for this project. Initial efforts were geared toward collection of background information on topics such as current procedures for testing barrier valves, associated drawbacks, and available subsea instrumentation. This information was then used in a brainstorming session held at SwRI for the purpose of identifying various technologies for barrier leak detection. Personnel involved with the technology identification came from a wide variety of technical backgrounds: geosciences, mechanical engineering, physics, materials engineering etc. Each of the selected technologies was graded using a set of evaluation criteria. The scores of each technology were used to rank the list and select the top-scoring technology for further assessment in a proof-of-concept task. The selected approach, well-specific modeling, was comprehensively evaluated to determine its effectiveness.

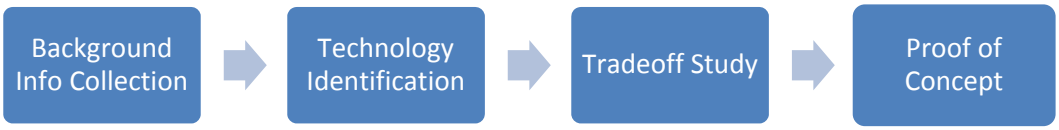

Figure 1.1. Project Progression Flowchart

1.3 Report Organization

Table 1.1 outlines the organization of the content of this report following the current section.

Table 1.1. Outline of Report Content

SECTION	TITLE	CONTENT
2	Tradeoff Study	Overview of evaluation process for selection of the technology to carry forward for remaining project tasks.
3	Proof of Concept	Chronology of efforts to further evaluate the chosen technology. Analysis of the effectiveness of the chosen system.
4	Conclusions	Overall project summary and conclusions.
5	References	Bibliography of references used in report.

2. TRADEOFF STUDY

A tradeoff study was conducted in order to select a technology most suited for improving the current testing methodology. A list of technologies was identified by means of a brainstorming session. This list was refined during several evaluation iterations. A list of evaluation criteria for final scoring was also generated and each parameter was assigned a relative weighting. The technologies were then graded using the evaluation criteria and a ranking list of the technologies was generated. Figure 2.1 illustrates this progression of steps for the tradeoff study.

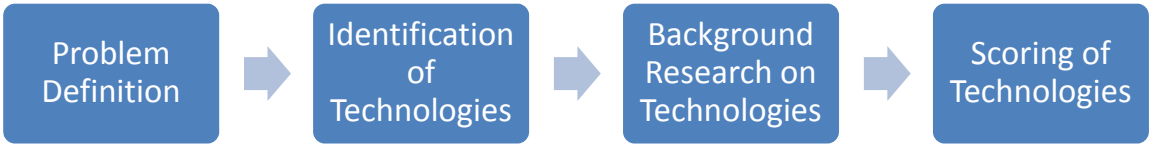

Figure 2.1. Process for Tradeoff Study

2.1 Brainstormed Ideas

A group of engineers and scientists from a broad range of fields was brought together to brainstorm possible testing approaches, as well as to determine the evaluation criteria for grading each technology.

A total of 73 ideas were brainstormed. Many of these concepts were permutations of other ideas. In an effort to make the list of ideas more manageable, the concepts were grouped into categories and the category title was used as the evaluated topic. For example, multiple ideas surrounding the use of tracer technology were identified. Instead of evaluating each one individually, a technology category called *tracer* was created and all similar topics were folded into this line.

The list was pared down by dismissing non-practical ideas. Additionally, the following list of ideas was excluded as the implementation of these methods would not result in a quantitative measure of leakage:

- Acoustic emissions
- Cameras
- Infrared monitoring
- Fluid conductivity measurements
- Introduction of oleophilic material
- Distributed temperature sensing

The original list of topics under consideration was:

- Computational data processing
- Direct fluid measurement
- Fluid injection rate
- Improved temperature and pressure measurement
- Level detection
- Mass gauging
- New valve hardware
- Tracers
- Thermal stabilization
- Ultrasonic
- Volume reduction

It was apparent that some of the identified methods were "new technologies," while others were simply means of improving the current pressure-monitoring approach. Since the

evaluation of these two broad categories may differ from each other, the technologies were originally divided into two groups. Table 2.1 and Table 2.2 provide the starting point for the tradeoff study.

Table 2.1. New Technologies Considered

FLOW MEASUREMENT	When a volume is trapped in a cavity and properties such as temperature are maintained, no additional flow into the cavity should be required to maintain pressure. If injection lines were left open and equalized, flow of methanol or gas could be utilized to quantify leakage rates. Gas pressurization could also be used.
FLUID DETECTION	Fluid downstream of the valve could be sampled and a local analysis performed to determine composition. Changes in fluid composition could be monitored by means of conductivity changes in the column.
LEVEL DETECTION	It is assumed that some amount of gas is present in the wells for which this testing would be performed. As soon as a cavity of fluid is sealed, separation will commence. If this process is accelerated and temperature conditions are maintained, the level should not change unless leaks are present. The level could be measured by direct pressure monitoring, utilizing ultrasonic or lasers, or by use of guided waves. The level conditions could be stabilized by injection of denser-than-oil fluids or known amounts of gas.
NEW VALVE HARDWARE	While not suitable for existing valves, new wells could utilize hardware or valves that were specifically designed with considerations for leakage measurement. An example would be to instrument gates or install flow meters into the tree. Secondary double-block-and-bleed valves could also be utilized.
TEMPERATURE PROFILE	Thermal profiling could be utilized to detect the migration of fluids. One example would be to utilize fiber optics or other temperature-measuring devices to detect Joules-Thomsen cooling of gases expanding past the valve seat. Alternatively, the fluid on one side of the valve could be heated and infrared or other means could be used to monitor temperature.
TRACER	A variety of tracers may be applicable for injection on one side of the valve. Examples would be RFID devices, radioisotopes, or fluids such as helium. Various means could be utilized to detect the tracer downstream of the valve seat.
ULTRASONIC	Various ultrasonic devices could be utilized to measure flow or the presence of bubbles. Ultrasonic detectors could be directly mounted to the valve.

Table 2.2. Means of Supplementing Existing Procedures

ALTERNATIVE TRANSMITTERS	Conduct testing in similar fashion as done today, but with improved instrumentation and/or instrumentation designed specifically for leak testing. One example would be the use of fiber optics for temperature measurement.
DATA PROCESSING IMPROVEMENTS	Supplementary data processing may allow for improved assessment of results. Examples include computer tomography, interferometry, or genetic algorithms. Computational fluid dynamics (CFD) could potentially be used to model valve-specific behavior.
THERMAL STABILIZATION	One of the significant obstacles in current test approaches is the fact that stopping flow will result in cooling of the fluid. Perhaps removing such temperature effects would improve test results. Accelerated heating could be used, as could injection of more thermally-stable fluids. Alternatively, the fluid could be *cooled* quicker by means of cooling coils or injection of seawater.
VOLUME REDUCTION	The relatively large volumes of fluid monitored during pressure decay testing amplify other test uncertainties. Reducing these volumes (particularly for subsurface valves), could dampen such effects. One potential idea would be to utilize an inflatable trap to reduce the volume.

2.2 Evaluation Criteria

The brainstorming session was also utilized to identify grading criteria for the tradeoff study. In addition to the selection of the criteria, relative weightings were also determined. The list of criteria and their weightings is provided Table 2.3 below. These ratings were reviewed by various operators and their recommendations were incorporated into the final weightings.

Table 2.3. Grading Criteria

CRITERIA	WEIGHTING	DESCRIPTION
Performance	10	The ability of the technology to accurately measure leakage in a repeatable fashion.
HSE	9	Health, safety, and environmental footprint. Specifically, minimizing "hoops to jump through" in order to deploy system.
Robustness	7	Ability of the technology to produce useful data, even in non-ideal circumstances.
Adaptability	7	Ability to work over a variety of types of wells (e.g., gas, multiphase, large bore, etc.) and with various hardware (horizontal trees, vertical trees, etc.).
System Reliability	7	Reliability of hardware to be ready-for-use when called upon.
Retrofittable	6	Ability of technology to be retrofitted to existing infrastructure.
Test Time	5	Amount of time required to execute one leakage test.
Direct Cost	3	The cost to install any hardware and direct costs associated with the execution of tests (not factoring in the loss of production or flow assurance remediation).
Technology Readiness Level	3	Maturity of technology and minimal developmental schedule required. Also includes developmental costs.

One of the grading criteria initially used in this work was *operational footprint*. This criterion was defined as the ability of the system to operate with minimal risk of impacting other equipment (in other words, not solving one problem at the expense of creating another). During analysis of each technology, however, a clear score could not be determined for most technologies, so this criterion was dropped from further assessment.

A list of grading guidelines is provided in Table 2.4. This arrangement allowed for consistent grading of each of the technologies.

Table 2.4. Guidance Utilized for Assessing Grades for Each Criterion

CRITERIA	WEIGHTING	1 – LOWEST	3 - MIDDLE	5 - HIGHEST
Performance	10	System only allows for relative measurement	System allows for qualitative measurement corresponding to half the range of allowed leakage	System can measure rate in reliable fashion to the order of several ccs/min or scfm
HSE	9	Corporate policies would prevent deployment of such technology	Some additional equipment or procedures would have to be put in place to ensure safe operation	No HSE impact
Robustness	7	Will not work unless ideal conditions are present	Particular conditions (e.g., multiphase separation, etc.) must be met in order to accurately measure leakage	Works independently of environment or well conditions
Adaptability	6	System will only work for specific wells or tree configurations	System can work on the majority of well and tree types	System can work on all well and tree types
System Reliability	7	Hardware malfunctions during testing	Some maintenance and testing required to ensure continued reliability	System hardware is always available when needed
Retrofittable	6	Can only be used in new wells with new hardware	Can be retrofitted to some valve and tree designs	Can be adapted to any existing well
Test Time	5	Test time longer than with current methods	Total test time same as current methods	Total test time no more than half of time of existing methods
Direct Cost	3	Considerable hardware must be purchased specifically for this test	Some well-specific equipment must be procured	No costs in addition to shut-down time
Technology Readiness Level	3	System several years and many dollars in investment away from reality	System could be brought online within a two-year period	System is available for use today

2.2.1 Technology Evaluation

Some additional research was conducted to further refine the list of appropriate technologies that were first presented in Table 2.1 and Table 2.2. A tradeoff study was then performed to rank the suitability of ten methods for barrier testing:

- Active ultrasonic
- Differential pressure level measurement
- Flow measurement
- Guided wave level detection
- Passive ultrasonic
- Radiometric level detection
- Thermally-stable pressure monitoring
- Tracer
- Volume-reducing pressure monitoring
- Well-specific modeling

Each of these technologies was graded (using a scale of 1-5, with 5 being the highest) on each of the criteria provided in Table 2.3. This scoring was based upon the expected performance of each technology for use in the testing of PMVs. While a later part of the report will discuss a refocusing on SCSSVs, the initial effort of this tradeoff study was on the PMVs.

The project definition of PMV came from early discussions with RPSEA staff and operators. For purposes of the spirit of this project, PMV and USV can be used interchangeably, as the general testing techniques could be utilized in either case.

The results are provided in Appendix A. These tables include a brief description of the technology, the grading for each criterion, and justification of the score provided. The current state-of-the-art, pressure monitoring, was also scored and appears first. The remaining technologies appear in alphabetical order. A more in-depth description of some of the technologies can be found in Appendix B.

Table 2.4 presents a summary of the rankings for each of the technologies for each of the criteria, along with the normalized score. The technologies are presented in order of their normalized score, with the "best" technologies being in the columns to the left.

Well-specific modeling scored as the most appropriate technology for safety barrier testing. The only other technology to be scored higher than the current pressure-monitoring approach was pressure monitoring with the addition of volume reduction. Pressure monitoring with thermal stabilization also scored relatively high. Modeling was, thus, selected as the technology to move into the proof-of-concept stage of the project.

Table 2.5. Scoring Summary

Well-specific modeling scored the highest.

Criteria	*Weighting*	*Well-Specific Modeling*	*Volume Reduction*	*Pressure Monitoring (Current)*	*Thermal Stabilization*	*Differential Pressure Level Detection*	*Tracer*	*Passive Ultrasonic*	*Active Ultrasonic*	*Flow Measurement*	*Guided Wave Level Detection*	*Radiometric Level Detection*
Performance	10	4	4	3	4	3	4	3	1	4	3	3
HSE	9	5	4	5	4	5	2	5	5	4	4	2
Robustness	7	3	3	2	3	3	5	3	3	4	3	3
System Reliability	7	4	5	5	4	5	4	3	3	2	4	3
Adaptability	6	4	4	4	4	3	4	3	4	4	3	3
Retrofittable	6	4	4	4	3	3	4	4	4	2	3	3
Test Time	5	4	4	3	5	3	4	3	5	4	4	4
Direct Cost	3	4	4	4	3	2	1	4	4	2	2	1
TRL	3	4	3	5	4	5	3	4	3	3	3	3
Normalized Score		**1.00**	**0.98**	**0.95**	**0.94**	**0.90**	**0.89**	**0.88**	**0.85**	**0.84**	**0.82**	**0.70**

2.3 Transition in Focus to Subsurface Valves

At the end of the tradeoff study, the operator members of the project team expressed confidence in the current approach for wellhead valves and that the proof-of-concept work should instead focus on the SCSSV. The tradeoff scoring was revisited for SCSSVs and the same technology, well-specific modeling, floated to the top of the list and was carried to the proof-of-concept work on this project.

3. PROOF OF CONCEPT

A trade-off study was conducted to select a concept for improved safety barrier testing. Well-specific modeling scored highest in this assessment, and was selected to advance to the proof-of-concept task. The goal of this work was to develop an approach that allows operators to input varying well-specific information, and then use the model to provide a more accurate assessment of valve leakage than current pressure-monitoring methods. Per operator input, the focus of this work was on surface-controlled subsurface safety valves (SCSSVs).

3.1 Current Industry Testing Procedures and Project Objectives

In offshore production wells, the SCSSV represents a critical barrier component to be used in the event of an emergency to shut off flow from the well. The SCSSV is installed below the mud line and its integrity needs to be verified on a periodic basis. API 14B provides in-situ test instructions for SCSSVs. The document acknowledges that standard procedures are difficult to apply to deepwater applications. The allowable leak rates for PMVs and SCSSVs are specified in API 14H and API 14B, respectively. In a gas-only environment, the allowable leakage is 15 scfm. In liquid-only environments, the allowable leakage is 400 cc/min.

The traditional methods of leak testing in API 14H and API 14B make the assumption that pressure is lost at a dry tree. Thus, the discharge pressure is atmospheric. In reality, wells with subsea trees, however, will discharge in normal operation to the back pressure of the downstream flow line to which they are attached. Thus, the loss of pressure at the wellhead will not result in a discharge pressure of atmospheric. At a minimum, the hydrostatic head from the water depth at the location of the wellhead will act against the flow. One complication in such a scenario is that the testing of the valve may be at a lower differential pressure than if the downstream were allowed to be vented to atmospheric. For valves with seals that require to be energized, such a scenario would be worst-case as sealing against lower pressures and could be more conducive to failure. However, valves that fail at higher differential pressures would exhibit the opposite effect.

In dry tree conditions, the actual liquid leakage through a PMV or SCSSV can be determined by means of volume collection. A downstream port can be connected to a tank or other reservoir and leakage ported to it to determine the volume of leaked product. In the case of a multiphase well in which the column segregates after shut-in, the excess gas pressure can be vented and the remaining column space filled with another fluid to allow for direct measurement of leak rate to occur. Obviously, such an approach is not possible for subsea trees.

One means of testing SCSSVs is monitoring pressure buildup. The wellhead can be closed to create a trapped cavity between the SCSSV and the wellhead. The cavity is then monitored for pressure buildup over a period of time. Theoretically, this pressure would not change unless leakage through the closure mechanism of the SCSSV occurred. However, such an application does not compensate for any thermal effects in the well.

Testing of SCSSVs using this procedure can be costly since such validation takes considerable time. Generally, any wellhead valves are tested first (test may take on the order of one hour), followed by the SCSSV (several hours). In addition to direct production losses, long shut-in periods can also lead to flow assurance issues in the restarting wells. Hydrate formation, in particular, is an area of concern in many subsea well locations.

Aside from difficulties arising from this testing process itself, results from this method do not provide direct correlation to leakage rates. As shown in Figure 3.1, there are opposing effects that influence pressure changes within the shut-in cavity. Cooling decreases pressure, due to gas cooling and volume change from liquid contraction, while leakage will increase it.

While a minimum of five minutes is recommended, discussion with operators revealed that one hour is more feasible given the relatively high uncertainty of the instrumentation to detect such small pressure deviations. For example, if a 500-m shut-in wellbore (50˚C, 150 bar) with an inner diameter of six inches has a gas volume of 50%, then 400 cc/min over five minutes represents only 0.044% of the total liquid volume, while 15 scfm over five minutes represents about 0.35% of the total gas volume. Allowing for longer shut-in times to reduce measurement uncertainty though, introduces further uncertainty due to cooling effects, which are not captured by current empirical models. Operators have investigated the possibility of using zonal temperature and pressure data to reduce uncertainty (Paino et al., 2004). However, wide-scale implementation of these types of techniques would require significant retrofitting for new instrumentation, e.g., distributed sensor fiber placement and multiple pressure gauges staggered the length of the wellbore.

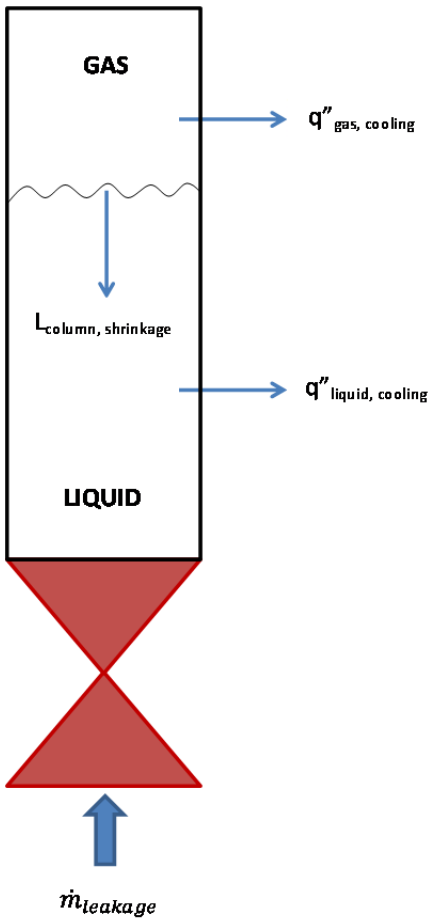

Figure 3.1. Heat Transfer and Mass Flow Mechanisms Influencing Shut-in Pressure
Cooling and liquid shrinkage decrease pressure, while inflow leakage raises the pressure.

3.1.1 Regulatory Context

While there are different regulations worldwide, points of emphasis for this project are operations in the Gulf of Mexico under jurisdiction of the U.S. Department of the Interior. The enforcement body of this department (BSEE) utilizes a mix of API standards and other line items to capture governance of these areas. In relating to PMVs (or even Underwater Safety Valves) and SCSSVs, testing is largely based on API 14H and API 14B, respectively. The typical test intervals are three months and six months, respectively. These requirements are spelled out in NTL No. 2009-G36 that went into effect on January 1, 2010. This notice utilizes the barrier method and establishes the allowable leak rate of both types of valves to be 400 cc/min for liquid service and 15 scfm for gas service.

3.1.2 Prior Efforts

Prior work had been conducted by one operator to use a well simulator (OLGA) to model the leakage through an SCSSV. OLGA models attempted to model a flow through a small office into a big volume and were unable to reliably converge. In essence, the model was not flowing, making a flowing model simulator not appropriate for such work. The differences in the assumption of discharge coefficient alone led to uncertainty on the order of 15%. The feeling of the operator was that the model was no better than ±40% uncertainty.

3.1.3 Path Forward

Since isolating potential leakage effects on pressure is not possible using the present testing procedure, one objective of the current project is to propose a testing process that will provide quantitative assessment of leakage rate. Along the same line, reduction in measurement uncertainty and criterion sensitivity are additional goals. Finally, a procedure that reduces the required shut-in time is a desirable feature. As stated in the previous section, well-specific modeling was chosen as the most promising leak detection technology for advancement to the proof-of-concept stage.

3.2 Computational Fluid Dynamics Modeling

It was determined to perform simulations using transient computational fluid dynamics (CFD). The numerical code CFX version 12.1 was utilized for initial simulation results. However, the software package was changed to FLUENT version 13.0, as detailed in Appendix C. Both software packages are produced by ANSYS, and include sophisticated multiphase models able to handle heat and mass transfer between solid-liquid/gas phases.

3.2.1 Modeling Progression Map

A roadmap for generating suitable CFD models is presented in Figure 3.2. An overview of each of these models is provided in Appendix C. Though modeling was chosen from the previous tradeoff study due to some significant advantages, it also has a higher likelihood than experimental testing of a particular test becoming very well-specific. Thus, the progression plan was based on starting with the simplest cases first, and progressing with increasing complexity. This approach allowed for neglecting processes that do not strongly impact the results. A variety of parametric studies on select variables allows for potential development of correlations that can be used over a broad range of well types.

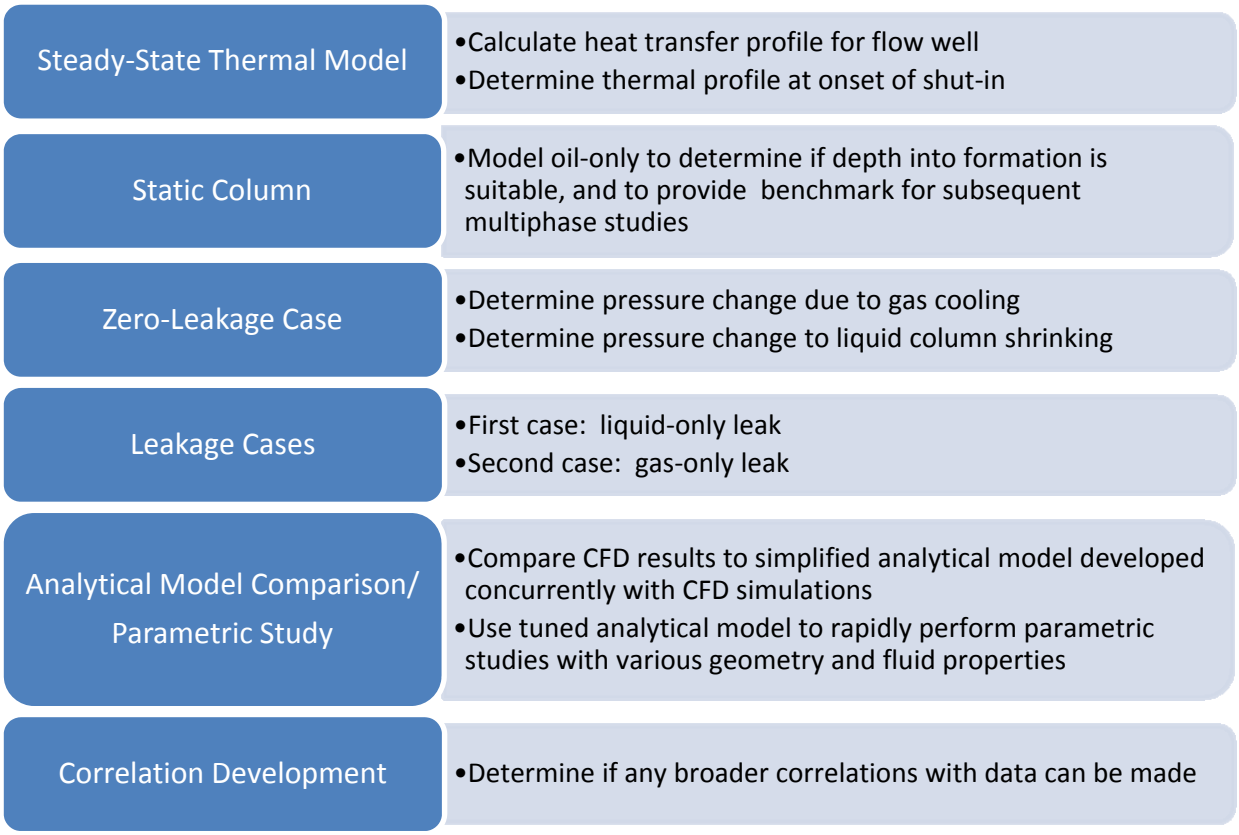

Figure 3.2. CFD Modeling Roadmap
CFD modeling was carried out in six discrete phases.

3.2.2 CFD Code Inputs and Setup Configuration

The physical setup of the CFD model is based in part on input received by operators that agreed to provide feedback for this project. Since the problem is symmetrical in nature, axisymmetric simulations have been employed. Figure 3.3 presents a schematic of the overall geometry that served as the baseline case for this project. The gas and liquid columns are contained by 500 m of steel tubing, and are bounded by the wellhead at the top and the SCSSV at the bottom. Outside the tubing are layers of gelled diesel in the annulus, carbon steel in the casing, cement for the annulus barrier, and formation rock in the far field. The respective thickness of each layer is given in Figure 3.3. It is necessary to have the formation rock thick enough that cooling effects are not felt at the boundary, while minimizing computational requirements associated with additional discretized domain cells. Five meters was chosen as an initial estimate, and this value was then verified from post-processed results to be a reasonable value based on two hours of simulation time from an example case.

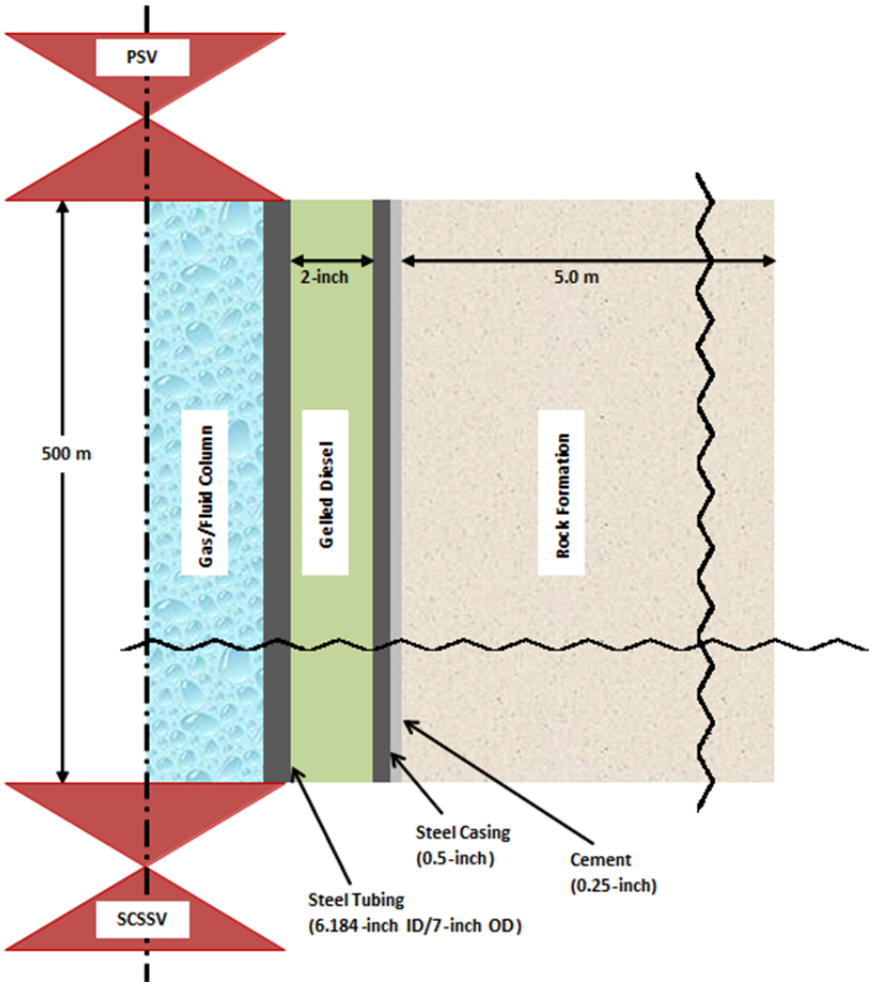

Figure 3.3. Shut-in Wellbore Schematic of Example Case

The region between the SCSSV and PMV is modeled for effects of leakage and cooling on pressure using the example geometry provided by the operator.

The left boundary is associated with axisymmetric symmetry. The bottom boundary is specified using the Dirichlet condition of constant 50˚C temperature to mimic reservoir temperature. The top boundary is also a Dirichlet condition, set to 4˚C. The right boundary is meant to simulate the temperature profile given an infinite formation distance from the wellbore. The temperature distribution is linear as a function of well depth, assuming a homogeneous formation with a constant thermal conductivity. Though formations are not generally homogeneous along the entire wellbore, it is felt that this is a reasonable approximation for the model.

Property information for the various solid layers was obtained from operator input and is given in Table 3.1. It should be noted that annulus fluid and formation rock properties can vary widely based on the physical location of the well. Fluids considered in this work are oil and methane gas (adhering to ideal gas law). The specific heat, viscosity, and thermal conductivity properties for the gas (NIST, 2011) are: 50.5 J/(kg-K), 0.0162 cP, and 0.053 W/(m-K), respectively. The oil was assumed to be incompressible with temperature-dependent density. Shrinkage of the liquid column, along with associated pressure changes in the gas, is accounted for through the thermal expansion coefficient of each fluid. The expansion coefficient is assumed to be constant at 0.001 K^{-1} for oil (Wolfram/Alpha, 2010); oil density at bottom-hole

conditions was set at 850 kg/m^3 based on operator input; specific heat (Wolfram/Alpha, 2010) was taken as 2,130 J/(kg*K); and thermal conductivity (ANSYS, 2010) was specified as a function of temperature to be $k\left[\frac{W}{m*^\circ C}\right] = 0.17 - 1.418e^{-4}T$, where T is in Kelvin.

Table 3.1. Solid Material Properties

Properties in the table were obtained from operator input.

Material	Region	k [W/(m*K]	ρ [kg/m^3]	c_p [J/(kg*K)]
Stainless Steel	Tubing	15	8100	500
Gelled Diesel	Annulus Fluid	0.2	810	1900
Carbon Steel	Casing	40	7850	480
Cement	Annulus Barrier	0.85	1650	900
Water-Saturated Shale	Formation Rock	3	2300	1000

3.2.3 CFD Conclusions

The motivation for utilizing CFD was to provide a robust means of comparing field data for a specific well. The expected pressure behavior of a well could be characterized for a particular set of conditions and trending could be accomplished to determine if the SCSSV was leaking more than allowed. Unfortunately, the CFD models, in general, did not demonstrate realistic pressure cases. Specifically, for cases with no leakage, the gas density and pressure increased, even though its volume increased and temperature decreased. Additionally, the CFD models require significant computational time that would likely not be available for field deployment over numerous wells. Thus, CFD is not an ideal candidate for supplementing existing pressure-monitoring approaches. However, the steady-state thermal models were useful for input to analytical models.

3.3 Analytical Model

CFD modeling is computationally-expensive and would likely not be feasible for individual well testing. A more straightforward analytical approach was developed in order to determine if such a method could gauge the dynamics of the well without the large computational cost of running CFD models.

This selected approach utilizes relatively simple equations to characterize the behavior in a well. Figure 3.4 provides the heat loads of the well architecture during the course of a test during shut-in. If the SCSSV leaks, the pressure in the tube will increase. This behavior is complicated by the fact that the shut-in fluid can lose heat to the surrounding rock formation through the materials making up the well cross section. These materials include the tubing itself, annular fluid, the well casing, and cement. The loss in heat will cause the liquid volume to decrease which, in turn, will increase the gas volume and reduce the overall gas cap pressure. In addition, the loss of heat from the gas itself will cause the gas pressure to decrease.

This analysis investigates the response of the fluid pressure to these processes:

1. Leakage of liquid into the shut-in space through the SCSSV (pressure increase).
2. Loss of heat from the liquid (pressure decrease).
3. Loss of heat from the gas (pressure decrease).

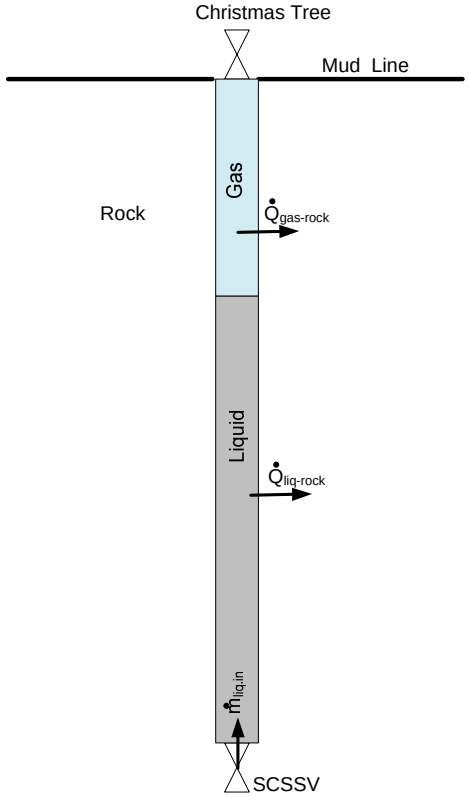

Figure 3.4. Heat Loads for Shut-in Conditions for SCSSVs
The gas and liquid exchange heat with the formation, but the heat transfer between the gas and liquid is assumed to be negligible.

3.3.1 Assumptions

The mathematical model for the thermal response of the shut-in fluid is based on the following simplifying assumptions:

1. The liquid and gas are already separated as a precondition to the application of this analysis. Stated differently, the user has to allow for sufficient time to elapse for gas bubbles to rise to the top of the closed well. This time lapse is addressed in subsection 3.6.
2. The gas/liquid interface can be located with sufficient precision based on the known GVF conditions, as measured at the wellhead or by extrapolation back from a downstream measurement location. Once the gas/liquid interface is established, it is further assumed that no gas comes out of the solution once the pressure measurement period begins (i.e., after the time established in subsection 3.6)
3. Gas does not leak from tubing.
4. The temperature is uniform in each gas and liquid subvolume. The gas and liquid temperatures in each subvolume change according only to the heat transfer to the surrounding rock.

5. The liquid composition is assumed to be uniform during the time this analysis is applied. This is a simplifying assumption for this form of the model, but is not a requirement. Future model improvements can include the oil/water composition effects on the liquid thermal properties in each subvolume.
6. Heat transfer between fluid subvolumes is neglected.
7. Fluids are assumed stationary - convective heat transfer is neglected.
8. The annular fluid (gelled diesel) is a good enough insulator such that the thermal capacitance of the tubing is included with the wellbore fluid.
9. Total volume of shut-in tubing is constant.
10. Hydrostatic pressure effects on density are negligible; so, a uniform nominal gas pressure is applied to the entire tube.
11. Gas volumes act as ideal gases. The impact of this assumption is addressed in subsection 3.6.

3.3.2 Rock Thermal Profile

The heat transfer from the tubing to the rock is dictated by the temperature difference between the fluid and the neighboring rock formation. A thermal analysis of the flowing fluid and a 5-m radius of the surrounding rock was performed to establish the temperature profile in the neighboring rock that is established after the production fluid has been flowing for a long period. The boundary conditions for this analysis were taken from typical data supplied by an operator from conditions measured in the field:

- Far-field rock temperature at 500 m below the mudline = 55°C.
- Temperature at the mudline = 4°C.
- Production fluid temperature = 50°C.

Other rock temperature profiles can be easily incorporated into the analysis.

A linear profile for the far-field rock temperature was assumed. The corresponding steady temperature profiles for the wellbore fluids, structures, and nearby rock for a flowing well are shown in Figure 3.5. For this figure, the right-most point on the x-axis represents the wellhead, while a value of zero is the location of the SCSSV. This profile was generated from steady-state thermal modeling and was input into the analytical model. It is seen that the nearby rock temperature is characterized by a bilinear profile. The temperature gradually decreases from about 55°C at a depth of 500 m to about 8°C at a depth of about 8 m (i.e., temperature gradient of 0.096°C/m). The temperature decreases from 8°C to 4°C in the uppermost 8 m of rock (temperature gradient of 0.5°C/m).

It is assumed that, after the well is shut in to perform the SCSSV leak test, the rock near the wellbore does not change appreciably during the time of the test. So, the profile of the nearby rock formation shown in Figure 3.5 is assumed to be constant with respect to time.

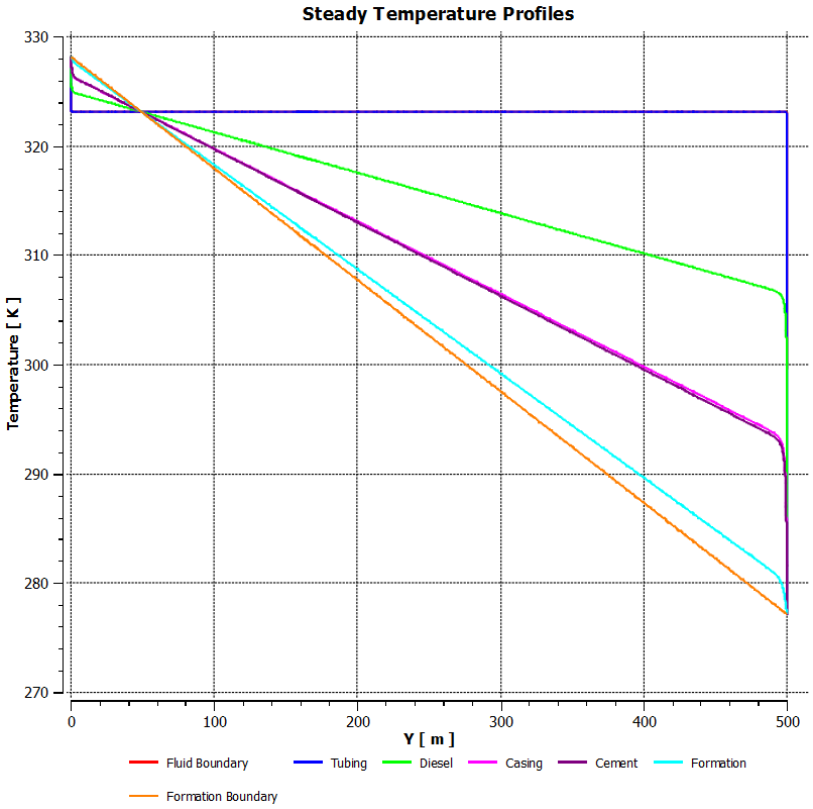

Figure 3.5. Steady Well and Formation Temperature for Flowing Well

The CFD predictions for the fluid temperature were used as an initial condition for the analytical model. The SCSSV is located at a value of 0 on the x-axis.

3.3.3 Material Properties

The properties of the various fluids and solid materials used in the analysis are as follows.

Production Gas

- Specific Heat: 700 J/(kg-K)
- Gas Constant: 518 J/(kg-K)

Production Oil

- Specific Heat: 2,130 J/(kg-K)
- Density (Baseline): 850 kg/m^3 (ρ_{lo})at 350 K (T_{lo})
- Thermal Expansion: 0.0008 1/K

Tubing

- Specific Heat: 500 J/(kg-K)
- Density: 8,100 kg/m^3
- Thermal Conductivity: 25 W/(m-K)

Gel Diesel

- Specific Heat: 1,900 J/(kg-K)
- Density: 810 kg/m^3
- Thermal Conductivity: 0.14 W/(m-K)

Casing

- Specific Heat: 480 J/(kg-K)
- Density: 7,850 kg/m3
- Thermal Conductivity: 25 W/(m-K)

Cement

- Specific Heat: 900 J/(kg-K)
- Density: 1,650 kg/m3
- Thermal Conductivity: 0.42 W/(m-K)

3.3.4 Model Description

A mathematical model of the thermal response of the production liquid and gas inside the shut-in section of the tubing is developed by applying the principles of conservation of mass and energy to the two fluids. The fluid volumes are divided into subvolumes, as shown in Figure 3.6.

The selection of two unequal subvolumes for the gas is based on the presence of a clear inflection point in the rock temperature vertical profile that serves as a boundary condition for this model. The selection of three subvolumes for the liquid is based on the simplicity of having equal mass in each liquid subvolume.

It is recognized that the subvolume represents a very coarse discretization of the wellbore and rock geometry. This level of detail is well suited to the software (Mathcad) chosen to demonstrate the efficacy of the model. This imposed resolution does not limit the use of the model and greater vertical resolution can readily be programmed into a different software system for future improvements of the model.

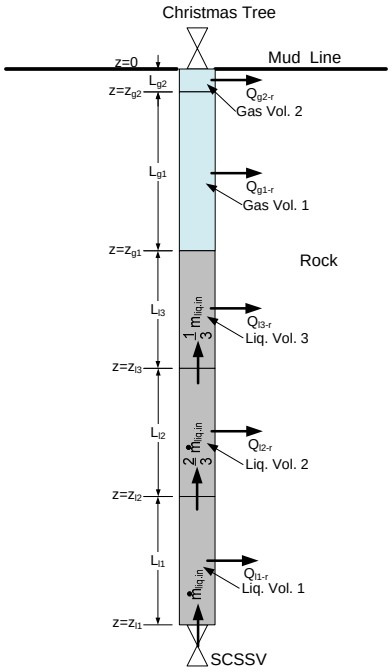

Figure 3.6. Model Subvolumes

The gas cap is divided into two subvolumes and the liquid into three subvolumes.

The subdivisions of the gas and oil are defined below in the description of the model equations below.

3.3.5 Liquid Density

The liquid density is assumed to be temperature-dependent according to a linear thermal expansion relation.

$$\rho(T) = \rho_{lo}[1 - \beta_l(T_l - T_{lo})]$$

3.3.6 Gas Volume

In keeping with the fact that the rock formation has a break in its thermal gradient, the gas is divided in to two subvolumes. The divide in the gas subvolumes is to be placed at the break in the rock temperature profile. It is assumed that the mass of each gas subvolume remains constant throughout the entire time.

3.3.7 Model Equations

The model equations for the gas subvolumes are based on the conservation of mass and energy.

3.3.8 Nomenclature

The nomenclature for the analytical model is defined below.

Variables

A_s	surface area
A_x	cross-section area
h	enthalpy
U	heat transfer coefficient
M	mass
E	total energy
e	mass-specific energy
P	pressure
V	volume
T	temperature
T_R	temperature of rock near a subvolume
$C_{v.gas}$	gas constant volume specific heat
C_{liq}	liquid specific heat
C_l	effective specific heat of liquid and wall materials
C_g	effective specific heat of gas and wall materials
$\dot{m}_{liq}$	leak rate through SCSSV
k	thermal conductivity
ρ	density
F_{g2}	fraction of total gas volume assigned to gas subvolume 2
$\dot{Q}$	heat transfer rate
$\dot{W}$	mechanical work rate (for fluid expansion)
GVF	gas volume fraction

Subscripts

g1 gas volume 1
g2 gas volume 2
l1 liquid volume 1
l2 liquid volume 2
l3 liquid volume 3

Gas-Liquid Interface

The sum of the gas and liquid volumes is constant; so,

$$-\frac{dV_g}{dt} = \frac{dV_l}{dt}$$

Recall that it is assumed that the gas volumes retain a constant ratio,

$$V_{g2} = F_{g2}V_g = F_{g2}(V_{total} - V_l) \quad \Rightarrow \quad \frac{dV_{g2}}{dt} = -F_{g2}\frac{dV_l}{dt} \qquad \text{Eq. 1}$$

$$V_{g1} = \left(1 - F_{g2}\right)V_g = \left(1 - F_{g2}\right)(V_{total} - V_l) \quad \Rightarrow \quad \frac{dV_{g1}}{dt} = -\left(1 - F_{g2}\right)\frac{dV_l}{dt} \qquad \text{Eq. 2}$$

The rate of change of the liquid volume is now defined from the definition of the density and the assumption (described below) that the liquid is divided into three subvolumes having equal mass.

$$V_l = \frac{M_l}{\rho_l} \quad \Rightarrow \quad \frac{dV_l}{dt} = \frac{V_l}{M_l}\dot{m}_{liq} + \rho_{lo}\beta_{lo}\left(\frac{V_{l1}}{\rho(T_{l1})}\frac{dT_{l1}}{dt} + \frac{V_{l2}}{\rho(T_{l2})}\frac{dT_{l2}}{dt} + \frac{V_{l3}}{\rho(T_{l3})}\frac{dT_{l3}}{dt}\right) \qquad \text{Eq. 3}$$

Conservation of Mass

Using the ideal gas equation of state and the assumption that the mass of each gas subvolume is constant, the following equations can be derived.

$$\frac{dM_{g1}}{dt} = \frac{M_{g1}}{P_g}\frac{dP_g}{dt} + \frac{M_{g1}}{(V_{g1} + V_{g2})}\frac{dV_{g1}}{dt} - \frac{M_{g1}}{(V_{g1} + V_{g2})}\frac{dT_{g1}}{dt} = 0$$

$$\frac{dM_{g2}}{dt} = \frac{M_{g2}}{P_g}\frac{dP_g}{dt} + \frac{M_{g2}}{V_{g2}}\frac{dV_{g2}}{dt} - \frac{M_{g2}}{T_{g2}}\frac{dT_{g2}}{dt} = 0$$

These can be combined with Eq. 2, and 3 to yield

$$\frac{dP_g}{dt} = \frac{P_g}{\left(V_{g1} + V_{g2}\right)}\frac{dV_l}{dt} + \frac{P_g V_{g1}}{T_{g1}}\frac{dT_{g1}}{dt} + \frac{P_g V_{g2}}{T_{g2}}\frac{dT_{g2}}{dt} \qquad \text{Eq. 4}$$

Conservation of Energy

From thermodynamics, the conservation of energy for a control volume surrounding a fluid is

$$\frac{dE}{dt} = \dot{Q} - \dot{W} + \dot{m}_{in}h_{in} - \dot{m}_{out}h_{out}$$

Applying this to the gas subvolumes (with no mass flow), we find

$$\frac{dE_{g1}}{dt} = M_{g1}C_g\frac{dT_{g1}}{dt} = -U_{g1}A_{sg1}\left(T_{g1} - T_{Rg1}\right) - P_g\frac{dV_{g1}}{dt} \quad \text{Eq. 5}$$

$$\frac{dE_{g2}}{dt} = M_{g2}C_g\frac{dT_{g2}}{dt} = -U_{g2}A_{sg2}\left(T_{g2} - T_{Rg2}\right) - P_g\frac{dV_{g2}}{dt} \quad \text{Eq. 6}$$

3.3.9 Liquid Volume

The liquid is divided into three subvolumes of equal mass to allow for flexibility of later modifications to the model requiring multiple subvolumes. The choice of three subvolumes was arbitrary. During a simulated event, the total mass of liquid can change, but the total mass is always divided equally among the three subvolumes. This provides for a very crude discretization of the liquid to allow for a variation in liquid density.

Conservation of Mass

The rate of change of liquid mass is

$$\frac{dM_l}{dt} = \dot{m}_{liq} \quad \text{Eq. 7}$$

By assuming that the mass of all of the liquid subvolumes are equal, the following expressions can be found.

$$\frac{dM_{l1}}{dt} = \frac{dM_{l2}}{dt} = \frac{dM_{l3}}{dt} = \frac{\dot{m}_{liq}}{3}$$

Conservation of Energy

Applying the conservation of energy expression subvolume 1 (the lowermost) results in

$$\frac{dE_{l1}}{dt} = M_{l1}\frac{de_{l1}}{dt} + e_{l1}\frac{dM_{l1}}{dt} = -U_{l1}A_{sl1}(T_{l1} - T_{Rl1}) - P_g\frac{dV_{l1}}{dt} + \dot{m}_{liq}h_{in} - \frac{2}{3}\dot{m}_{liq}h_{l1}$$

After rearranging and making use of the thermodynamic relation $h=e+pv$, the equation becomes

$$M_{l1}C_l\frac{dT_{l1}}{dt} = -U_{l1}A_{sl1}(T_{l1} - T_{Rl1}) + \dot{m}_{liq}C_l\left(T_{liq} - T_{l1}\right) \quad \text{Eq. 8}$$

Similarly, the conservation of energy for the other liquid subvolumes is:

$$M_{l2}C_l\frac{dT_{l2}}{dt} = -U_{l2}A_{sl2}(T_{21} - T_{Rl2}) + 2/3\,\dot{m}_{liq}C_l(T_{l1} - T_{l2}) \quad \text{Eq. 9}$$

$$M_{l3}C_l\frac{dT_{l3}}{dt} = -U_{l3}A_{sl3}(T_{l3} - T_{Rl3}) + 1/3\,\dot{m}_{liq}C_l(T_{l2} - T_{l3}) \quad \text{Eq. 10}$$

3.3.10 Heat Transfer

It is assumed here that the gas and liquid do not move appreciably so that convection heat transfer is negligible. The effective heat transfer coefficient between the production fluids and

the rock formation are due to the combined conduction through all the wellbore materials. For the upper gas volume, this is expressed as

$$U_{g2} = \left[\frac{D_{i.tube} ln\left(\frac{D_{o.tube}}{D_{i.tube}}\right)}{2k_{tube}} + \frac{D_{i.tube} ln\left(\frac{D_{o.diesel}}{D_{o.tube}}\right)}{2k_{diesel}} + \frac{D_{i.tube} ln\left(\frac{D_{o.casing}}{D_{o.diesel}}\right)}{2k_{casing}} + \frac{D_{i.tube} ln\left(\frac{D_{o.cement}}{D_{o.casing}}\right)}{2k_{cement}} \right]^{-1}$$

Expressions for the other cross sections are similar.

Note that in this expression for the overall heat transfer coefficient, it is assumed that gelled diesel between the tube and casing remains stationary. If this layer mixes due to convection, then the effective thermal conductivity must be modified accordingly. For now, it is assumed that the gelled diesel does not flow, but the model can be modified to include site-specific changes in the properties of this material.

3.3.11 Thermal Capacity

In the energy equations listed above, the terms for the mass and thermal capacity must include the effects of some of the solid materials with the corresponding fluid volumes. Inspection of the model predictions shows that the gelled diesel is a reasonably good insulator compared to the other materials. Consequently, the tubing closely follows the fluid temperatures and the casing and cement are closer to the rock temperatures. For this reason, the mass and thermal capacity of the tubing are combined with those of the fluids.

$$M_{l1} = L_{l1}\left[A_{x.fluid}\rho_l(T_{l1}) + A_{x.tube}\rho_{tube}\right]$$

Similar expressions can be written for the other liquid and gas subvolumes.

The effective specific heat is obtained by a mass-weighted average of the constituent materials,

$$C_l = \frac{\left[C_{liq}A_{x.fluid}\rho_l(T_{l1}) + C_{tube}A_{x.tube}\rho_{tube}\right]}{A_{x.fluid}\rho_l(T_{l1}) + A_{x.tube}\rho_{tube}}$$

$$C_g = \frac{\left[C_{v.gas}A_{x.fluid}\left(P_g/R_{gas}T_g\right) + C_{tube}A_{x.tube}\rho_{tube}\right]}{\left[A_{x.fluid}\left(P_g/R_{gas}T_g\right) + A_{x.tube}\rho_{tube}\right]}$$

In both these expressions, it is probably sufficient to use the initial pressure and temperature of the liquid and gas to define their respective densities. These expressions for the subvolume mass and the effective specific heats must be modified to include other materials if the thermal analysis shows that the casing and cement are closer to the fluid temperature than the rock temperature.

3.3.12 Model Summary

The numbered equations listed above, Eqs. 1-10, form a set of ten coupled ordinary differential equations. The equations are non-linear and it is not clear that a closed form solution

can be obtained. For the purposes of this analysis, the model equations were coded into a Mathcad sheet.

3.4 Analytical Results

A series of simulations were run to study how various features of the well influence the results. In these examples, the input values (unless otherwise noted) were:

- Gas cap of 20% of the column height between the SCSSV and the wellhead. For the purposes of this modeling work, it has been assumed that sufficient time has elapsed to allow for complete segregation of phases. Background for such an assumption is provided in subsection 3.6 of this report.
- Liquid temperature of 50°C at the time of shut-in.
- Rock temperature profile as shown in Figure 3.5.
- Initial gas cap pressure of 100 bar.
- 500 m of 7-inch (6.184-inch ID) tubing.

3.4.1 Zero-Leakage Behavior

Figure 3.7 shows the pressure decay for a zero-leakage case over the period of four hours. As expected, the pressure in the gas cap falls as the gas temperature cools and the liquid column cools and contracts. The second curve shows the same condition, but with the model feature for liquid shrinkage disabled. Thus, if only the gas cap temperature was known (or estimated), the difference would be on the order of 1 bar/hr. Over the course of four hours, the overall gas cap pressure decreased on the order of 7 bar. Figure 3.8 shows the pressure decay for a non-leak case with various volumes of gas cap. The rate-of-decay is more pronounced for smaller gas caps as there is more impact from the larger liquid column.

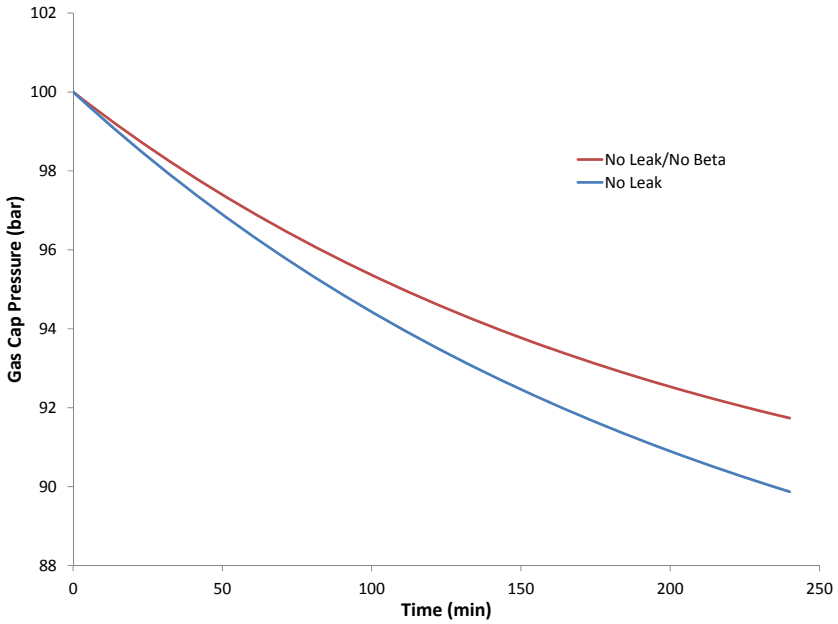

Figure 3.7. Change in Gas Cap Pressure With and Without Accommodation for Changes in Liquid Column (No Thermal Contraction, β)

The figure compares pressure decay over time for a tight flapper. The shallower curve represents a model condition that does not account for contraction of the liquid column.

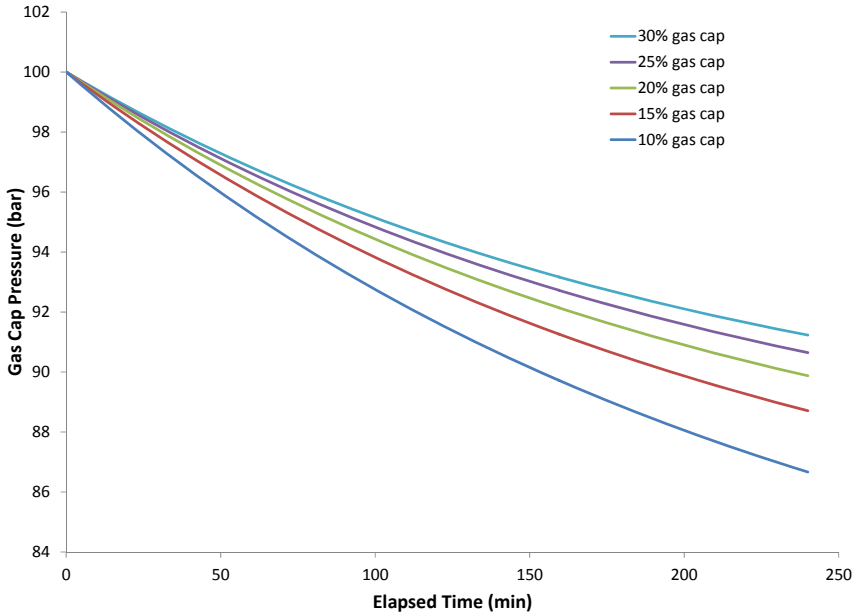

Figure 3.8. Gas Cap Decay Rate for Non-Leak Case of Various Gas Cap Percentages

The greater the initial volume of the gas cap, the less overall pressure decay is observed, as there is less of a liquid column to shrink.

An item of particular interest is the percent difference between model runs that do and do not account for the shrinking of the liquid column. In other words, this deviation is the error that would be incurred by not accounting at all for shrinkage of the column (the latter may be an approach used to simplify calculations). Figure 3.9 plots this difference for three representative gas caps. As the figure shows, there is less than 1% difference in the results for the first few hours for gas caps 20% and larger. This behavior would be expected as the liquid column is shorter and, thus, not accounting for it would have fewer consequences.

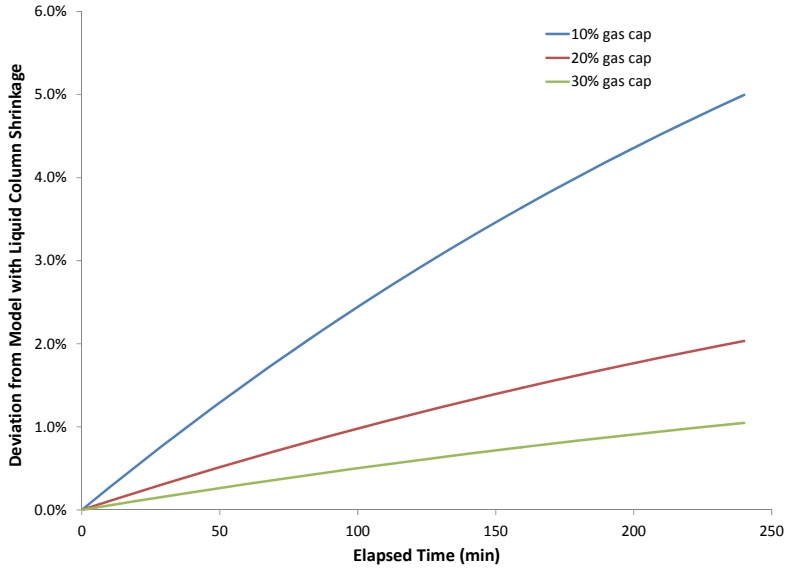

Figure 3.9. Percent Difference in Models That Include and Do Not Include Shrinkage of Liquid Column

The percent difference is equal to the model error that would be introduced by only accounting for cooling of the gas cap.

3.4.2 Leakage Cases

The fundamental motivation for performing these various calculations is to determine if a leak would present a pressure profile distinct enough from the "natural decay" of the system. As a baseline value, 400-cc/min leakage is used as an acceptance criteria in API 14B and serves as a regulatory reference point. Figure 3.10 shows the pressure decays for various leak rates, including 400 cc/min. As the curves show, small leaks are somewhat indistinguishable from the zero-leakage case. However, the 400-cc/min case is markedly different and would likely be distinguished from the zero-leakage case. Note that this plot represents one specific well geometry and boundary condition set.

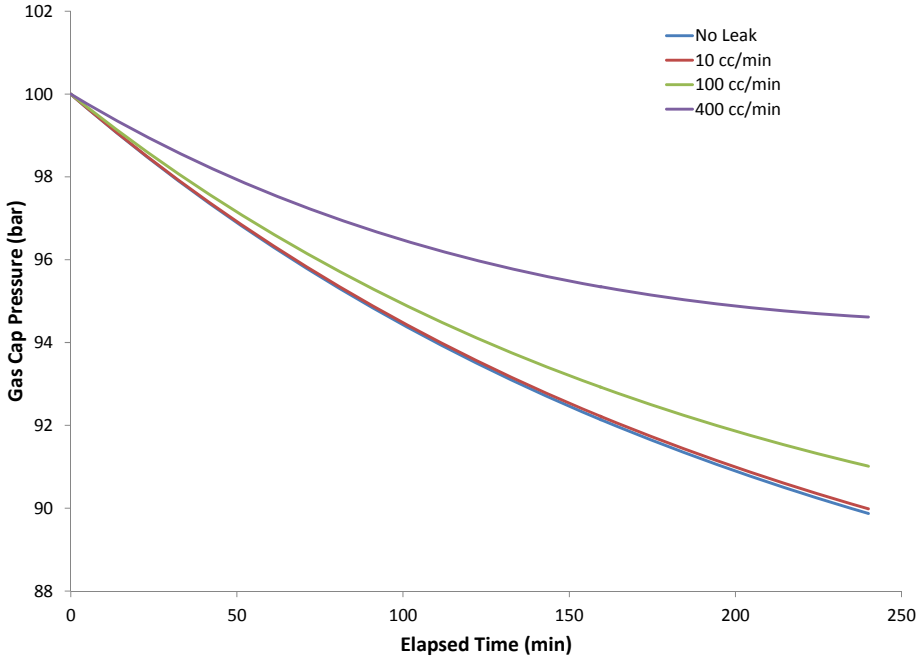

Figure 3.10. Pressure Profile for Various Leak Rates

At the common regulatory allowable rate of 400 cc/min, there is a significant difference in that curve versus the zero-leakage condition. Thus, it is likely that such leaks can be found in a relatively short time period as compared to existing approaches.

A different illustration of this behavior is presented in Figure 3.11. For leaks 100 cc/min and smaller, there is less than a 1% change over most of the monitoring period compared with the zero-leakage case. In some regards, the stark differences in the 400-cc/min rate are promising as they indicate such leaks could be detected using pressure monitoring. However, it is likely that trending and not absolute calculations would be used in the field. In other words, the pressure decay curve from one test would be superimposed on one from the previous test to see if the curve shifted. Figure 3.12 shows the same behavior for leaks of 400 cc/min at different gas caps. As expected, the smaller gas caps (lower gas caps) are more sensitive to leaks.

To determine whether or not a leak would be detected in the field, some context is needed as to how fast such a change in valve performance is observed. If the valve was "bubble tight" on one check and then leaked 400 cc/min on the next, it would be fairly easy to conclude such from the pressure decay curves. However, small changes from test to test might be masked by the uncertainty of the measurement. Thus, several past test results should be used to provide some context to the results.

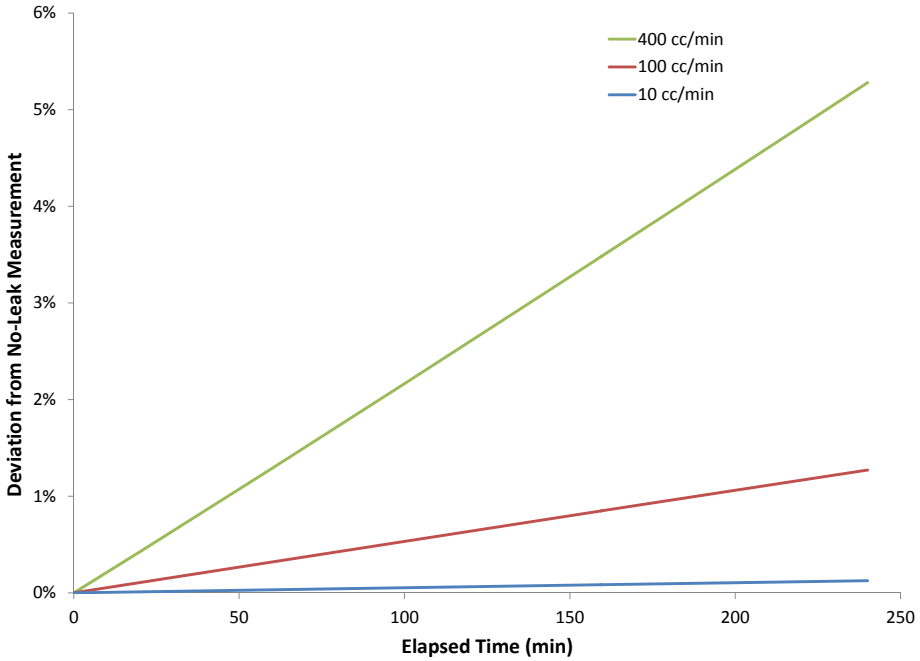

Figure 3.11. Difference in Pressure Decay for Various Leak Rates in Comparison with Zero-Leakage Case

For relatively small leaks (<100 cc/min), there is less than 1% difference with the non-leak case and, thus, such leaks may be within the overall margin of error. Leaks near the regulatory threshold of 400 cc/min are easier to distinguish.

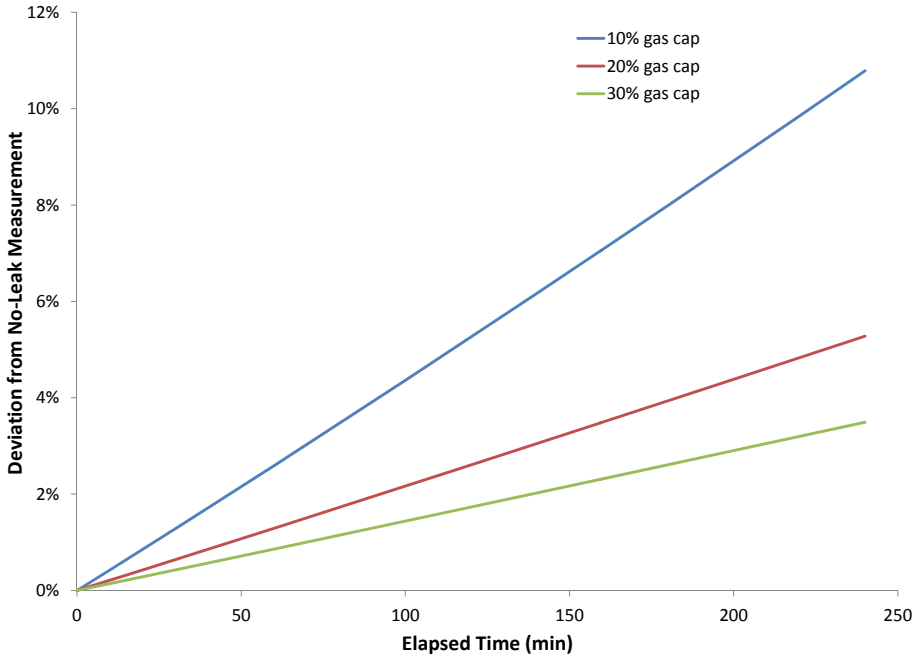

Figure 3.12. Difference in Zero-Leakage versus 400-cc/min Leak for Various GVFs

To some degree, volume leaked can be thought of as gas volume displaced, so smaller gas volumes will be more strongly affected by leaks.

It is conceivable that well conditions would change from time to time and any trending could be adjusted accordingly. Figure 3.13 shows the pressure decay in terms of absolute change

in pressure over the testing window for three different line pressures. When these curves are normalized to the starting pressure, the result is exactly the same. Thus, a particular comparison curve could be used on the same well, even if the pressure conditions changed.

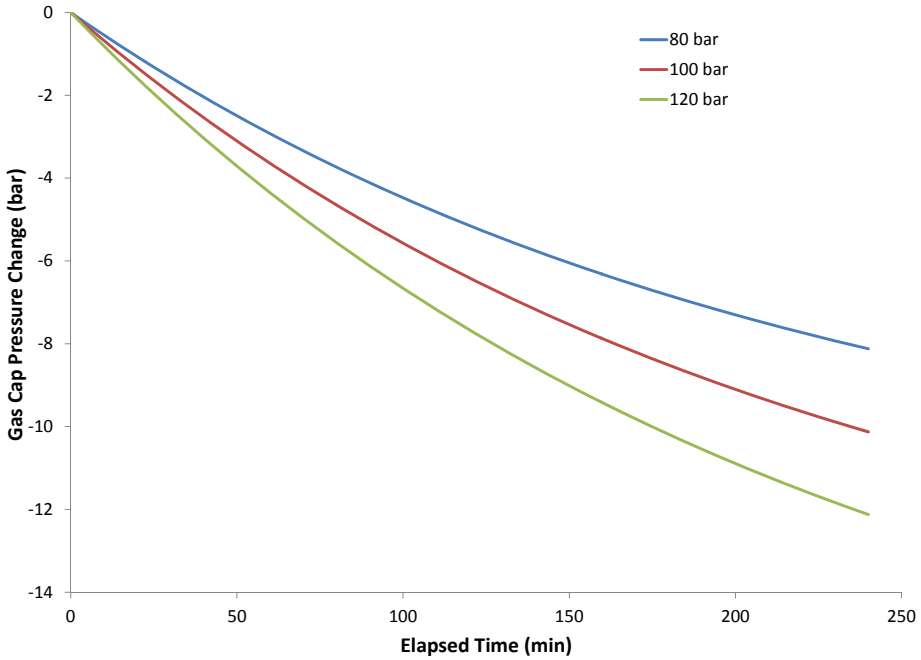

Figure 3.13. Pressure Decay for Various Starting Tubing Pressures
When normalized against initial pressure, these curves sit exactly on top of each other. Thus, once a particular well was modeled, the same trending curve could be used, even if the line pressure changed from test to test.

Well geometries and conditions are complex and often in flux. Instead of trying to use pressure-decay curves to establish absolute leakage rates, an alternative is to utilize relative trending. For a given SCSSV, the pressure decay curve, under similar conditions, should not change. If the decay rate changes significantly, that could signal problems with the valve. Figure 3.14 revisits an earlier chart on the relative difference between decay rates for leak cases and non-leak cases. It should be noted that the deviation in curves increases with time, so lengthening testing intervals would add to the accuracy. However, as noted earlier in this report, reducing the overall testing time is one of the objectives of this work.

There is a certain amount of measurement and modeling uncertainty that accompany any of these curves. In the case of relative measures for the same well, the driving uncertainty will be the pressure measurement. As a baseline case, consider a condition in which the confidence of pressure measurements is 1% of measured range. The intersection of the curves on Figure 3.14 with the dotted line indicates the elapsed test time required to differentiate the leak from the baseline zero-leakage case. For a leak of 400 cc/min, a test time of over 40 minutes would be required, while over one hour would be required for a leak of 300 cc/min. Note that the results shown in Figure 3.14 neglect the effects of uncertainty in the pressure decay of the "zero-leakage" case. If uncertainty bands are assigned to both the leak case and the zero-leakage case, additional time is required to differentiate a leak. For example, if ±1% bands are used for the zero-leakage case and a case with a 400-cc/min leak, Figure 3.15 shows that about 90 minutes is required for the deviation to fall outside of the respective uncertainty bands. This approach is extended to other uncertainty conditions in Figure 3.16. In Figure 3.16, it is seen that about three

hours is required to detect a leak if the uncertainty is ±2%. Over 12 hours is required to differentiate a leak of 100 cc/min for the 2% uncertainty case.

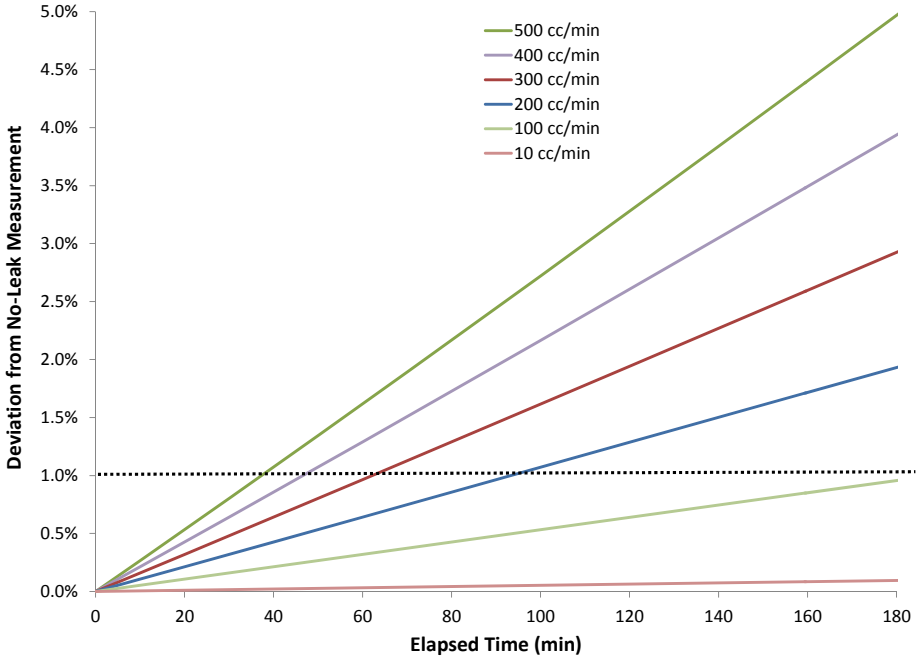

Figure 3.14. Deviation of Pressure Curves for Leak Cases When Compared to Zero-Leakage Cases

As an example, if the overall measurement/modeling uncertainty was 1%, it would require 50 min of monitoring to determine that the valve performance had diminished if the leakage rate was 400 cc/min.

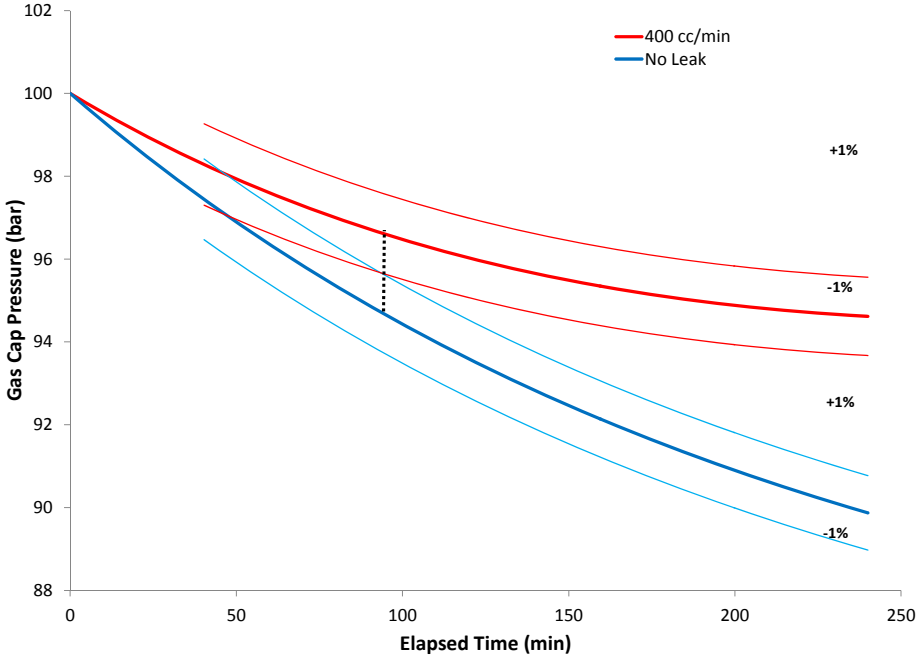

Figure 3.15. Decay Curves for Zero-Leakage and 400-cc/min Leak Cases With 1% Uncertainty Bands

For the given uncertainty bands, 90 min of test time would be required to differentiate the leak from the baseline case.

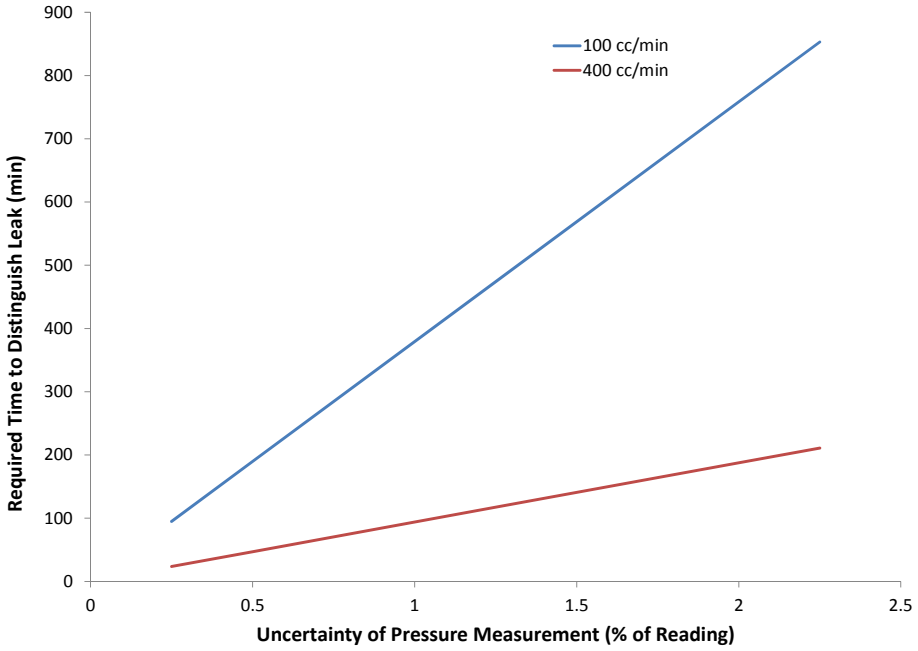

Figure 3.16. Required Time to a Detect Leak as a Function of System Uncertainty
For typical field instrumentation, the required test time could be compressed when compared to current practices.

3.4.3 Wellbore Characteristics

Various modeling runs were performed to determine if the previously-noted results were unique to the specific geometry and fluid properties used or if the model could be applied to a range of well conditions. The initial temperature of the fluids (liquid and gas) was varied from 50°C to 70°C. Figure 3.17 shows how the gas cap pressure was affected when the gas cap percentage was kept at 20% with zero leakage. After four hours, there is approximately a 6-bar difference between the 50°C and 70°C curves. When this same case was modeled for a 10% gas cap percentage, there was an 8-bar difference between the 50°C and 70°C curves (graph not shown). As the gas cap percentage increases, the difference between the 50°C and 70°C curves at four hours decreases.

The temperature of the rock formation was varied from uniform temperatures of 30°C to 50°C. The resulting pressure curves were compared to the original temperature case, as shown in Figure 3.18. The original temperature profile of the rock is linear in two parts. It begins at the mudline at 5°C and increases to 22°C in the first 8 m. The rock profile continues from 22°C to 50°C in the remaining 492 m.

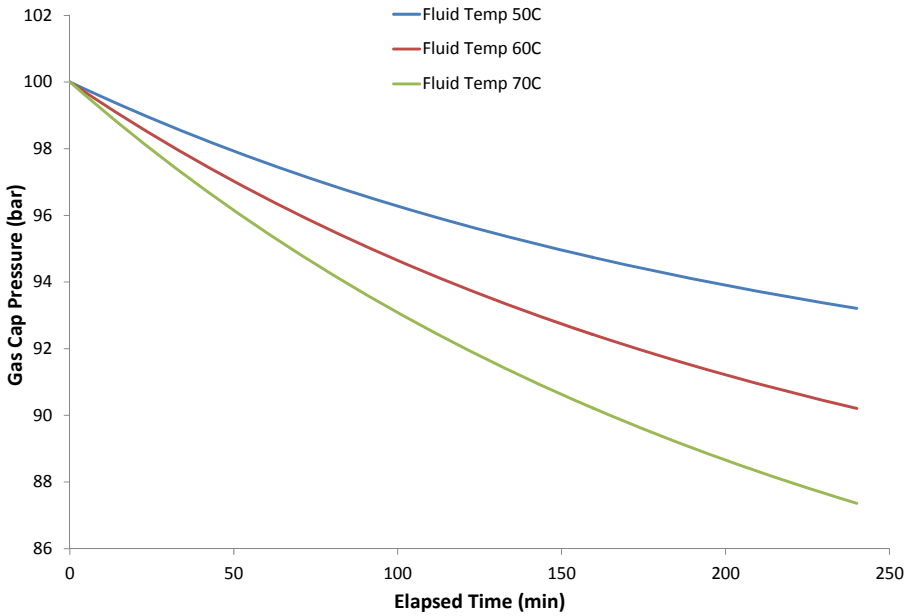

Figure 3.17. Pressure Response for Various Fluid Temperatures with 20% Gas Cap and No Leakage

The difference in temperature from the fluid to the surroundings will affect how much the liquid column grows, (and, therefore, how much the pressure increases on the gas cap) due to thermal expansion.

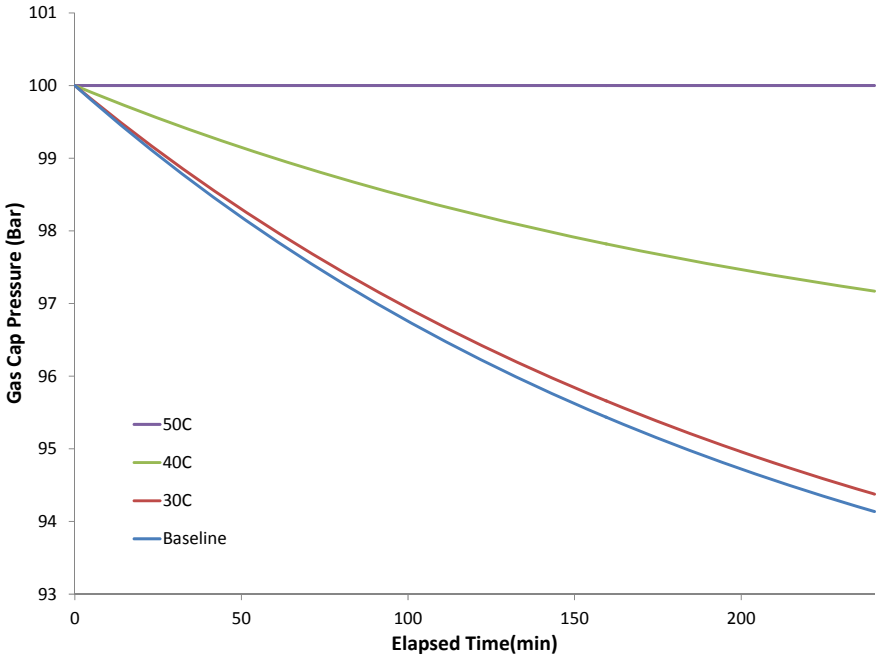

Figure 3.18. Decay Curves for Varied Rock Profile Temperatures with 30% Gas Cap Percentage and Zero Leakage

When the temperatures of the fluid and rock are equal, the gas cap pressure is a straight line whose slope is based on the leak rate. The top line in this graph demonstrates this concept.

The overall heat transfer coefficient between the fluids and the well bore was calculated based on assumed values of the tubing, casing, diesel, and cement. The calculated value of

3.819 watt/m^2·K was varied by ±20% to determine the sensitivity of the system to the heat transfer coefficients. Figure 3.19 shows the gas cap pressure for 30% gas cap and zero leakage. In this case, the ±20% change in the heat transfer coefficient resulted in less than a ±1% change in the gas cap pressure. Thus, the model is not overly dependent upon accurately knowing the thermal properties of the constituent wellbore components.

Additional cases were run to determine the system's response to different gas fractions and leak rates. Figure 3.20 shows the change in the gas cap pressure normalized to an overall heat transfer coefficient of 3.819 watt/m^2·K. Changing the heat transfer coefficient causes a greater variation in gas cap pressure when the gas cap percentage is small (< 30%). Though not shown here, pressure curves were also calculated for a system with these parameters and a 400-cc/min leak rate. If you were to overlay the 400-cc/min deviation curves on top of the 0-cc/min deviation curves in Figure 3.19, they would be nearly identical.

The following illustrations show how various changes in the well geometry affect the gas cap pressure curve. The well geometry changes that were studied in detail are the inside diameter of the tubing, and the length of the shut-in portion of the well. These geometry adjustments were modeled with many of the previous changes to well properties and compared against the original geometry to determine the magnitude of the effect on the gas cap pressure.

When the inside diameter of the tubing was decreased to 5.0 in, the thickness of the annulus was increased to maintain the same outside diameter of the casing. Gas cap pressure curves were compared for these two geometries with a 400-cc/min leak and zero leakage. The resulting pressure curves are shown in Figure 3.21.

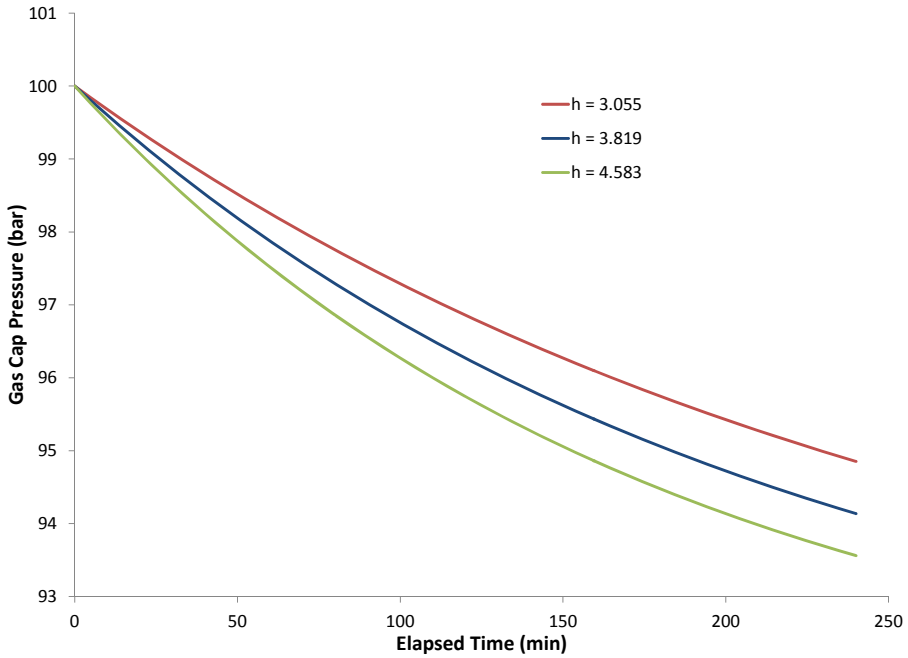

Figure 3.19. Decay Curves for Varied Overall Heat Transfer Coefficients with Zero Leakage
A ±20% change in the heat transfer coefficient caused less than ± 1% change in the gas cap pressure at 30% gas cap percentage.

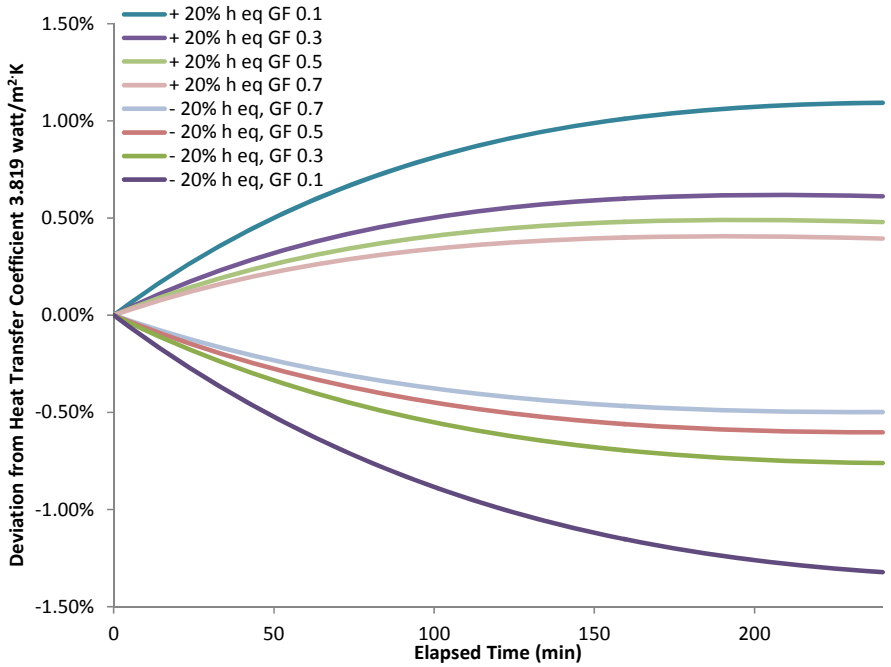

Figure 3.20 Difference in Pressure Decay for Various Overall Heat Transfer Coefficients Normalized to 3.819 watt/m^2·K

As the gas fraction decreases, the change affected by the heat transfer coefficient increases. The larger the liquid column, the greater capacity it has to affect the system. These parameters were also graphed for a 400-cc/min leak rate. The resulting curves matched these zero-leakage results to within 0.09%.

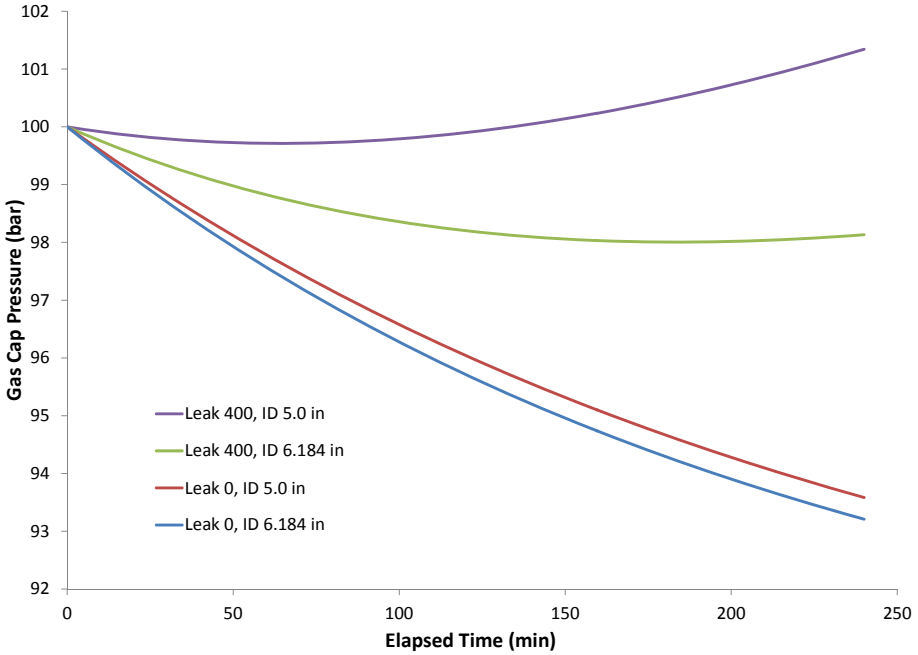

Figure 3.21. Pressure Decay Comparing 400 cc/min Leak and Zero Leakage with Tubing Inside Diameters of 6.184 inches and 5.0 inches

The column of fluid in a well with a leak will rise faster in a smaller diameter. This causes a greater difference in the pressure at four hours in the leak case than that demonstrated by the non-leakage case.

The inside diameter of the tubing was also varied with fluid temperatures of 50°C, 60°C, and 70°C. When the gas cap pressure curves were compared to those of the original well geometry, there was less than 0.75% difference in the pressure at four hours.

To test the sensitivity of the tubing diameter to system temperatures further, the rock formation temperature was changed to a uniform temperature of 40°C. Gas cap pressure curves were computed for gas cap percentages of 10%, 30%, 50%, and 70% in a zero-leakage environment. After four hours, every curve was 0.15% higher than the cases run with a tubing diameter of 6.184 in.

The reduced tubing ID was also modeled with ±20% of the equivalent heat transfer coefficient. When the gas cap pressure curves are normalized against those created by the original geometry, the maximum pressure difference is approximately 0.3%. This value is representative of the 10% gas cap percentage at four hours. For the 30% gas cap percentage case, there was about 0.05% difference in pressures after four hours.

The original length of the tubing between the SCSSV and the shut-off valve is 500 m. The well length was also modeled at 250 m and 1,000 m to determine the effects of this parameter on the gas cap pressure. Figure 3.22 shows the gas cap pressure resulting from these well lengths in a 400-cc/min vs. zero-leakage case.

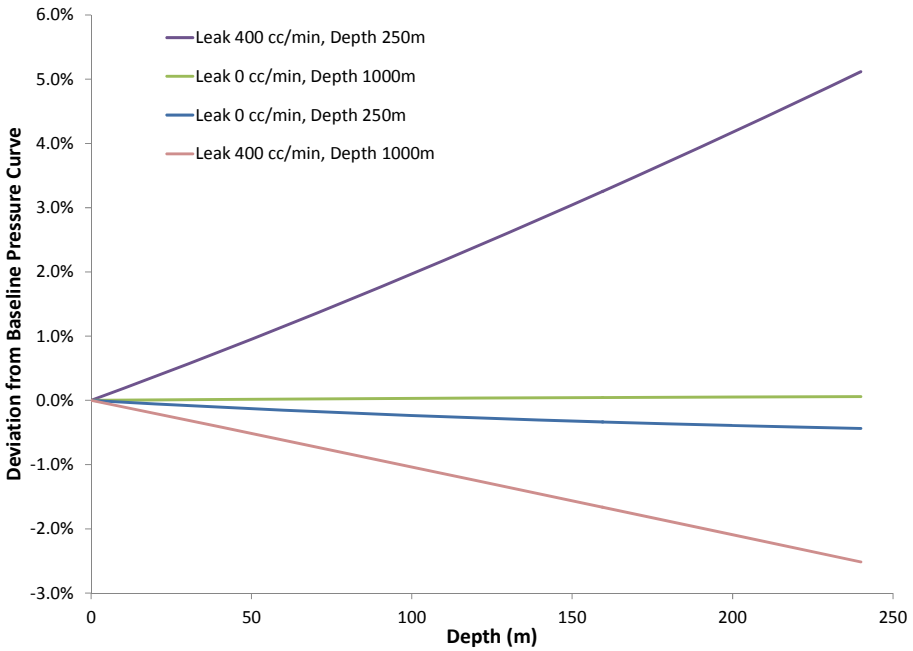

Figure 3.22. Deviation of Pressure Curves for Various Well Lengths and Leak Cases when Compared to the 500-m Depth Model

Introducing a leak into the system causes the greatest gas cap pressure deviation from the original model.

The gas cap pressure curves for the 250-m and 1,000-m cases were normalized against the 500-m case while varying the fluid temperature in the well. The 250-m well gas cap pressure deviated 0.3% after four hours. The 1,000-m well's gas cap pressure deviated 0.05% after four hours.

When a uniform rock temperature is modeled with each well length, the result is identical gas cap pressure curves, however; utilizing a temperature gradient, like that in the original model, causes some deviation. When normalized to the 500-m well, there was a 0.4% deviation in pressure in the 250-m well at four hours. The deviation observed in the 1,000-m well was 0.05% after four hours.

The equivalent heat transfer coefficient was varied at ±20% with each well length. After four hours, the gas cap pressure in the 250-m well was 0.5% higher than the 500-m well. The 1,000-m well gas cap pressure was 0.1% lower than the 500-m well.

It was observed for all cases modeled that the pressure curves from the 250-m well deviated further from the 500-m case than the pressure curves from the 1,000-m well.

The analytical model is a promising approach for assessing wellbore pressure conditions without the need for further instrumentation. This model would allow for relative trending of pressure data, as well as the ability to predict the amount of test time required for a specific set of conditions. One of the key findings of this work is that temperature effects cannot be ignored or the resulting pressure curves will not have the context for proper evaluation.

3.5 Real Gas Effects

Wellbore pressure can be in excess of 100 bar. Under these conditions, there are significant effects of pressure and gas composition that will cause the gas compressibility factor to be other than Z=1. The ideal gas assumption was allowed to stand for the sake of simplicity in order to demonstrate the usage of the model as described in subsection 3.4. The impact of this assumption is addressed here.

The industry standard for approximating the thermodynamic properties of hydrocarbon gases is the so-called AGA-8 method (Starling et al., 1992). This methodology is far too complicated for use in the model described here; instead, the simpler methodology described by Estele-Uribe and Jaramillo (2005) was adopted for this analysis. In this method, a virial equation of state is used to compute the compressibility factor as a function of gas composition (incorporated via mixture relations to define pseudo-critical properties), temperature, and pressure. The gas compressibility was incorporated into the thermal model above by modifying Eq. 4 to account for Z being a function of temperature and pressure. It is still assumed that gas composition is constant. The software was modified accordingly.

The non-ideal gas form of the model and the ideal gas form of the model were applied to the baseline case defined in subsection 3.4. For the sake of this example calculation, the gas was assumed to be pure methane.

The predictions of these two approaches for the gas pressure and the temperature of the upper gas subvolume are compared in Figure 3.23. In this graph, a positive deviation indicates that the non-ideal mode prediction is greater than the ideal gas prediction. First it is seen that the prediction for the gas temperature using the ideal gas model is in very close agreement with the non-ideal gas model. The other model parameters (temperatures, volumes) show even closer agreement and have not been included in this graph.

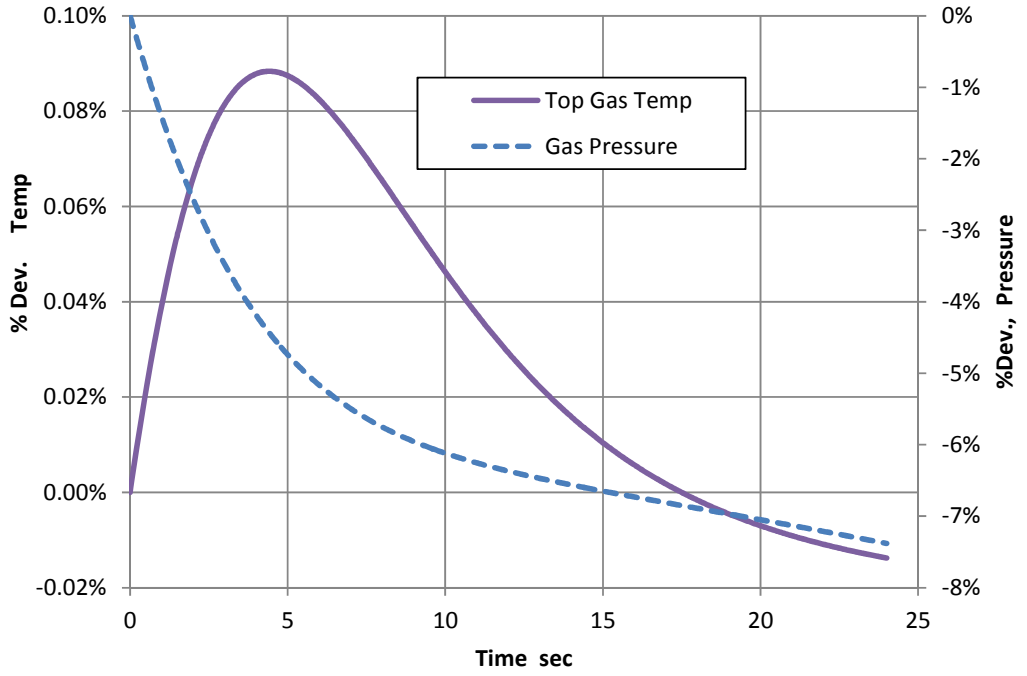

Figure 3.23. Comparison of the Ideal Gas and Non-Ideal Gas Forms of the Thermal Model for the Baseline Case

The other fluid temperatures showed even better agreement that the upper gas subvolume temperature shown here.

3.6 Phase Separation

Once the well is shut in for a leak test, the gas and liquid phases in the production fluid immediately begin to separate in the well. The time it takes for the two phases to completely separate is governed by the rate the gas can come out of the solution, form bubbles, and rise to the gas cap. Complete separation time ranges from a matter of minutes to several hours and depends on the conditions of the well just prior to shut in. Field experience suggests that a shut-in well separates very quickly. Xiao et al. reported that in a typical well, the liquids and gasses separate in approximately one hour (Xiao, 1995). However, these reports are based on pressure changes at the gas cap, as opposed to fluid samples from the well. Therefore, it is useful to develop a simple model to estimate the total time required to fully separate the liquid and gas phases in a shut-in well.

The properties that can affect separation time include:

- Bubble size at shut-in
- Gas-to-liquid ratio
- Shut-in pressure
- Fluid temperature
- Interfacial tension of the gas and liquid phase
- Density of the gas and liquid phase
- Viscosity of the gas and liquid phase
- Diameter of the pipe
- Length of the well

A model that accurately predicts the separation time of the liquid and gas phases in a well would take all of the above factors into account. In a flowing well, gas bubbles in the production fluid are continuously being sheared by liquid phase in the well. This shearing governs the maximum stable bubble size in a flowing fluid, where higher liquid flow rates produce smaller bubbles. Once a well is shut in, these bubbles begin to coalesce and grow until they reach their maximum stable size in a stagnant fluid. For this model, it is assumed that the bubbles coalesce quickly into their maximum stable size shortly after the well has been shut in and that the coalescing time will be neglected. Also, it is assumed that liquid holdup is such that phase change is not occurring.

The separation time is governed by the maximum stable bubble size in the stagnant well. Each bubble will reach a terminal velocity as it rises to the gas cap. In general, the larger the bubble size, the higher the bubble terminal velocity, causing a shortened separation time. However, well conditions such as pressure and temperature can cause exceptions to this generality.

In order to estimate the separation time in the well, the following assumptions were made:

1. All gas bubbles reach their maximum stable diameter quickly after the well is shut in. Therefore, the coalescence time is negligible.
2. Each bubble rises independently and its rise velocity is not affected by other bubbles rising near it.
3. The separation time of the well is said to be equal to the time it takes a bubble from the bottom of the well to rise to the bottom of the final gas cap. This location is determined by applying the gas volume fraction to the total depth of the well. This implies that the total volume of liquid and gas in the well remains constant during separation and that no mass enters or exits the well during shut in.
4. The continuous liquid phase is comprised of 100% oil and no solids are present in the well.

The nomenclature for this model is defined below.

Variables

A_r	variable for determining the terminal velocity of the bubble
F	variable for determining the terminal velocity of the bubble
D	inner diameter of the process tubing
d_{max}	maximum stable bubble diameter in a stagnant well
E_o	Eövtös number
g	gravitational constant
GVF	gas volume fraction
k	variable for determining the terminal velocity of the bubble
L_{well}	depth of the well
m	variable for determining the terminal velocity of the bubble
M	Morton number
R	buoyancy Reynolds number
R_e	Reynolds number
U_t	terminal velocity of a bubble in stagnant media

$U_{t,w}$ terminal velocity of a bubble in stagnant media with wall effects considered
t_s separation time of the well
μ viscosity
r density
Dr differential between the density of the continuous and dispersed fluid
s interfacial surface tension

Subscripts

c property of the continuous fluid phase
d property of the dispersed fluid phase

Previous studies have developed theoretical and empirical models to predict the maximum stable bubble diameter in a stagnant fluid. Grace et al. predicted the maximum stable bubble diameter by defining an applicable range of disturbance wavelengths that would cause a bubble in stagnant fluid to become unstable and break up (Grace). However, the resulting method requires an interactive solution method to determine the maximum stable bubble size, making it impractical for many applications. Kitscha et al. recognized the need for a practical breakup correlation for rising bubbles in stagnant media and defines the maximum stable bubble diameter of a rising bubble in a stagnant liquid as:

$$d_{max} = 27.07\left(\frac{\sigma}{g\,\Delta\rho}\right)^{\frac{1}{2}}\left[1+\left(\frac{{\mu_c}^2}{\rho_c\left(\frac{\sigma}{g\,\Delta\rho}\right)^{\frac{1}{2}}}\right)^{\frac{1}{2}}\right]^{0.83}$$

Based on this equation, Kitscha found an average error of 13.9% between published experimental data and predicted maximum bubble diameters. Comparing this error to Grace's published average error of 28%, the Kitscha model was chosen for this model.

Since the maximum stable bubble diameter is dependent on the difference in density between the continuous and dispersed phases, the hydrostatic pressure on the bubble from the liquid column affects the diameter. A larger density difference creates bubbles of decreasing size. For example, the maximum stable bubble diameter can be 25% larger at the bottom of a 4,500-m well, as opposed to just below the gas cap. However, even though a bubble can have a larger stable diameter at the base of the well, the rise velocity may be slower than the smaller bubble higher in the well. At the base of the well, the smaller density difference between the continuous and dispersed phases retards the buoyancy effects of the bubble, reducing the bubble rise velocity.

Once the maximum stable bubble size is calculated, the well separation time can be estimated as the time it takes a single bubble to travel from the bottom of the well to the bottom of the final gas cap. The terminal velocity of a bubble rising in stagnant fluid depends on the fluid properties of the continuous and dispersed phases in the well (μ_c, μ_d, r_c, r_d, and s) and the inner diameter of the well. Two dimensionless parameters that characterize bubble shape and terminal velocity are the Morton number, *M*, and the Eötvös number, E_o. The Morton Number

gives an indication to the strength of the viscous effects and the inertial effects on the bubble and is defined as:

$$M = \frac{g\,\mu_c{}^4\,\Delta\rho}{\rho_c{}^2\sigma^3}$$

A higher Morton number indicates that the viscous effects play a larger role in bubble flow characteristics.

The Eötvös number shows the relationship between the gravitational effects and the surface effects on the bubble and is defined as,

$$E_o = \frac{g\,d_{max}{}^2\,\Delta\rho}{\sigma}$$

Figure 3.24 shows the dependence of the rise velocity, expressed as the Reynolds number, on the Morton and Eötvös numbers.

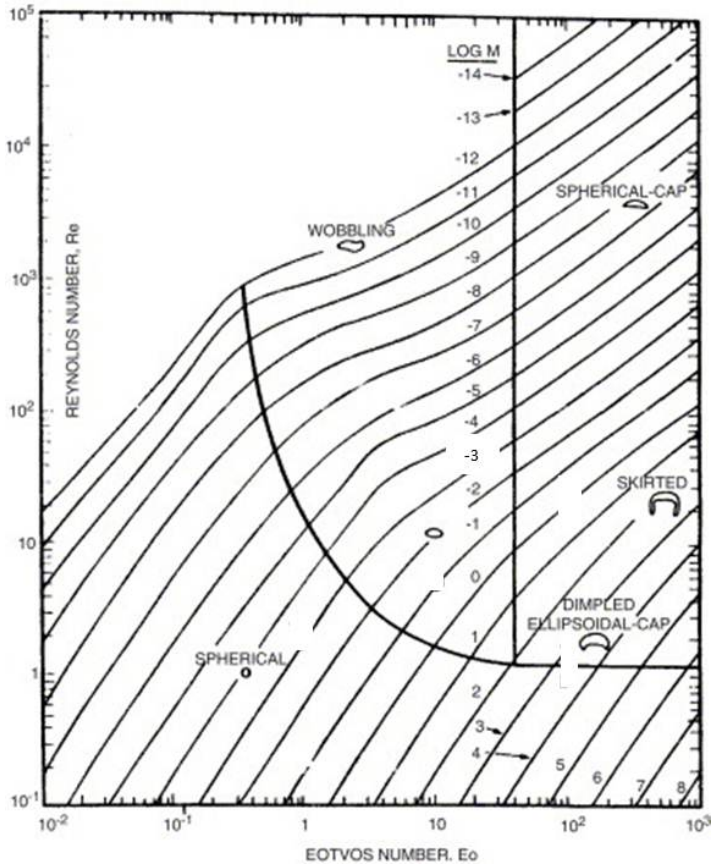

Figure 3.24. The Effects of the *M* and E_o on the Terminal Velocity of a Bubble
The figure also shows the most likely bubble geometry for the conditions (Clift et al.)

Bubbles rising through a semi-infinite media have been extensively investigated. A common correlation for semi-spherical bubbles rising in infinite media was outlined by Clift et al. and Grace et al. as:

$$U_t = Re\,\frac{\mu_c}{\rho_c d_{max}}$$

where

$$Re = \frac{1}{2}\left[(F^2 + 2A)^{\frac{1}{2}} - F\right] \qquad \text{for M} > 0.01$$

$$Re = 0.70 A_r^{\frac{1}{2}} \qquad \text{For M} < 0.01 \text{ and } E_o \geq 40$$

and

$$A_r = \frac{E_o^{\frac{3}{2}}}{M^{\frac{1}{2}}} \qquad\qquad F = \frac{3\left(2 + 3\frac{\mu_d}{\mu_c}\right)}{1 + \frac{\mu_d}{\mu_c}}$$

A bubble rising in a confined space, such as a pipe, will travel slower than a bubble in a semi-infinite extent. Therefore, the rise velocity calculated using the above equations must be corrected to account for the effect of wall proximity. As the ratio of the maximum bubble diameter to the inner diameter of the well bore increases to $d_{max}/D \leq 0.6$, the terminal velocity in a confined extent can be estimated by (Wallis):

$$U_{t,w} = U_t\left(1 + 1.6\frac{d_{max}}{D}\right)^{-1}$$

Above a diameter ratio of 0.6, the bubbles act as Taylor bubbles and are mostly dependent on the geometry of the tube (Wallis). Figure 3.25 shows flow patterns in vertical multiphase wells. Stagnant separation patterns most closely mimic "bubble" or "slug" flow. Slug flow contains large Taylor bubbles and some smaller bubbles. For this project, we will consider the bubble pattern to be comprised entirely of Taylor bubbles or entirely of small bubbles.

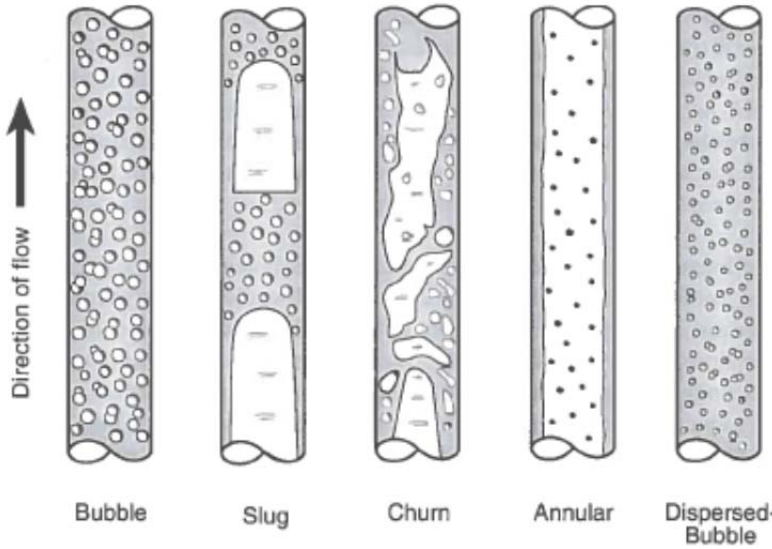

Figure 3.25. Flow Patterns in Vertical Flowing Pipes
Stagnant separation flow would most likely mimic bubble or slug flow (Shoham).

The correlations for rise velocity of Taylor bubbles have been well vetted. Most Taylor bubble rise velocity correlations depend entirely on gravitational forces and pipe geometry, and carry no dependence on fluid properties. Further, many of these correlations were developed in air and water systems and are empirical in nature. Wallis proposed a bubble rise correlation that

takes the fluid properties, such as the viscosity of the continuous phase and the interfacial tension, into account, where the velocity is found by:

$$U_t = k\left[\frac{Dg(\rho_c - \rho_d)}{\rho_c}\right]^{\frac{1}{2}}$$

where

$$k = 0.345\left(1 - e^{\frac{-0.01R}{0.345}}\right)\left(1 - e^{\frac{3.37 - E_o}{m}}\right)$$

and R is the buoyancy Reynolds number:

$$R = \frac{\left[\frac{Dg(\rho_c - \rho_d)}{\rho_c}\right]^{\frac{1}{2}}}{\mu}$$

m is a function of R and is assigned the following values:

R> 250:	$m = 10$,
18 < R < 250:	$m = 69R^{-0.35}$,
R < 18:	$m = 25$.

The Wallis correlation accounts for the viscous effects through the buoyancy Reynolds number. However, the rise velocity is a weak function of viscosity, as seen from the equation for k.

Once the bubble rise velocity has been determined, the separation time is estimated as the time it takes a single bubble to rise from the bottom of the well to the bottom of the final gas cap. Therefore, separation time can be calculated using the well gas volume fraction, *GVF*, according to:

$$t_s = \frac{L_{well}\,(1 - GVF)}{U_t}$$

Table 3.2 shows the approximate separation time for a variety of tubing diameters and oil viscosities. The following fluid properties are held constant:

Upstream Pressure: 100 bar
Average well temperature: 323 K
Interfacial surface tension between the liquid and dispersed phases, σ: 11 dyne/cm
The interfacial tension is based on a crude oil with 30 ºAPI and 100 bar (Brill)
Density of the continuous phase, ρ_c: 850 kg/m^3
Density of the dispersed phase at atmospheric conditions, ρ_d: 0.668 kg/m^3
The density of the dispersed phase is adjusted based on the pressure in the well.

The separation time estimates take wall proximity effects, viscosity effects, and bubble origination depth into account.

Based on this simple model, it is recommended that the operator wait approximately 30-40 minutes per 500 m of well depth. In general, larger diameter wells separate faster than smaller diameter wells. Also, it is interesting to note that the viscosity plays a relatively important role in the bubble rise velocity. Lower viscosity fluids (1 cP and 10 cP) are unable to maintain large stable bubble diameters. However, they offer less resistance to the bubbles

traveling to the surface. Higher viscosity fluids (100 cP and 1,000 cP) promote large stable bubbles, while very large viscosity fluids (1,000 cP) act to slow the rise velocity of the bubbles.

Table 3.2. Rise Velocity and Time for a Single Bubble to Travel from 500 m Below the Gas Cap to the Bottom of the Final Gas Cap

Values in bold were calculated as 100% Taylor bubble flow. All others were calculated as smaller bubbles ($d_{max}/D < 0.6$).

Rise Velocity (m/s)	Oil Viscosity (cP)			
Tubing ID (in.)	1	10	100	1,000
2.5	0.206	0.207	**0.258**	**0.178**
3	0.223	0.224	**0.283**	**0.222**
3.5	0.237	0.239	**0.305**	**0.261**
4	0.248	0.251	0.261	**0.296**
4.5	0.258	0.261	0.276	**0.327**
5	0.267	0.270	0.289	**0.352**
5.5	0.274	0.278	0.300	**0.374**
6.184	0.283	0.287	0.314	**0.402**

Rise Time (minutes per 500 m)	Oil Viscosity (cP)			
Tubing ID (in.)	1	10	100	1,000
2.5	40.5	40.3	**32.3**	**46.8**
3	37.4	37.2	**29.4**	**37.5**
3.5	35.2	34.9	**27.3**	**31.9**
4	33.6	33.2	31.9	**28.2**
4.5	32.3	31.9	30.2	**25.5**
5	31.2	30.9	28.8	**23.7**
5.5	30.4	30.0	27.8	**22.3**
6.184	29.4	29.0	26.5	**20.7**

As previously mentioned, the pressure and temperature of the bubble formation location in the well determine its maximum stable size and rise velocity. The velocity changes by 11% to 15%, based on the viscosity of the fluid and depth of the well. Table 3.3 shows this effect on the rise velocity and time required to rise 500 m in the well based on the bubble location. Figure 3.26 shows the total separation time based on the bubble velocity outlined in Table 3.3.

Table 3.3. Rise Velocity and Time for a Single Bubble to Travel 500 m Upward, Based on its Location in the Well

Values in bold were calculated as 100% Taylor bubble flow. All others were calculated as smaller bubbles ($d_{max}/D < 0.6$).

Rise Velocity (m/s)	Oil Viscosity (cP) 6.184" pipe			
Height of liquid column (m)	1	10	100	1,000
500	0.283	0.287	0.314	**0.402**
1000	0.279	0.283	0.309	**0.394**
1500	0.275	0.280	0.304	**0.387**
2000	0.272	0.276	0.299	**0.380**
2500	0.268	0.272	0.294	**0.372**
3000	0.264	0.267	0.289	**0.365**
3500	0.259	0.263	0.284	**0.357**
4000	0.255	0.259	0.278	**0.349**
4500	0.251	0.254	0.273	**0.340**

Rise Time (minutes per 500 m)	Oil Viscosity (cP) 6.184" pipe			
Height of liquid column (m)	1	10	100	1,000
500	29.4	29.0	26.5	**20.7**
1000	29.9	29.4	27.0	**21.2**
1500	30.3	29.8	27.4	**21.5**
2000	30.6	30.2	27.9	**21.9**
2500	31.1	30.6	28.3	**22.4**
3000	31.6	31.2	28.8	**22.8**
3500	32.2	31.7	29.3	**23.3**
4000	32.7	32.2	30.0	**23.9**
4500	33.2	32.8	30.5	**24.5**

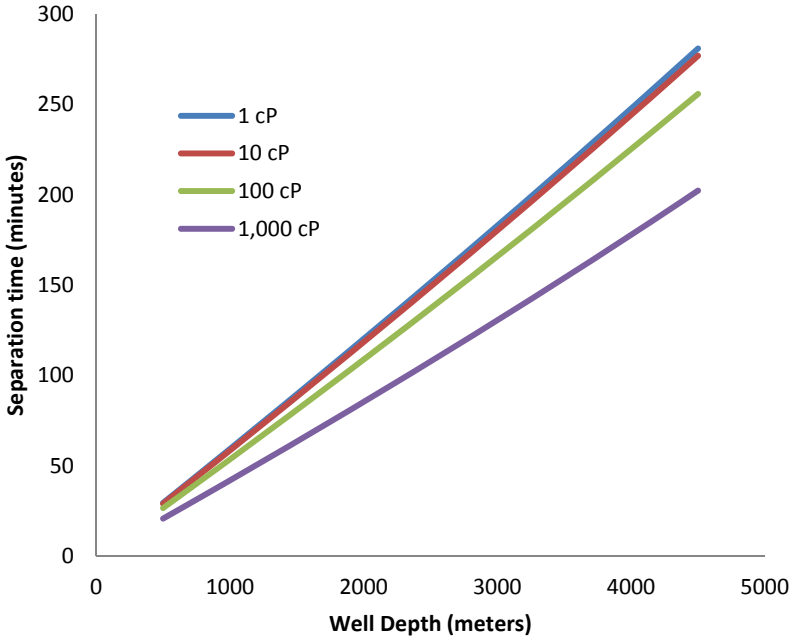

Figure 3.26. Total Separation Time in Minutes as a Function of Well Depth at Four Viscosities
The chart assumes that the bubbles travel at a constant velocity in each 500-m section of the well and change velocity as they travel toward the wellhead.

A less conservative method to estimate well separation time is to assume that all of the available gas in the system coalesces to a Taylor bubble immediately after shut in. This would cause rapid separation, especially in less viscous wells (where μ_c < 100 cP). Field experience tells us that the pressure in the gas cap rises during well separation as the gas comes out of the solution, forms bubbles, and rises to the gas cap. Field experience has also shown that the largest gas cap pressure change occurs shortly after shut in (within the first hour). Therefore, this less-conservative well separation time estimate may be practical for valve leakage testing, since it will estimate the time it takes the majority of the gas from the well to rise to the surface. The smaller bubbles, which move slower, will have a smaller effect on the gas cap pressure increase.

Table 3.4 shows the rise velocity and separation time for the first 500 m of a well, assuming that the bubbles in the well form only Taylor bubbles. The Taylor bubble rise velocity was calculated using the equation from Wallis. This equation, as mentioned previously, has a weak dependence on viscosity. Therefore, the change in rise velocity based on viscosity is insignificant in the 1-cP, 10-cP, and 100-cP well separation times. However, at 1,000 cP, the rise velocity is moderately slower than the lower viscosities.

Based on this less conservative approach, it is recommended that the operator wait approximately 20 - 30 minutes per 500 m of well depth, where larger diameter tubes require less separation time.

Table 3.4 Rise Velocity and Time for a Single Bubble to Travel 500 m to the Gas Cap, Based on the Tubing Inner Diameter

All bubbles are assumed to be Taylor bubbles where the maximum diameter is nearly the inner diameter of the tubing.

Rise Velocity (m/s)	Oil Viscosity (cP)			
Tubing ID (in.)	1	10	100	1000
2.5	0.262	0.262	0.262	0.182
3	0.287	0.287	0.287	0.227
3.5	0.310	0.310	0.310	0.267
4	0.332	0.332	0.332	0.302
4.5	0.352	0.352	0.352	0.332
5	0.371	0.371	0.371	0.358
5.5	0.389	0.389	0.389	0.381
6.184	0.413	0.413	0.413	0.408

Rise Time (minutes per 500 m)	Oil Viscosity (cP)			
Tubing ID (in.)	1	10	100	1000
2.5	31.8	31.8	31.8	45.8
3	29.0	29.0	29.0	36.7
3.5	26.9	26.9	26.9	31.2
4	25.1	25.1	25.1	27.6
4.5	23.7	23.7	23.7	25.1
5	22.5	22.5	22.5	23.3
5.5	21.4	21.4	21.4	21.9
6.184	20.2	20.2	20.2	20.4

3.7 Revisiting of PMV

While the focus of the project was primarily on the SCSSV, a similar modeling approach was utilized for PMVs. Since the PMV and underwater safety valves (USVs) have similar testing requirements, industry practices for USVs were utilized as a baseline.

3.7.1 Overview

The current version of API 14H provides an example problem of how to interpret results from a pressure buildup test. This example utilizes a large downstream volume with a liquid-gas mixture. It assumes only gas leaks by the USV. The work outlined in this section also assumes that no liquid is leaking past the valve, though some of the downstream cavity may be occupied by liquid. It is assumed that the liquid hold-up is such that no phase change occurs during this testing.

All things considered, the existing example provides a relatively straightforward means of implementation. There are two aspects of this example, however, that warrant further evaluation:

1. The calculation assumes a fixed leak rate. What is not stated, but had to have been assumed, is that the leak is in choked flow. In other words, the upstream pressure is significantly higher than the downstream pressure and that changes in the downstream pressure are not affecting the velocity through the leak path. However, such an arrangement will not always be present in such tests. In tests with large differentials, the upstream pressure will reduce to the point where choked flow will no longer exist and the downstream pressure will then affect the flow rate. In tests with small differentials (likely due to inability to further reduce downstream pressure), the leak may never be in choked flow.
2. The calculation assumes a constant temperature. For a USV on a subsea tree, it is possible that significant thermal changes may occur and such changes would impact the results.

To study alternative approaches, and to assess the relative error in non-choked flow and a changing thermal environment, both a numerical and an analytical model were developed.

3.7.2 Numerical Model

A numerical model was developed to capture the thermal effects that may be present during such pressure buildup testing. It was assumed that the entire downstream cavity is filled with gas and that the leakage through the valve is gas phase. The following calculations assume ideal gas with a constant specific heat.

The change in mass in the downstream cavity is equal to the mass flow through the valve:

$$\frac{dM_2}{dt} = \dot{m}_L$$

where

M_2 = mass of gas in downstream cavity
$\dot{m}_L$ = leakage flow rate

If a control volume is drawn around the valve and the upstream and downstream cavities, the conservation of energy can be expressed as:

$$\frac{dE_2}{dt} = \dot{Q} - \dot{W} + \dot{m}_{in}h_{in} - \dot{m}_{out}h_{out}$$

where

E_2 = energy in trapped cavity
$\dot{Q}$ = heat transfer rate to gas
$\dot{W}$ = work done by gas
$\dot{m}_{in}$ = mass flow rate into cavity
h_{in} = enthalpy of inlet gas
$\dot{m}_{out}$ = mass flow rate out of cavity
h_{out} = enthalpy of outlet gas

Since no work is done by the gas and no gas flows out of the cavity, the previous equation can be expressed as:

$$\frac{dE_2}{dt} = M_2 C_v \left(\frac{dT}{dt}\right) + \dot{m}e_2 = \dot{Q} + \dot{m}_{in}h_{in}$$

where C_p is the specific heat (constant pressure) of the gas and e_2 is the internal energy of the gas.

From the ideal gas law, the time-rate-of-change of the temperature of the gas can be written as:

$$\frac{dT}{dt} = \frac{V}{MR_{gas}}\left(\frac{dP}{dt}\right) - \frac{PV}{MR_{gas}}\dot{m}$$

Substituting this expression into the previously-derived energy equation and then rearranging yields:

$$\frac{dP_2}{dt} = \dot{Q}\frac{R_{gas}}{C_v V_2} + \frac{R_{gas}kT_1}{V_2}\dot{m}$$

where C_v is the specific heat (constant volume) of the gas and k is the ratio of specific heats. This equation can be integrated numerically to calculate the pressure in the downstream cavity at a given time. The mass flow rate, however, can vary, depending on whether or not choked flow is present. The flow of gas through a leaking valve can be modeled as an orifice with a flow area much smaller than the inlet pipe. The non-choked compressible flow through an orifice is given as:

$$\dot{m} = KAY\sqrt{2\rho_1(P_1 - P_2)}$$

For choked flow, this equation would be

$$\dot{m} = KAY\sqrt{2\rho_1 P_1(1 - x_c)}$$

where

$$Y = 1 - (0.41 + 0.35\beta^4)\left(\frac{P_1 - P_2}{\gamma P_1}\right)$$

The critical pressure ratio is:

$$x_c = \left(\frac{2}{k+1}\right)^{k/k-1}$$

For an assumed value of k = 1.293 for methane, x_c is 0.547.

β is the ratio of the orifice to the pipe diameter. The value of K, however, is unknown. However, for purposes of the application of this model to leakage through a valve, the "starting" leak rate can be defined to be the maximum allowed leak rate. In that scenario, the equations can be re-written to be, for initial non-choked flow:

$$\dot{m} = \frac{\dot{m}_i}{Y_1\sqrt{2\rho_1(P_1 - P_2)}} Y\sqrt{2\rho_1(P_1 - P_2)}$$

and initial choked flow:

$$\dot{m} = \frac{\dot{m}_i}{Y_{choked}\sqrt{2\rho_1 P_1(1 - x_c)}} Y\sqrt{2\rho_1(P_1 - P_2)}$$

Both of these equations assume current flow is non-choked. These equations can then be inserted into the numerical integration.

3.7.3 Analytical Model

API 14H and the existing regulations in the CFR utilize a fixed volumetric leak rate (e.g., scfm) over an undefined test interval. Inherently, this approach assumes that the leak rate is not changing. For such a scenario to manifest, two conditions must be met:

1. The flow through the leak path is in choked flow.
2. The upstream volume is sufficiently large enough that its pressure does not decrease during the test duration, even as it loses gas to the downstream side of the valve. The reason for this stipulation is to ensure constant mass flow through the leakage path.

Thus, it would be prudent for an operator to ensure that the testing interval does not extend into a non-choked regime. Assuming ideal gas (compressibility factor, Z = 0) with no heat transfer to the seawater, the time for choked flow can be represented as:

$$t_c = (x_c - x)\frac{P_1 V_2}{k R_{gas} T \dot{m}}$$

where:

t_c = time at choked flow transitions to non-choked flow
x_c = critical pressure ratio
x = pressure ratio (P_2/P_1) at start of test
P_1 = upstream pressure
V_2 = downstream volume
k = ratio of specific heats
R_{gas} = gas constant
T = temperature
$\dot{m}$ = leakage flow rate

This equation came from taking

$$\frac{dP_2}{dt} = \dot{Q}\frac{R_{gas}}{C_v V_2} + \frac{R_{gas} k T_1}{V_2}\dot{m}$$

and setting the heat transfer to zero before integrating. The resulting equation for choked flow is:

$$P_2 = P_{2i} + \frac{R_{gas} k T_1}{V_2}\dot{m}$$

where P_{2i} is the initial downstream cavity pressure. A set of calculations was performed to study the relative importance of pressure and volume. In all calculations, methane was utilized with a gas constant of 518 J/(kg-K). An allowed leakage rate of 15 scfm was used with a density at standard conditions of 0.667 kg/m3.

Two volume scenarios were used:

- Small (perhaps within the tree) – 10 feet of 5" ID pipe = 0.039 m^3
- Large (discharge into flowline) – 1,000 feet of 3" ID pipe = 1.39 m^3

Table 3.5 provides a summary of these sample calculations. For large volumes, it will not be a problem to remain in choked flow. For smaller volumes, the time is critical relative to the actual volume. It would be interesting to get information from manufacturers of subsea trees as to the typical "smallest" volumes available.

Table 3.5. Calculated Time to Reach Non-Choked Flow

PARAMETER	UNIT	CASE 1	CASE 2	CASE 3	CASE 4	CASE 5	CASE 6
Upstream Pressure (P_1)	bar	150	150	100	150	150	100
Initial Downstream Pressure (P_2)	bar	50	1	5	50	1	5
Volume (V_2)	m^3	0.039	0.039	.039	1.39	1.39	1.39
Temperature (T)	K	323	323	323	323	323	323
Time for choked flow	**min**	**2**	**5**	**3**	**73**	**183**	**112**

The monitoring of pressure in a closed cavity will be significantly impacted by the temperature of the gas. There are several possible heat transfer scenarios that may be working in concert during such a test:

- The temperature of the gas in the downstream cavity will decrease as it loses heat to the surrounding seawater through the walls of the cavity (even if well-insulated).
- For relatively small volumes, the heat of compression during leakage will increase the temperature in the cavity.
- If gas is allowed to expand into a lower-pressure volume, Joules-Thomsen cooling may decrease the gas temperature.

In regards to loss of gas temperature to the seawater, calculations were separately performed for natural and forced convection. The time constant in the natural convection cases was an order of magnitude higher than the expected testing duration, so it would be reasonable to neglect such temperature changes. The impact of forced convection can spill into the test interval, depending on the cavity geometry, wall thickness, and insulation. The complexity of assessing such temperature changes for a given well could introduce more problems than it might solve if the calculations are used incorrectly. Thus, it is recommended that, for most applications, such heat transfer be ignored.

In regards to heat of compression and Joules-Thomson cooling, two different approaches were used to derive an equation that allows the user to calculate the pressure as a function of time for a fixed leak rate. The first, presented here, assumes that the downstream gas is isothermal. Such assumptions are currently utilized in Appendix A of API 14H.

$$P_2 = P_{2i} + \frac{\dot{m} Z R_{gas} T}{V_2} t$$

where

P_2 = pressure in the trapped cavity
P_{2i} = pressure in the trapped cavity at the start of the leak test
$\dot{m}$ = leakage flow rate
Z = gas compressibility (=1 for ideal gas)
R_{gas} = gas constant
T = temperature
V_2 = downstream volume

Another route involves drawing a control volume around the entire cavity and using conservation of energy. If heat transfer to the seawater is set to zero, the resulting equation is:

$$P_2 = P_{2i} + \frac{\dot{m} k R_{gas} T}{V_2} t$$

where

P_2 = pressure in the trapped cavity
P_{2i} = pressure in the trapped cavity at the start of the leak test
$\dot{m}$ = leakage flow rate
k = ratio of specific heats
R_{gas} = gas constant

T = temperature
V_2 = downstream volume

In using both of these equations, the analyst sets the flow rate to the maximum allowed leakage rate. The computed pressure, P_2, is the pressure in the closed volume that would be achieved at this flow rate in the specified time, t. If the measured pressure is less than the predicted pressure, then the leakage rate is less than the maximum allowable value. Conversely, if the measured pressure is more than the predicted value, then the actual leakage rate is more than the allowable value. The first of the two equations is most suitable for cases in which the downstream volume is sufficiently large or the expected leak rate sufficiently small.

3.7.4 Non-Choked Flow

It was previously noted that non-choked flow presents unique challenges. The downstream pressure response for non-choked flow conditions was derived under the assumptions of ideal gas and no heat transfer from the gas. Additionally, it was assumed that the effective C_v of the leakage path does not change during the process. The downstream pressure during the time of non-choked flow is:

$$P_{2,nc} = P_1 - \frac{kP_1}{0.41}\left[\frac{A_1 e^{-\varepsilon\sqrt{0.41/kP_1}(t-t_c)} - A_2}{A_1 e^{-\varepsilon\sqrt{0.41/kP_1}(t-t_c)} + A_2}\right]^2$$

where

$$A_1 = 1 + \sqrt{\frac{0.41}{kP_1}}\sqrt{P_1 - P_{2i}} \quad \text{and} \quad A_2 = 1 - \sqrt{\frac{0.41}{kP_1}}\sqrt{P_1 - P_{2i}}$$

and

$$\varepsilon = \frac{1}{Y\sqrt{P_1 - P_{2i}}}\left(\frac{kR_{gas}T}{V_2}\dot{m}\right) \quad \text{and} \quad Y = 1 - 0.41\left(\frac{P_1 - P_2}{kP_1}\right)$$

t = current time
t_c = time when the choked flow ended (set to zero if flow is never choked)
P_{2i} = downstream pressure at the beginning of the flow

This set of equations came from taking

$$\frac{dP_2}{dt} = \frac{R_{gas}kT_1}{V_2}\dot{m}$$

and substituting

$$\dot{m} = \frac{\dot{m}_i}{Y_1\sqrt{2\rho_1(P_1 - P_2)}}Y\sqrt{2\rho_1(P_1 - P_2)}$$

before integrating. As in the case of choked flow, the analysis sets the flow rate to the maximum allowed flow. This flow is used to establish a flow coefficient of the leakage path so that the downstream pressure can be estimated from the theory.

The actual pressure as a function of time is the superposition of the choked and non-choked cases. If the measured pressure over the test time, t, is less than the predicted pressure, then the actual leakage rate is less than the maximum allowable value.

3.7.5 Model Comparison

When heat transfer is set to zero in the numerical model, the results mirror those of the closed-form analytical model. Figure 3.27 shows the resulting pressure and temperature curve for the "small-volume" case without any heat transfer; the numerical and analytical results sit on top of each other. The same trend can be found for the "large" volume. Figure 3.28 shows the same comparison for cases in which a heat transfer coefficient of 5 W/m^2-K was applied to the numerical model. In the first few minutes of the test, the temperature increases due to compression of the gas. However, the gas begins to cool soon thereafter due to heat loss to the seawater. Figure 3.29 shows the same behavior for a large volume. The volume is sufficiently large that the heat of compression is dominated by heat transfer to the seawater. For this case, there is a larger difference between the two models. The same trends were observed for other values of the heat transfer coefficient.

As noted in a previous section, it is ideal to maintain choked flow during the leak test as the leak rate is harder to quantify when non-choked flow is present. Figure 3.30 shows a case of this transition for a leak that started at 2.5 scfm. There is choked flow present for just over 12 minutes. During this duration, the leak rate is constant. However, the leak rate quickly falls in the non-choked region and eventually goes to zero just prior to the 60-minute interval.

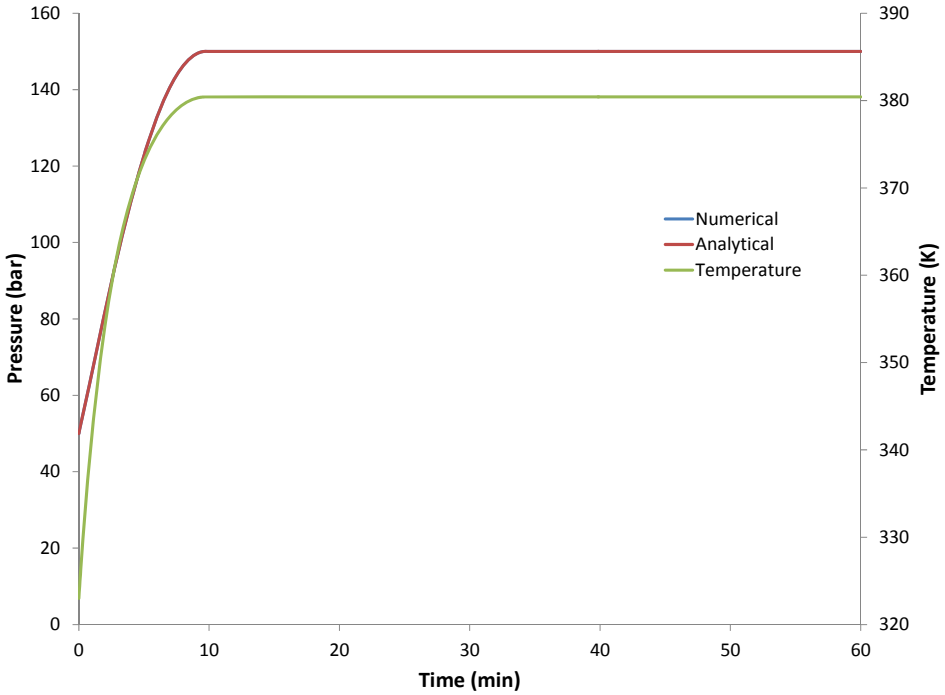

Figure 3.27. Comparison of Numerical and Analytical Model for No Heat Transfer
This comparison for a small volume shows no appreciable difference between the two models when heat transfer is not considered. The numerical and analytical curves sit on top of each other and are indistinguishable.

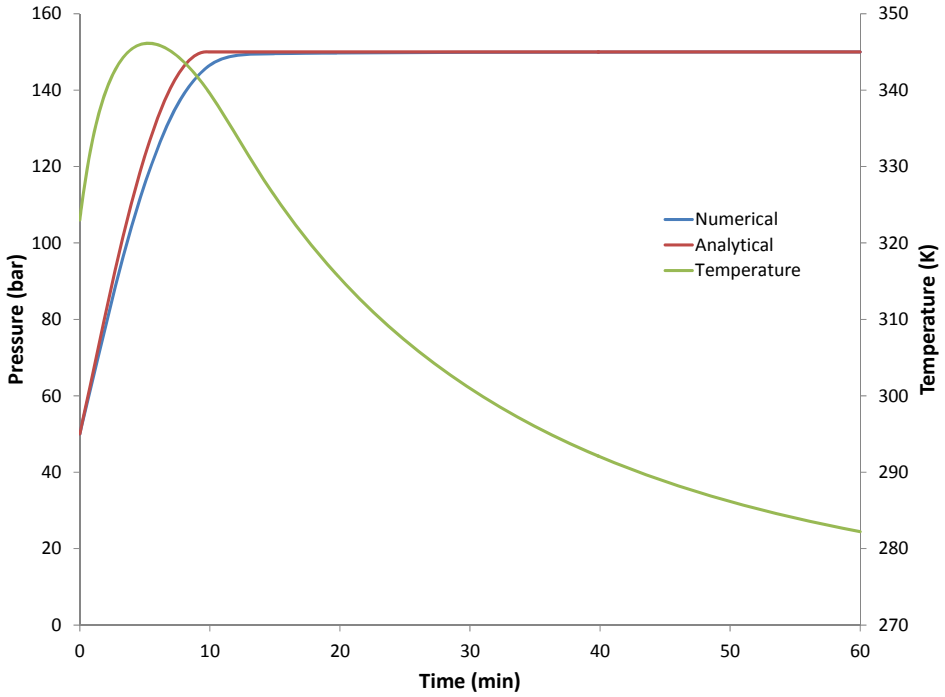

Figure 3.28. Comparison of Numerical and Analytical Model When Heat Transfer is Introduced
In this small volume, the temperature rises initially due to compression of the gas before it begins to cool as heat is lost to the seawater.

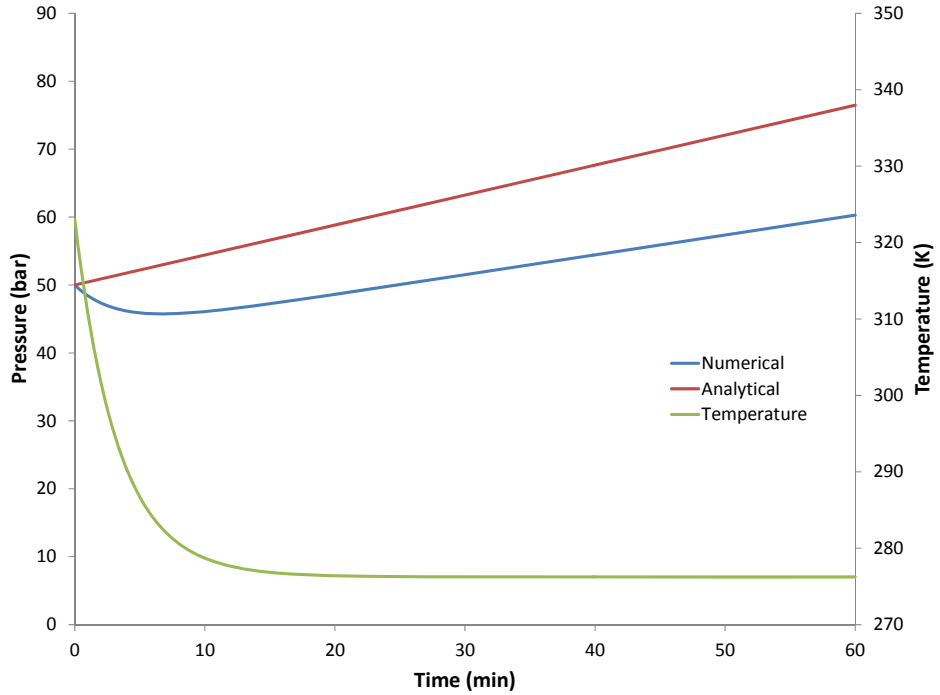

Figure 3.29. Comparison Between Models for Large Volume
There is a larger disparity between the two models, as compared to a case with a relatively small volume.

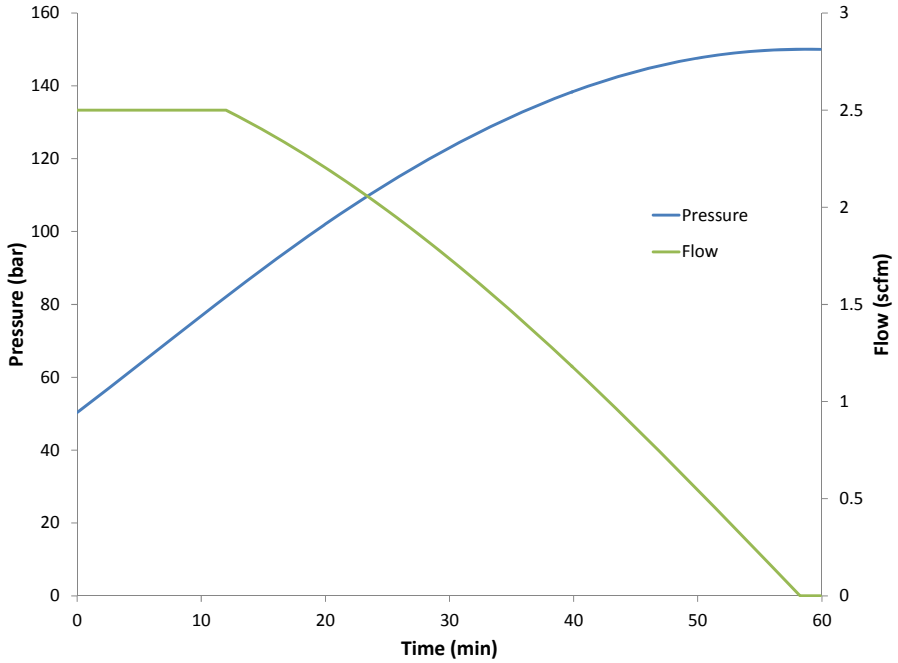

Figure 3.30. Pressure and Flow Curve for Choked Flow Transition

Choked flow is present for 12 minutes before transitioning to non-choked flow.

3.8 Proof-of-Concept Conclusion

The work on this part of the project highlighted shortcomings of utilizing CFD for the modeling of such wellbore conditions. The exaggerated aspect ratio of the problem complicates the setup of CFD and does not allow for such an approach to characterize well behavior without significant loosening of model assumptions. Some of the results, including the increase in density during cooling of the gas, suggest that the model uncertainty does not make such a tool suitable for studying complex behavior in a well. Additionally, the long run times of such models do not make it feasible to implement this approach for multiple wells.

As noted in the introduction section of this report, a new approach to safety barrier testing should have at least one of three features: the ability to reduce test time, the ability to directly quantify the leak rate, and the ability to work in multiphase conditions. Advances in at least one of the three areas would represent an improvement over current methods for testing, provided that the cost to implement new technology is not too high.

Utilization of the numerical model developed for this project would allow for an operator to predict the amount of time elapsed to quantify a specific leak rate. Additionally, this model uses multiphase conditions and, thus, two of the desired criteria outlined in the previous paragraph are met using this approach.

The numerical model is a promising approach for assessing wellbore pressure conditions without the need for further instrumentation. This model would allow for relative trending of pressure data, as well as the ability to predict the amount of test time required for a specific set of conditions. One of the key findings of this work is that temperature effects cannot be ignored or the resulting pressure curves will not have the context for proper evaluation.

Modeling work of pressure buildup testing for wellhead valves such as PMVs and USVs also demonstrated the impact of temperature on the results. These results are significantly

impacted by the overall volume of the pressure cavity. Also of note in the modeling of wellhead valves is the importance of retaining choked flow during the entire observation period.

4. CONCLUSIONS

Existing pressure-monitoring techniques for evaluating leakage in production master valves (PMVs) and surface-controlled subsurface safety valve (SCSSVs) where a subsea tree exists do not account for thermal and other environmental effects. This approach to leak detection has significant uncertainty and requires extended periods of time to complete. During these long shut-in periods, there is a loss of production, as well as an increased likelihood of flow assurance events.

A project was undertaken to determine if an alternate means of conducting this testing was possible. A number of technologies were identified and subsequently ranked. Due to the high number of existing wells with the need for testing, it was decided to largely avoid technologies that required retrofitting of existing infrastructure, particularly for SCSSVs. The resulting tradeoff study picked well-specific modeling as the candidate technology. This approach is able to capture thermal and other environmental effects.

An analytical model was developed that allows for determination of leakage rates, as well as the required test duration. The model is computationally-inexpensive and allows for the operator to conduct simple trending of results. The sensitivity of various criteria was also explored. One significant finding of this work is that thermal effects of the well must be accounted for in order to properly interpret pressure results. Utilization of this model can reduce overall test times and give operators a sense of the level of uncertainty in interpreting measured pressure changes.

Overall, this project demonstrated that such a model can improve the existing approaches to testing of safety barriers. There is room for improvement in future efforts if the modeling approach is revisited. Example improvements could be extension of the calculations to non-ideal gas behavior and accommodation of thermal effects such as convection. The results from the model also highlighted the relative importance of such parameters as temperature distribution and level measurement for the liquid column. Invoking technologies, such as distributed temperature sensing, that could reduce overall uncertainty would benefit the use of such models. The testing of safety barriers in deepwater environments remains a challenge, but the contents of this report provide several tools that can be used to augment existing practices in the field.

5. REFERENCES

American Petroleum Institute (API) Recommended Practice 14A, *Specification for Subsurface Safety Valve Equipment*, 11th Edition, July 2005.

American Petroleum Institute (API) Recommended Practice 14B, *Recommended Practice for Design, Installation, Repair and Operation of Subsurface Safety Valve Systems*, 4th Edition, July 1994.

American Petroleum Institute (API) Recommended Practice 14H, *Recommended Practice for Installation, Maintenance and Repair of Subsurface Safety Valves and Underwater Safety Valves Offshore*, 5th Edition, August 2007.

ANSYS 13.0 Theory Guide, "Section 10.1.1. Discretization of the Governing Equations," SAS IP Inc. (2010).

Boisvert, J., "Keep Measurements on the Level – Choose the Right Technology for Your Application," Siemens Energy and Automation, reprinted from Chemical Processing: November 2006, http://www.sea.siemens.com/us/internet-dms/ia/ProcessInstruments/Level/RadarLevel/Chem-Processing-Article-06.pdf.

Brill, J., and Beggs, H., "Two-Phase Flow in Pipes," Sixth Edition, 1978.

Chemical Tracers Inc., http://www.chemtracers.com, 2007.

ClampOn AS, ClampOn DSP Leak Monitor brochure, Bergen, Norway, August 2009.

Clift, R., Grace, J. R., and Weber, M. E., "Bubbles, Drops, and Particles," Academic Press, Inc., London, UK, 1978.

Dictionary.com, "tracer," in © *Encyclopedia Britannica, Inc*., Source location: Encyclopedia Britannica, Inc., http://dictionary.reference.com/browse/tracer.

Emerson Process Management, Level Measurement: http://www2.emersonprocess.com/en-US/brands/rosemount/Level/Pages/index.aspx.

Emerson Process Management, *Daniel® Model 3804 Liquid Ultrasonic Flow Meter Product Datasheet*, publication DAN-MODEL3804-LIQ-USM-DS-0810, August 2010.

Endress+Hauser, Level Measurement: http://www.us.endress.com.

Estele-Uribe, F., Jaramillo, J., "Generalised Virial Equation of State for Natural Gas Systems," Fluid Phase Equilibria, Vol. 231, 2005, pp. 84-98.

Farstad, J. E., and Cremean, S. P., United States Patent number 5,361,636, *Apparatus and Process for Measuring the Magnitude of Leaks*, November 8, 1994.

FMC Technologies, *Smith Meter® Ultra⁶ Ultrasonic Liquid Flowmeter Specifications*, publication SSLS001 Issue/Rev. 0.4, June 2010.

Grace, J. R., T Wairegi, and J. Brophy, "Break-up of Drops and Bubbles in Stagnant Media," Canadian Journal of Chemical Engineering, Vol. 56, pp. 3-8, February 1978.

Grimley, T. A., "Multipath Ultrasonic Flow Meter Performance," *Proceedings of the 1996 North Sea Flow Measurement Workshop*, Peebles, Scotland, October 1996.

Grimley, T. A., *Ultrasonic Meter Testing For Storage Applications*, Final Report to U.S. Department of Energy, DOE Cooperative Agreement No. DE-FC21-96MC33033, December 1998.

Instanes, G., and Pedersen, A., "Acoustic Leak Monitoring on Subsea Valves," *Proceedings of the 2008 SPE Asia Pacific Oil & Gas Conference and Exhibition*, paper SPE 114256, published by the Society of Petroleum Engineers, Richardson, Texas, October 2008.

Kitscha J. and Kocamustafaogullari, G., "Breakup Criteria for Fluid Particles," International Journal of Multiphase Flow, Vol. 15, pp. 573-588, July 1989.

K-Tek, Level Measurement: http://www.ktekcorp.com/dnn20/Default.aspx?tabid=54#.

Lansing, J., "Benefits of Calibrating Ultrasonic Meters," *Proceedings of the 2002 AGA Operations Conference*, Chicago, Illinois, published by the American Gas Association, Washington, D.C., May 2002, paper 02-OP-60.

Lansing, J., "Ultrasonic Meter Station Design Considerations," *Proceedings of the 2003 Western Gas Measurement Short Course*, Victoria, British Columbia, Canada, May 2003.

Miller, R. W., *Flow Measurement Engineering Handbook, Third Edition*, McGraw-Hill.

National Institute of Standards and Technology (NIST) Chemistry WebBook, http://webbook.nist.gov, keyword: CH4 (2011).

Paino, W. F., Tengah, N. H., Woodward, M. I., Snaith, N., Salleh, H., and Brown M., "Using Intelligent Well Technology to Define Reservoir Characterization and Reduce Uncertainty, SPE 88533 (2004).

Ronan Measurement Divisions: http://www.ronanmeasure.com/pages/default.asp.

Schnake, J. "Liquid Level Measurement – Basics 101, Part 1," Endress+Hauser White Paper

Schnake, J. "Liquid Level Measurement – Basics 101, Part 2," Endress+Hauser White Paper

Schnake, J. "Liquid Level Measurement – Basics 101, Part 3," Endress+Hauser White Paper

Shoham, O., "Mechanistic Modeling of Gas-Liquid Two-Phase Flow in Pipes," Society of Petroleum Engineers, Texas, USA, 2006.

Siemens A/S, SITRANS F ultrasonic flow meter brochure, publication E20001-A60-P730-V2-7600, June 2010.

Siemens, Level Measurement: http://www.sea.siemens.com/us/Products/Process-Instrumentation/Process-Sensors-Transmitters/Pages/Level-Measurement.aspx

Southwest Research Institute, *Ultrasonic Flow Meter Workshop*, sponsored by Southern Gas Association, Sept. 6-7, 2006.

Starling, K.E., Savidge, J.L., "Compressibility Factors of Natural Gas and Other Related Hydrocarbon Gases," AGA Transmission Measurement Committee Report 8, American Gas Association, 1992.

Tannehill, J. C., Anderson, D. A., and Pletcher, R. H., *Computational Fluid Mechanics and Heat Transfer*, 2nd Ed., Taylor and Francis, Philadelphia, PA (1997).

U. S. Department of Labor, OSHA, Radiation Detection Instruments, http://www.osha.gov/SLTC/radiationionizing/introtoionizing/radiationdetectioninstru.html.

U.S. Department of the Interior, Minerals Management Service, Gulf of Mexico OCS Region, "Using Alternate Compliance in Safety Systems for Subsea Production Operations," NTL No. 2009-G36, January 1, 2010.

Wauquier, J. P., *Petroleum Refining, Vol. 1: Crude Oil, Petroleum Products, Process Flowsheets*, Editions Technip, Paris, 1995.

Whitehouse, W. J. and Putman, J. L., *Radioactive Isotopes – An Introduction to their Preparation, Measurement and Use*, Oxford University Press, London, England, 1958.

Witte, J. N., "Ultrasonic Gas Meters from Flow Lab to Field: A Case Study," *Proceedings of the 2002 AGA Operations Conference*, Chicago, Illinois, published by the American Gas Association, Washington, D.C., May 2002, paper 02-OP-34.

Wolfram|Alpha knowledge base, http://www.wolframalpha.com, keyword: crude oil (2011).

World Nuclear Association, Radioisotopes in Industry, http://www.world-nuclear.org/info/inf56.html, February 2010.

Xiao, J., Fuentes-N, F. and Reynolds, A., "Modeling and Analyzing Pressure Buildup Data Affected by Phase Redistribution in the Wellbore." SPE 26965, 1995.

Zemel, B., Chapter 7 – Downhole Tracers & Chapter 8 Tracers in Facility Operations, *Tracers in the Oilfield*, Vol. 43 1995, pp. 293-426.

APPENDIX A

Technology Evaluation Results

TECHNOLOGY EVALUATION RESULTS

As described in the body of the report, each of the identified leak detection technologies, including the current technology of pressure monitoring, were scored for how well they met the grading criteria identified in Table 2.3. The scoring (using a scale of 1-5, with 5 being the highest) was based upon the expected performance of each technology for use in testing of PMVs.

Table A.1. Scoring for Pressure-Monitoring Method

PRESSURE MONITORING		
GENERAL TECHNOLOGY DESCRIPTION		
The current means of testing valves involve closing in a cavity, creating a differential pressure across the test valve, and monitoring the cavity for pressure buildup or decay.		
CRITERIA	**DESCRIPTION**	**SCORE**
Performance	Correlation of the pressure is required, so sensitivity is reduced to some degree. Many factors (temperature, fluid composition, etc.) can impact pressure.	3
HSE	No HSE implications have been identified.	5
Robustness	Any uncertainty about the fluid composition, temperature fluctuations, etc., reduces performance.	2
System Reliability	In addition to other valves for sealing the cavity, the only other "on demand" hardware is pressure transmitters.	5
Adaptability	With a few possible exceptions, the system can work in most wells and trees.	4
Retrofittable	This approach can be utilized in any tree with access for installation of a pressure transmitter.	4
Test Time	Testing can take considerable periods of time due to allowing for fluid settling and temperature stability.	3
Direct Cost	Acquisition of pressure transmitters and perhaps some software is required.	4
Technology Readiness Level	This approach is currently in use by operators.	5

Table A.2. Scoring for Active Ultrasonic

ACTIVE ULTRASONIC		
GENERAL TECHNOLOGY DESCRIPTION		
Devices that detect ultrasonic energy may be used to measure flow rates through leaking valves. Existing ultrasonic technologies incorporate active sensors that generate ultrasonic pulses and use transit-time measurements to determine fluid flow rates. Active ultrasonics are commonly used in flow meters for gas and liquid pipelines, but have poorer uncertainties at the expected leakage rates than passive units. This technology is available in non-intrusive, clamp-on versions that could be attached to the outside of a valve assembly or tree.		
CRITERIA	**DESCRIPTION**	**SCORE**
Performance	This technology likely cannot detect leak rates at low-enough velocities required for this application.	1
HSE	Active units can be clamped to pipes non-intrusively. Under the assumption that these instruments are already in place, or procedures exist to add subsea taps, HSE impact is negligible.	5
Robustness	No active units known to exist for subsea applications. Technology expected to function well only in single-phase flows.	3
System Reliability	This approach would require hardware and sensors that would occasionally be prone to downtime.	3
Adaptability	Technology can adapt to changes in gas pressure and temperature, but are not expected to function well if multiphase flows are present in the cavity. Initial test conditions with a single-phase medium can be created to improve performance.	4
Retrofittable	Active technology can be adapted to wells with sufficient straight lengths of pipe. Requires pressure and temperature instrumentation on the system; under the assumption that these instruments are already in place, minimal retrofitting is expected.	4
Test Time	Active technology can provide measurements over a period of a few minutes. Time required for passive measurements is unknown.	5
Direct Cost	Manufactured equipment would be generic to a variety of wells.	4
Technology Readiness Level	Active equipment is available for topside applications, but current approach would require redesign for subsea applications.	3

Table A.3. Scoring for Differential Pressure Level Detection

DIFFERENTIAL PRESSURE LEVEL DETECTION		
GENERAL TECHNOLOGY DESCRIPTION		
Level detection could be used to observe whether the liquid-to-gas ratio in a confined volume immediately downstream of a valve changes in response to a leak.		
CRITERIA	**DESCRIPTION**	**SCORE**
Performance	Assuming an average well bore radius of 5½ inches with a cylindrical shut-in geometry volume, to detect 2 ml/min liquid flow in one hour, a minimum resolution of 1.96 mm would be needed by a level gauge. For 200 ml/min over ½ hour, this resolution would be 98 mm, and for 200 ml/min over ten minutes, it would be 32.6 mm. Allowing one hour of testing time, most level gages would be well within their accuracy thresholds for a 10-ml/min liquid leak. For PMVs in a horizontal orientation, it is likely a significantly greater volume of leaked liquid would be required to raise the level a detectable amount.	3
HSE	There are no identifiable HSE issues with this technology.	5
Robustness	Level detection operates under the inherent assumption that the gaseous and liquid phases are separate at the time of measurement. However, other than minimal emulsion, this should occur fairly rapidly after the downstream volume is shut-in and isolated.	3
System Reliability	Aside from differential pressure transmitters, no additional hardware is required for implementation of this technology.	5
Adaptability	Long horizontal distances or well bores with very large radii will tend to decrease liquid level change-to-volume change ratios and, thus, testing would take longer to assure minimum flow rates are not being exceeded.	3
Retrofittable	Gas injection points will also be required if process lines are expected to carry solely liquid. Pressure differential detection would require taps be placed on both sides of the barrier valves.	3
Test Time	The act of determining the change in liquid level requires very little time for all of the level detection technologies. However, for a 120-ml total amount of leaked fluid (2 ml/hr for one hour) with an average 5 ½-inch bore inner well tube radius, the height change of the liquid column would only be about 2 mm if a cylindrical volume is assumed. For 1,200 ml in one hour (200 ml/min), this would be about 20 mm. Two millimeters is, in general, just at the resolution level of the level detection instrumentation. Thus, testing time would be expected to take about ten minutes to one hour.	3
Direct Cost	This technology would require liquid injection (and possibly gas) ports be installed upstream of the PMV and SCSSV.	2
Technology Readiness Level	There is little further work required to bring such technology to field-ready status.	5

Table A.4. Scoring for Flow Measurement

FLOW MEASUREMENT		
GENERAL TECHNOLOGY DESCRIPTION		
This technology involves utilizing a regulator of some sort that keeps the pressure within a trapped cavity at constant pressure. If there is a leak and additional fluid has to be metered in to maintain pressure, the flow rate could be measured and the leak rate determined. A fluid such as methanol could be utilized for injection into the cavity.		
CRITERIA	**DESCRIPTION**	**SCORE**
Performance	The accuracy of the measurement would only be limited by the accuracy of a flow meter.	4
HSE	Other than utilization of methanol and additional joints, there are no HSE issues.	4
Robustness	The well fluid would be purged from the cavity, so conditions like temperature would be more easily captured.	4
System Reliability	This approach would require numerous hardware (regulators, injection valves, flow meters) that could go down.	2
Adaptability	Since the well fluid would be purged, geometry constraints would not play a large role in the performance of this system.	4
Retrofittable	Due to the required additional hardware, such an approach would not be likely to be used on existing trees.	2
Test Time	Testing would proceed in a relatively quick manner.	4
Direct Cost	The additional hardware would make this approach expensive in comparison with those approaches that did not require additional components.	2
Technology Readiness Level	Such an approach is likely two or three years away from being implemented in the field.	3

Table A.5. Scoring for Guided Wave Level Detection

GUIDED WAVE LEVEL DETECTION		
GENERAL TECHNOLOGY DESCRIPTION		
Level detection could be used to observe whether the liquid-to-gas ratio in a confined volume immediately downstream of a valve changes in response to a leak.		
CRITERIA	**DESCRIPTION**	**SCORE**
Performance	Assuming an average well bore radius of 5½ inches with a cylindrical shut-in geometry volume, to detect 2 ml/min liquid flow in one hour, a minimum resolution of 1.96 mm would be needed by a level gauge. For 200 ml/min over ½ hour, this resolution would be 98 mm, and for 200 ml/min over ten minutes, it would be 32.6 mm. Allowing one hour of testing time, most level gages would be well within their accuracy thresholds for a 10-ml/min liquid leak. For PMVs in a horizontal orientation, it is likely a significantly greater volume of leaked liquid would be required to raise the level a detectable amount.	3

CRITERIA	DESCRIPTION	SCORE
HSE	Health and safety considerations for guided wave radar liquid level measurements would be minimal. Insertion of the tool must be considered.	4
Robustness	Level detection operates under the inherent assumption that the gaseous and liquid phases are separate at the time of measurement. However, other than minimal emulsion, this should occur fairly rapidly after the downstream volume is shut-in and isolated. Ambient conditions or foam at the interface would not present a problem for the instruments.	3
System Reliability	This approach would require hardware and sensors that would occasionally be prone to downtime.	4
Adaptability	Long horizontal distances or well bores with very large radii will tend to decrease liquid level change-to-volume change ratios and, thus, testing would take longer to assure minimum flow rates are not being exceeded. May have problems on horizontal tree.	3
Retrofittable	Two liquid injection points would need to be installed upstream of the valves to be tested for gas leaks. Guided wave detection would likely require installation of a side chamber with the emitter and guide cable/rod equipment.	3
Test Time	The act of determining the change in liquid level requires very little time for all of the level detection technologies. However, for a 120-ml total amount of leaked fluid (2 ml/hr for one hour) with an average 5 ½-inch bore inner well tube radius, the height change of the liquid column would only be about 2 mm if a cylindrical volume is assumed. For 1,200 ml in one hour (200 ml/min), this would be about 20 mm. Two millimeters is, in general, just at the resolution level of the level detection instrumentation. Thus, testing time would be expected to take about ten minutes to one hour, depending on the technology and the rate of leakage needed to get an accurate measurement. For horizontal distances after the PMV valve, the time would increase proportionally with level-to-volume ratio.	4
Direct Cost	Guided wave technology would require significant retrofitting to allow for positioning the cable chamber with adjoining valves next to the main wellbore. Liquid injection ports would need to be installed upstream of the PMV and SCSSV.	2
Technology Readiness Level	Already successfully employed in a range of operations and areas under a variety of harsh environmental conditions. However, several years of development are likely required for subsea applications.	3

Table A.6. Scoring for Passive Ultrasonic

PASSIVE ULTRASONIC		
GENERAL TECHNOLOGY DESCRIPTION		
Devices that detect ultrasonic energy may be used to measure flow rates through leaking valves. Existing ultrasonic technologies incorporate passive sensors that listen for acoustic signals generated by leaks and other events. Passive ultrasonic technologies have been tested for their ability to quantify leak rates through valves, and show some promise in safety barrier testing applications. This technology is available in non-intrusive, clamp-on versions that could be attached to the outside of a valve assembly or Christmas tree.		
CRITERIA	**DESCRIPTION**	**SCORE**
Performance	Passive technology exists that can measure gas-in-gas leakage rates down to 15 scfm in subsea applications, and less than 1 scfm in topside applications. Only manufacturer specs found for detectable liquid leakage rates.	3
HSE	Passive design requires static pressure measurements; active design requires pressure and temperature measurements. Under the assumption that these instruments are already in place, or procedures exist to add subsea taps, HSE impact is negligible.	5
Robustness	Passive units are unaffected by topside environment. Passive units are available for subsea, but with poorer lower measurement limit.	3
System Reliability	This approach would require hardware and sensors that would occasionally be prone to downtime.	3
Adaptability	Technology can adapt to changes in gas pressure and temperature, but are not expected to function well if multiphase flows are present in the cavity. Initial test conditions with a single-phase medium can be created to improve performance.	4
Retrofittable	Active technology can be adapted to wells with sufficient straight lengths of pipe. The location of passive sensors is less restricted. Both require pressure and temperature instrumentation on the system; under the assumption that these instruments are already in place, minimal retrofitting is expected.	4
Test Time	The time required for passive measurements is unknown.	3
Direct Cost	Manufactured equipment would be generic to a variety of wells.	4
Technology Readiness Level	Passive designs are now available for use in both topside and subsea environments.	4

Table A.7. Scoring for Radiometric Level Detection

RADIOMETRIC LEVEL DETECTION		
GENERAL TECHNOLOGY DESCRIPTION		
Level detection could be used to observe whether the liquid-to-gas ratio in a confined volume immediately downstream of a valve changes in response to a leak.		
CRITERIA	**DESCRIPTION**	**SCORE**
Performance	Assuming an average well bore radius of 5½ inches with a cylindrical shut-in geometry volume, to detect 2 ml/min liquid flow in one hour, a minimum resolution of 1.96 mm would be needed by a level gauge. For 200 ml/min over ½ hour, this resolution would be 98 mm, and for 200 ml/min over ten minutes, it would be 32.6 mm. Allowing one hour of testing time, most level gages would be well within their accuracy thresholds for a 10-ml/min liquid leak. For PMVs in a horizontal orientation, it is likely a significantly greater volume of leaked liquid would be required to raise the level a detectable amount. Another item to note is that if there were any hysteresis with regard to valve leakage direction, it may be problematic that the case with gas upstream of the valve requires a negative pressure differential using this technology.	3
HSE	Personnel performing installations and calibrations would run the risk of exposure from mishandling. Additionally, when the source is used, ocean life nearby could receive mild levels of radiation exposure.	2
Robustness	Level detection operates under the inherent assumption that the gaseous and liquid phases are separate at the time of measurement. However, other than minimal emulsion, this should occur fairly rapidly after the downstream volume is shut-in and isolated. Ambient conditions or foam at the interface would not present a problem for the instruments.	3
System Reliability	This approach would require hardware and sensors that would occasionally be prone to downtime.	3
Adaptability	Long horizontal distances or well bores with very large radii will tend to decrease liquid level change-to-volume change ratios and, thus, testing would take longer to assure minimum flow rates are not being exceeded. Horizontal trees may be an issue.	3
Retrofittable	Two liquid injection points would need to be installed upstream of the valves to be tested for gas leaks. Radiometric level detection itself is non-invasive and would require mounting on the outside of the wellbore, but inside the casing.	3

CRITERIA	DESCRIPTION	SCORE
Test Time	The act of determining the change in liquid level requires very little time for all of the level detection technologies. However, for a 120-ml total amount of leaked fluid (2 ml/hr for one hour) with an average 5 ½-inch bore inner well tube radius, the height change of the liquid column would only be about 2 mm if a cylindrical volume is assumed. For 1,200 ml in one hour (200 ml/min), this would be about 20 mm. Two millimeters is, in general, just at the resolution level of the level detection instrumentation. Thus, testing time would be expected to take about ten minutes to one hour, depending on the technology and the rate of leakage needed to get an accurate measurement. For horizontal distances after the PMV valve, the time would increase proportionally with level-to-volume ratio.	4
Direct Cost	Radiometric measurements would be quite expensive for the source material, as well as in obtaining necessary permits and trained radiological safety personnel. Liquid injection ports would have to be installed upstream of the PMV and SCSSV.	1
Technology Readiness Level	Already successfully employed in a range of operations and areas under a variety of harsh environmental conditions. However, several years of development are likely required for subsea applications.	3

Table A.8. Scoring for Thermal Stabilization

THERMAL STABILIZATION		
GENERAL TECHNOLOGY DESCRIPTION		
One of the major shortcomings of the current method is that pressure monitoring is sensitive to temperature changes. Temperature changes introduce uncertainty into the measurements and can result in having to wait for the temperatures to stabilize before conducting testing. The technology scored here is one in which pressure monitoring is supplemented by a mechanism that can quickly heat or cool all of the fluid being tested and keep it at a relatively constant temperature.		
CRITERIA	**DESCRIPTION**	**SCORE**
Performance	One factor in the existing approach is that temperature changes can affect pressure readings. One way to reduce these effects is to stabilize the temperature. This should reduce some uncertainty in the measurement.	4
HSE	The heating or cooling elements would perhaps have some safety hurdles that must be passed.	4
Robustness	Should offer a slight improvement over current methods as temperature fluctuation is taken out of the mix.	3
System Reliability	The heating or cooling elements would be prone to occasional outages.	4
Adaptability	With a few possible exceptions, the system can work in most wells and trees.	4
Retrofittable	Some effort would be required to install the heating or cooling elements on the existing infrastructure.	3
Test Time	Offers significant time savings as test does not have to wait for temperature to stabilize.	5
Direct Cost	Some additional cost would be required for hardware.	3
Technology Readiness Level	Commercially-available systems would like be acceptable for use.	4

Table A.9. Scoring For Tracer

TRACER		
GENERAL TECHNOLOGY DESCRIPTION		
Tracer particle concentration may be used to measure flow rate leaked through PMV and SCSSV barriers. The most common method in the industry, i.e., radioisotope detection, is likely the most feasible for such an application since it is noninvasive and does not require direct sampling of the process fluid stream. Tracer particles suspended in a stable, low-density gas would be injected upstream of the barrier valve. The downstream blocked-in volume would then be monitored over time to track rising radiation levels resulting from any leakage. Further details on a method for using tracers are provided in the supporting text.		
CRITERIA	**DESCRIPTION**	**SCORE**
Performance	Radiation intensity may be linked quantitatively to volume of leaked fluid, which may in turn be tracked in time to compute a flow rate. Radioisotope detection is sensitive, even with a low concentration of tracer particles. The method requires the assumption that tracer particles remain homogenously distributed in suspension fluid upstream of the barrier valve for the duration of the test.	4
HSE	Personnel performing calibrations and transporting radioisotopes would run the risk of exposure from mishandling. Additionally, ocean life nearby could receive very mild levels of radiation exposure during the test. In the case of a leak, this dosage might increase substantially. Documentation, procedures, and controls for a full radiation safety program would likely need to be instituted.	2
Robustness	Assuming adequate calibration and functionality of injection and detection equipment, there should be no impediment to using this method on any well, under any well conditions.	5
System Reliability	It would be recommended that periodic calibration of detection equipment be performed to ensure continued accuracy. However, it is not expected that the equipment would require high levels of maintenance. Some method of monitoring injection lines for tracer gas leakage may be necessary.	4
Adaptability	The proposed system is adaptable to all well types and configurations.	4
Retrofittable	Implementation requires only creation of an injection port on the wellbore upstream of the test valves. Radiation detectors may then be installed noninvasively outside the process stream region near the upstream blocking valves.	4
Test Time	Depending on the radioisotope selected as a tracer, radiation intensity levels can be detected for very low concentrations of leaked fluid.	4
Direct Cost	It will likely be expensive to set up a radiation safety/monitoring program, in addition to purchasing and installing injection and detection equipment. Also, significant quantities of radioisotopes must be procured on a regular basis for testing.	1
Technology Readiness Level	Radioisotope tracers have been reliably used in various industries for measurement of flow rate via radiation intensity levels.	3

Table A.10. Scoring for Volume Reduction

VOLUME REDUCTION		
GENERAL TECHNOLOGY DESCRIPTION		
The current pressure-monitoring approach can often times be applied to systems with large fluid volumes. The larger the volume, the more uncertainty is introduced into the measurement as issues like compressibility and gas content are heightened. Additionally, thermal effects take longer to evolve with large volumes. The approach scored here is to utilize the existing testing approach, while at the same time inserting an inflatable trap or other device to reduce the fluid volume.		
CRITERIA	**DESCRIPTION**	**SCORE**
Performance	Reducing the volume decreases the uncertainty in pressure measurements, increases sensitivity of calculations, and should lead to improved performance.	4
HSE	The volume-reducing element will likely require some additional safety protocols for its use.	4
Robustness	This approach slightly reduces the impact of well conditions.	3
System Reliability	There is little hardware required for this system that could experience downtime.	5
Adaptability	With a few possible exceptions, this system can work in most wells and trees.	4
Retrofittable	This approach would work on most existing valves, though additional hardware may be required.	4
Test Time	The added time for insertion of the device should be less than the savings in time during test.	4
Direct Cost	Some additional hardware would be required.	4
Technology Readiness Level	The system is likely a year or two away from implementation.	3

Table A.11. Scoring for Well-Specific Modeling

WELL-SPECIFIC MODELING		
GENERAL TECHNOLOGY DESCRIPTION		
This approach would be to develop models in which well-specific criteria could be entered and a more accurate means of capturing fluid behavior would be developed. Examples would be to collect temperature profiles using DTS or other transmitters, monitoring density and other criteria, introducing CFD, and using other data-mining technologies.		
CRITERIA	**DESCRIPTION**	**SCORE**
Performance	It would be expected that this approach would have better accuracy than current methods. This method still relies upon indirect measurement.	4
HSE	No anticipated HSE concerns have been identified.	5
Robustness	Would reduce sensitivity to some well conditions, but some features may still impact results. It is required to know well conditions in order to model them.	3
System Reliability	A few more instruments would likely be required.	4
Adaptability	With a few possible exceptions, the system can work in most wells and trees.	4
Retrofittable	Unless modeling requires instrumentation that cannot be universally installed, there are no immediate retrofit problems.	4
Test Time	Should be able to reduce time for a given test.	4
Direct Cost	A few additional pieces of instrumentation will be required for this approach.	4
Technology Readiness Level	The system could be initiated within one year, though the process would be evolving.	4

APPENDIX B

Technology Descriptions

TECHNOLOGY DESCRIPTIONS

The purpose of this appendix is to provide a detailed description of several of the technologies assessed for the project. Specifically, this text provides additional context to technologies in which several individual items were wrapped into one subject heading.

B.1 Active Ultrasonic Techniques

Ultrasonic technologies are well-established for measuring flow rates within pipelines. Most ultrasonic flow meters use an active technique to infer the flow rate in a natural gas or liquid pipeline. In the active approach, ultrasonic energy is transmitted and received by pairs of transducers. The transit path passes diagonally across the flow area (see Figure B.1), and in some meter designs, may be reflected one or more times by the meter walls. The transit time of the acoustic energy between transducers changes, depending on whether the sound waves are traveling upstream or downstream. The average flow velocity along the acoustic path can be calculated from these upstream and downstream transit times and from the transducer geometry. The calculation is independent of the speed of sound in the medium, so the composition of the gas or liquid stream does not need to be known beforehand (Miller, 1996; SwRI, 2006).

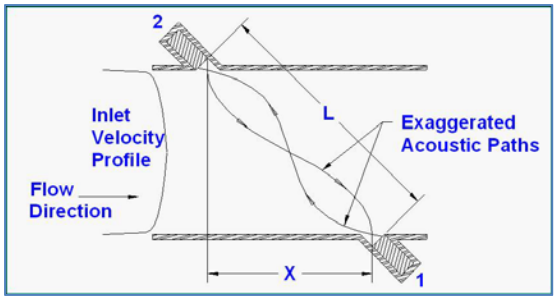

Figure B.1. Example of an Active Transducer Pair Used in Flow Measurement, with Key Geometric Criteria (SwRI, 2006)

Active, time-of-flight ultrasonic flow measurement has been in use for some time to measure flow rates in natural gas and liquid pipelines. Clamp-on ultrasonic meters are available (Siemens, 2010) that can be mounted externally to a pipeline to measure flow rates without disruption of flow. The following are considerations for applying active ultrasonic flow techniques to measure leakage in subsea assemblies:

- Although knowledge of the speed of sound is not needed, the equations for flow velocity require the sound speed to be constant along the acoustic path. This requires that there be no density gradients along the acoustic path.
    - Suppose the cavity between the blocked valves is initially filled with gas or a light liquid such as methanol, and the fluid injection lines are left open and equalized to the cavity. If oil (or a liquid denser than the phase filling the cavity) enters through the leaking valve, it would remain at the bottom of the cavity, regardless of tree orientation, and displace the methanol or fill gas. It may be possible to measure the displacement rate of the fill fluid using a clamp-on ultrasonic meter, and infer the leakage rate into the cavity. However, such measurements would only be possible until the interface between the two phases crosses the acoustic path and the density along the path becomes discontinuous.
    - The approach is expected to be less successful if the phase leaking into the cavity is less dense than the fill fluid. Small gas bubbles, for example, could scatter or

reflect acoustic energy back to the receiving transducer, as well as attenuate acoustic pulses traveling along the design path. Multiple reflections at the receiving transducer would require additional signal processing beyond what is performed by current clamp-on meters.

- Temperature gradients along the acoustic path will cause density variations and velocity measurement errors. If a significant temperature difference exists between the fluid in the cavity and the environment, heat transfer may induce such temperature gradients. Accurate ultrasonic flow measurements would require thermal equilibrium between the test cavity and the surroundings. Depending on whether the well and valve assembly are on the ocean floor or above the surface, and on the temperature of the fluids produced by the well, effort may be required to maintain thermal equilibrium between the valve assembly and its environment.
- Commercial ultrasonic flow meters have low-flow cutoff limits, below which the meter will not report a flow rate. For commercially-available natural gas flow meters, this limit is typically below a superficial velocity of 10 ft/s; brochures for liquid ultrasonic meters (Emerson Process Management, 2010; FMC, 2010), including a clamp-on meter (Siemens, 2010) report low-flow cutoffs on the order of 1 ft/s to 2 ft/s. The limit may be influenced by a number of factors, some of which are listed below. Limits may change as the technology is applied to leak detection for subsea wells.
    - Lansing (2002, 2003) reported that many natural gas meters have nonlinear meter responses below 10 ft/s, and that the cutoff may have been chosen to allow a single meter factor to be used over the meter flow range. Lansing suggested that piecewise linearization of calibration data at low flow rates would allow the meters to be used accurately below this cutoff.
    - Witte (2002) reported a characteristic decrease in repeatability below superficial velocities of 10 ft/s for a series of gas ultrasonic meters. The meters used multiple ultrasonic paths, and were designed for use on 12-inch-diameter pipelines. The threshold for poor repeatability may vary with the size and design of the meter, and with the flowing fluid, but may be a consideration for the use of ultrasonic meters in measuring valve leakage rates.
    - Grimley (1996, 1998) attributed poor repeatability of several ultrasonic natural gas meters below 3.3 ft/s to the resolution of transit time measurements. For 12-inch meters, scatter exceeded ±1% at superficial velocities below 3.3 ft/s (a volumetric flow rate of approximately 9,500 scfm at the test conditions). For a typical 8-inch meter, the bias related to transit time measurement resolution was ±1.34% at 1 ft/s (about 270 scfm), and exceeded ±8% at 0.15 ft/s (about 41 scfm). The averaging performed by multipath meters reduced the scatter below that from single-path meters.

B.2 Passive Ultrasonic Techniques

The use of externally-mounted ultrasonic sensors to passively detect and quantify valve leaks has developed as a separate technology. Farstad and Creaman (1994) filed a patent describing a method to attach calibrated accelerometers to a pipe wall, measure acoustic pressure waves generated by a leaking valve, and estimate the magnitude of the leak through signal analysis. They advocated this approach over the use of microphones, which would need to be inserted into the flow through the pipe wall.

Using theory and dimensional analysis of laboratory test data, Farstad and Creaman identified several variables that influence the acoustic pressure level in a pipe flow downstream of a leaking valve:

1. The mass flow rate of fluid leaking through the valve.
2. The distance from the valve.
3. Time-averaged pressures upstream and downstream of the valve.
4. The inside diameter of the downstream pipe.
5. The effective diameter of the valve leak.
6. The composition of the fluid in the pipeline.

They proposed that the leak flow rate could be estimated if the other criteria are known.

In the field, the effective diameter of the leak through the valve is always unknown, but the method proposed in the patent accounted for this through an empirical relationship between the remaining variables. Background noise would be eliminated by the use of a band-pass filter. In the patent, a frequency band of 30 kHz to 40 kHz was advocated for detecting leaks in natural gas valves, but it was noted that acoustic energy levels tend to decrease with increasing frequency, so lower frequencies should be chosen where practical. The empirical relationship also required that the pipe sizes of interest have a large number of natural frequencies in the frequency band of interest so that Statistical Energy Analysis could be used, and that the location of the transducer would not be critical. A general schematic of the signal processing approach listed in the patent is shown in Figure B.2.

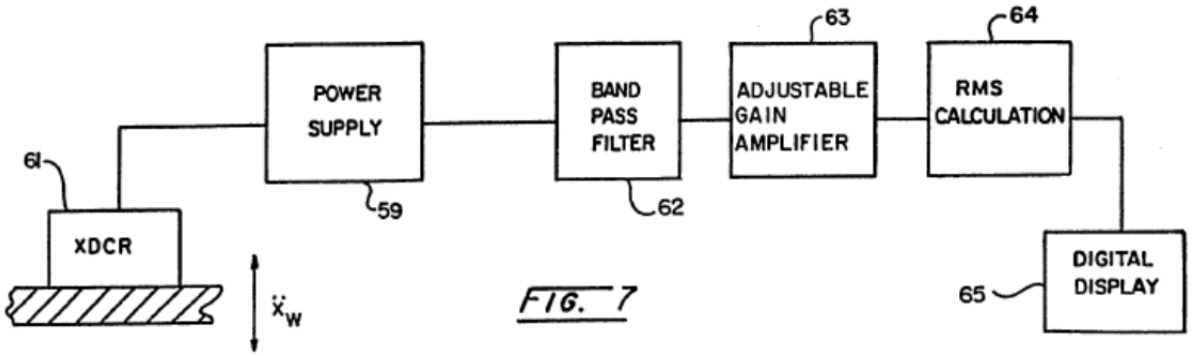

Figure B.2. General Schematic of Instrumentation for Measuring Flow Rates From Leaking Valves (Farstad and Cremean, 1994)

To apply the technique in field locations where access taps for microphones may not be available, a relationship was developed between pipe wall vibration and acoustic pressure, based on vibration measurement data at field installations. Sensors (such as accelerometers or acoustic sensors) should be chosen based on frequency response and sensitivity. The patent noted the need to securely bond the device to the pipe wall to eliminate relative motion between the pipe and sensor, and suggested the use of (1) adhesive bonding or (2) a threaded connection to a plate joined with silver solder to a flat surface on the pipe.

The patent noted that the leak flow rate predicted by the original method was only accurate to within a factor of two or three, but would be sufficient to determine whether valve repair or replacement is economically justified. However, the patent applicants encouraged modifications, such as the use of software algorithms to accept raw data and calculate leak flow rates.

The general principles described in the patent have been applied to a commercial sensor (ClampOn, 2009). As in the original patent concept, the ClampOn DSP Leak Monitor distinguishes ultrasonic leak noise from background noise, and uses a program with a database of field leakage measurements to convert acoustic readings leakage rates. The devices are available in versions for topside and subsea use, and can be used to detect leaks in either gas or liquid flows. Two subsea versions are available, depending on the required water depth. Published performance specifications of the devices are listed in Table B.1.

Table B.1. Published Performance Specifications for the ClampOn DSP Leak Monitor (ClampOn, 2008)

Principle of operation	Passive acoustic sensor
Flow regimes	Oil, gas, water, and multiphase flows
Minimum detectable leakage	0.1 l/min, liquid or gas
Minimum DP across leak for detection	Liquid: $\Delta P \geq 3$ bar across leak Gas: $\Delta P \geq 1$ bar across leak
Repeatability	1%
Pipe surface temperature limits	-40°C to 225°C (-40°F to 437°F); high-temperature fixtures available for pipes up to 500°C
Subsea design depth and pressure	Compact unit: 3,000 m, 333 bara (4,830 psia) Deepwater unit: 4,500 m, 675 bara (9,790 psia)

The topside version of the ClampOn monitor was recently tested on a 20" ball valve similar to those used on subsea installations (Instanes and Pedersen, 2008). Blind flanges were placed on both valve ports, and static pressure transmitters were mounted through each flange and on a vent port to the valve body cavity (Figure B.3). Before each test, the valve seat was intentionally damaged with a hand file. The blind flanges were put back in place, and the upstream side of the valve body was pressurized with nitrogen to induce leaks. Leakage rates were measured using a reference mass flow meter and the leak monitors, in conjunction with pressure measurements from the valve body.

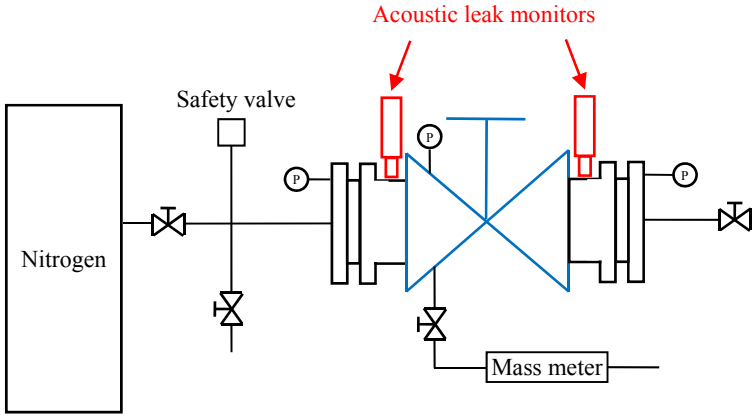

Figure B.3. Instrumentation Setup for the Leak Detector Demonstration Tests by Instanes and Pedersen (2008)

The sensors used in the tests carried a minimum required ΔP across the valve of 5 bar, though the commercial instruments with lower ΔP thresholds are available. Example comparisons between the reference mass flow meter and the ClampOn monitor are shown in

Figure B.4. Based on these results, the units were found to successfully measure gas leakage rates of less than 1 standard m^3/hr (0.59 scfm). However, the tests were performed with atmospheric air around the valve; for subsea, welded-in valves, some acoustic energy could be expected to escape to the water and reduce the signal level to the sensors. Under subsea conditions, higher detection thresholds were estimated, on the order of 42 standard m^3/hr (25 scfm) for a ΔP across the valve of 50 bar, and 27 standard m^3/hr (16 scfm) for a ΔP of 5 bar. The authors suggested varying the upstream pressure during leak monitoring, if possible, to increase the quality of data.

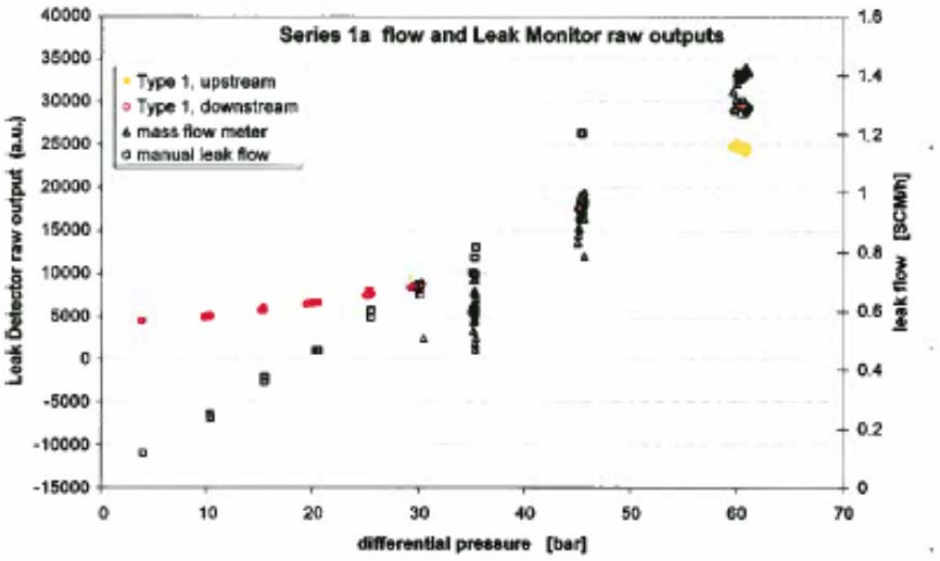

Figure B.4. Comparison of Reference Leakage Rate Measurements (Triangles and Squares) with Measurements by Acoustic Sensors (Instanes and Pedersen, 2008)

B.3 Level Detection

Level detection is based on measurement of the change in liquid level over time for a blocked-in region downstream of the test valve. Implementation of this technology would be dependent on the process fluid of the well at the time of testing. It would be required that the high-pressure side upstream of the valve being tested contain only one phase in order to provide a viable means of gauging leakage flow rates. However, downstream of the valve, a separated mixture of liquid and vapor should be present to provide contrast.

For cases where liquid is upstream of the valve, the region downstream could be injected with gas to give a negative pressure differential across the valve with respect to the normal direction of flow during production. If the valve leaked, the liquid level in the blocked-off section would fall. For cases with gas upstream of the valve, it would be necessary to have a liquid injection port in the blocked-in region. For a sufficient quantity of injected fluid, the pressure differential across the valve would become negative with respect to the direction of normal flow. After injection ceases, liquid levels would be monitored for any decrease that would indicate a leak through the valve.

One thing to note for level detection technology is that unless the pressure differential across the valve is maintained for the conditions that would be experienced during a failure, the rate of flow will tend to be altered. Thus, it would be difficult to provide a one-to-one

correlation with expected performance in case of emergency shut-down. This occurs with the current method employed by the industry as well. A pressure regulator on the gas injection line downstream of the test valve would allow for maintaining constant pressure in the blocked-in region during testing.

The first obvious manner of measuring liquid levels is simply through direct differential pressure monitoring. Two probes, one at the low side to measure vapor pressure above the liquid, and one at the high side located near the bottom to measure the liquid plus vapor pressure, are needed. The level of liquid is then obtained from the difference of the two pressure measurements. This technology is dependent on having a liquid with a known density. For oil/water mixtures, the reliability of the level measurement would be suspect if the relative ratios of each fluid are unknown. However, if the valve(s) upstream of the test valve were closed and methanol or a similar low-density liquid were injected to displace all other liquid, then when the test valve is closed liquid density would be known. Thus, for decreasing liquid levels a leakage volumetric flow rate could be computed. The accuracy of pressure differential measurements is along the order of ±0.065% of span (Emerson Level Measurement).

Other viable level detection technology alternatives considered as part of this study included float, capacitance, ultrasonic, non-contact radar, guided wave radar, and radiometric/gamma. Note that any system should include the ability to measure the pressure differential across the valve being tested, especially for the case of gas upstream of the test valve. If the pressure differential remained positive during the latter testing, it is possible that the liquid levels would not change, even if a leak developed, since the liquid would be incompressible compared to the gas. Thus, gas density in the blocked-off region would increase, while the liquid level could remain the same.

Like the previous differential pressure monitoring technology, magnetic or other types of float/displacer technologies are hampered by the fact that the fluid will not generally be a homogeneous mixture. Since the float is sized to the density of the liquid, the buoyancy force on it will differ for different density fluids (i.e., oil and water). Thus, without foreknowledge of fluid proportions, it is difficult to precisely relate float displacement to liquid level. Low density methanol injection could be used to first displace all other liquid in the blocked-in region, in the same manner as suggested for the differential pressure technology method of level detection. An advantage of employing floats is that such technology is not impacted by a foam interface. However, in general, their accuracy is not as good as other methods.

Liquid level detection based on capacitance operates for non-conductive liquids (e.g., hydrocarbons) by using a metal capacitance probe as one electrode, the metal wall of the containment vessel as a second probe, and the liquid as the dielectric. For conductive liquids, the metal probe must be insulated, and instead acts as the dielectric. Because the dielectric constants of water and oil are so different, this technology would not be suitable for such multiphase mixtures. Another potential issue with the technology for this application is that accuracy is only moderate compared to other technologies. For example, it is around ±5 mm for Endress Hauser products.

Measurements of reflected ultrasonic sound waves can have fairly good accuracies of about ±1 mm to 6 mm. However, pressure thresholds are generally specified to be below 250 psi (Boisevert 2006), which tends to limit their usefulness for deepwater well applications. Moreover, since temperature has such a high influence on speed of sound, accuracy is highly

dependent on the space between the sensor and the liquid remaining homogeneous (Schnake). Any foam on the surface of the liquid will also create measurement problems for the instrument. In summary, ultrasonic level gages are not ideal for the testing of safety barriers of subsea wells.

Non-contact and guided wave radar are both based on measurement of microwave signals, which (like other electromagnetic waves) travel at the speed of light in a vacuum. One large advantage of this technology for the present application is that ambient conditions (gas type, temperature, pressure, humidity) have little effect on measurements. Additionally, accuracies up to ±0.5 mm can be achieved (Schnake). Non-contact, as the name implies, requires no physical contact with the liquid interface in order to determine measurements. However, this configuration requires the liquid to have a minimum dielectric constant of about 1.5. Note that petroleum oil has a dielectric number of approximately two. This is rather close to the lower limit, and could create problems. Furthermore, foam at the gas-liquid can also be problematic for this technology. Guided wave radar still depends on microwave signals, but guides these using a flexible cable or rod contacting the liquid. This measurement technique works better for liquids with lower dielectric constants, as well as for applications with foam. Shown below is a schematic of a potential method of using this technology to evaluate the leakage rates of valve safety barriers. Retrofitting of existing wells could be carried out by attaching the small chamber to the side of the wellbore with valves to allow the liquid level in the chamber to equilibrate.

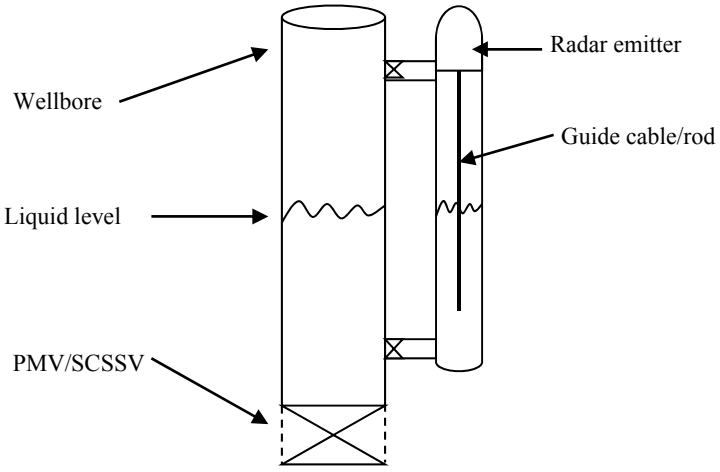

Figure B.5. Level Detection Conceptual Arrangement

Another technique is radiometric level measurement. Instead of microwaves, gamma ray signals are emitted and received to determine liquid height in a vessel. A primary advantage of this technology is that it can be completely non-invasive, with all equipment located external to the container. However, the significant disadvantages of dealing with the safety concerns arising from nuclear source material and high capital costs may hinder widespread adoption of this technology.

B.4 Tracer

A tracer may be defined as any detectable substance added to a chemical, biological, or physical system in order to follow its process or to study its distribution in the system. The technology is based on the assumption that addition of the tracer particles does not affect the chemical or physical properties of the system. Instead, they are meant to be passively carried

along with the media being transported and/or dispersed. A number of detection methods are available for which appropriate tracer particles may be selected based on desired properties. These include optical, chemical, electrical, magnetic, or radiation detection.

In reference to leak testing of safety barriers, the first thing to note is that tracers injected upstream of closed test valves will tend to disperse backwards into the process fluid as time progresses if their density is comparable to or greater than the process fluid (gas or liquid). Thus, quantitatively linking tracer concentration to flow rate would be difficult when initial concentrations are constantly changing. Downstream of the test valve, the flow must be blocked in to allow concentration levels of tracers to rise with time and provide a reliable means of volumetric flow rate. A second concern is that tracer concentrations in this blocked-in region may not be spatially homogeneous, since dispersion of the particles is a finite rate process and high-concentration tracer fluid leaked from the test valve can continually flow into the fixed volume with different rates and velocity profiles. Therefore, it is not clear where fluid samples could be taken to adequately represent a bulk concentration level. A solution to the two issues listed above would be to use tracers and suspension fluids that are less dense than the process components. This would produce results similar to the schematic shown below. Light tracer gas may be injected upstream of the test valve in sufficient quantities to cover the entire seat of the valve where leaks could occur. Assuming homogeneous suspension of tracer particles in the injected gas, concentration levels should remain constant in any leaked fluid. Gas leaked through the valve will then be lifted by buoyancy force toward the upper region of the blocked-in volume.

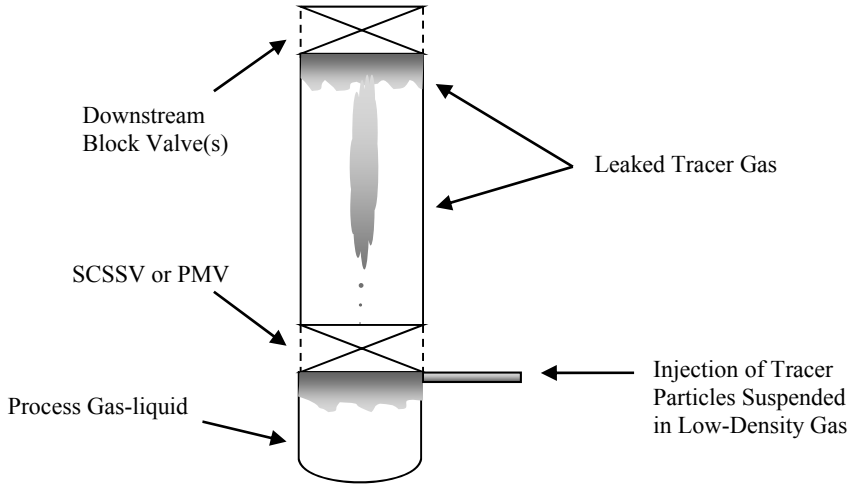

Figure B.6. Conceptual Arrangement of Tracer Leak Detection

Optical detection of tracers would be difficult to perform at the pipe itself. High-resolution cameras might be employed in conjunction with fluorescing tracer particles. However, cameras would need access to the entire region where the low-density particles will tend to collect in order to ascertain the total volume. Additionally, pressure and temperature conditions within the blocked-in volume must be held constant in order to keep the density of the tracer gas from changing – thereby changing the volume of the leaked fluid. From a practicality and time-management standpoint, siphoning off samples at the top of the blocked-in section and sending them to the surface for analysis is not realistic. Similarly, chemical tracer detection would likely require samples be taken to the surface for mass spectroscopy or other forms of analysis. Electrical tracers would be problematic, since there would be unknown quantities of

water either mixed with oil or in wet gas. The dielectric constant of water is quite high, being near 80. This would be likely to confuse readings unless samples were individually calibrated for percent water concentration. Magnetic tracer detection methods may also tend to be influenced by water concentration, and tracer particles are, in general, too large for such an application. In summary, none of the discussed tracer technologies up to this point are good candidates for accurately and efficiently determining leakage flow from barrier valves.

Radioactive tracers are the most widely used among all industries. They are commonly employed for medical applications to show the rate and location of uptake into various organs and glands. They are also used in botany to show the path of water or minerals. The oil industry utilizes them as a means of custody transfer. For example, different oil companies share pipelines, and each is assigned a radioactive tracer. Technicians downstream monitor radiation levels to determine when oil from a different company begins to pass their station.

Advantages of radioisotope detection include high sensitivity in low concentrations compared to nonradioactive isotopes. Additionally, it is possible to perform concentration measurements noninvasively using detectors outside the main process line. These could easily be arranged to target the upper region of the blocked-in volume where they would be expected to collect. Since radiation detection is based solely on intensity of radiation particles, changes to temperature/pressure of the suspension gas are not important. Radioisotopes have potential health hazards, however, and are expensive to track and dispose of. Particular tracer species can be selected based on a minimum required half-life for testing in order to mitigate hazards to personnel and the environment. Overall, radioisotopes represent the most feasible option for tracer technology in this application.

APPENDIX C

Computational Fluid Dynamics (CFD)

COMPUTATIONAL FLUID DYNAMICS (CFD)

The purpose of this appendix is to provide documentation of the efforts in utilizing CFD to study wellbore behavior. Results for various models are described here in detail.

C.1 Steady-State Thermal Model

Figure C.1 shows a steady-state thermal model that is the first step for CFD modeling of SCSSV wellbore behavior. Results from this simulation were needed as initial conditions for the thermal profile of the solids at the onset of well shut-in. These results were also used as a baseline for checking that the modeled diameter of the formation rock is sufficient for avoiding any boundary effects.

To set up the steady-state model, the fluid region was removed from the domain, leaving the left boundary to be the inner wall of the steel tubing. This temperature was specified as 50˚C since the fluid temperature prior to well shut-in has a relatively constant value near that of the reservoir temperature. Figure C.2 provides an illustration of the domain setup. An element-based finite volume method was used for solution of the system of equations generated through domain discretization. Specifically, the ANSYS high-resolution advection scheme (ANSYS, 2010) was employed. Double-precision was used for all calculations. A stringent RMS residual target of 10^{-10} was specified for the steady-state convergence criteria.

The temperature contour results from the steady-state case are shown in Figure C.2. As expected, the temperature remains high near the fluid-solid boundary, decreasing towards the far field formation rock. The highest thermal gradients are located in the upper left corner where the seabed and fluid-solid boundary meet. Since the reservoir and fluid temperatures are comparable, the gradients are relatively low near the bottom of the domain. Results from the steady-state thermal model are used as initial condition input for subsequent cases.

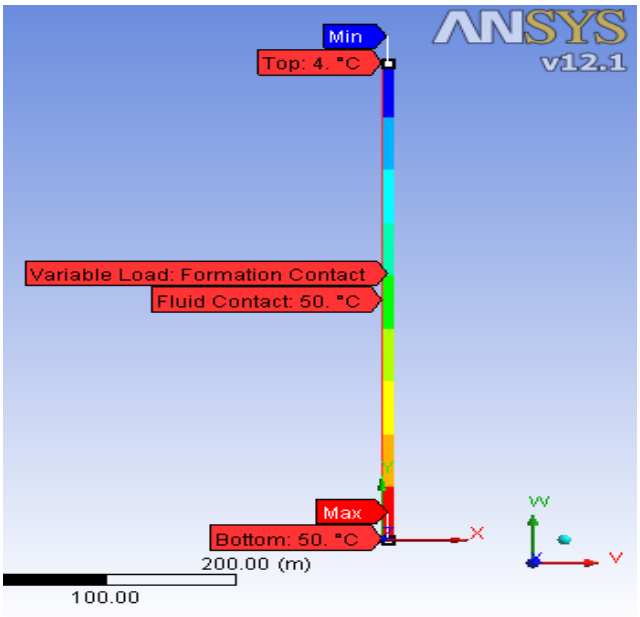

Figure C.1. Thermal Boundary Conditions of Steady-State Model
For the steady-state thermal model, the fluid regions are removed and a 50˚C constant temperature is enforced at the tubing wall.

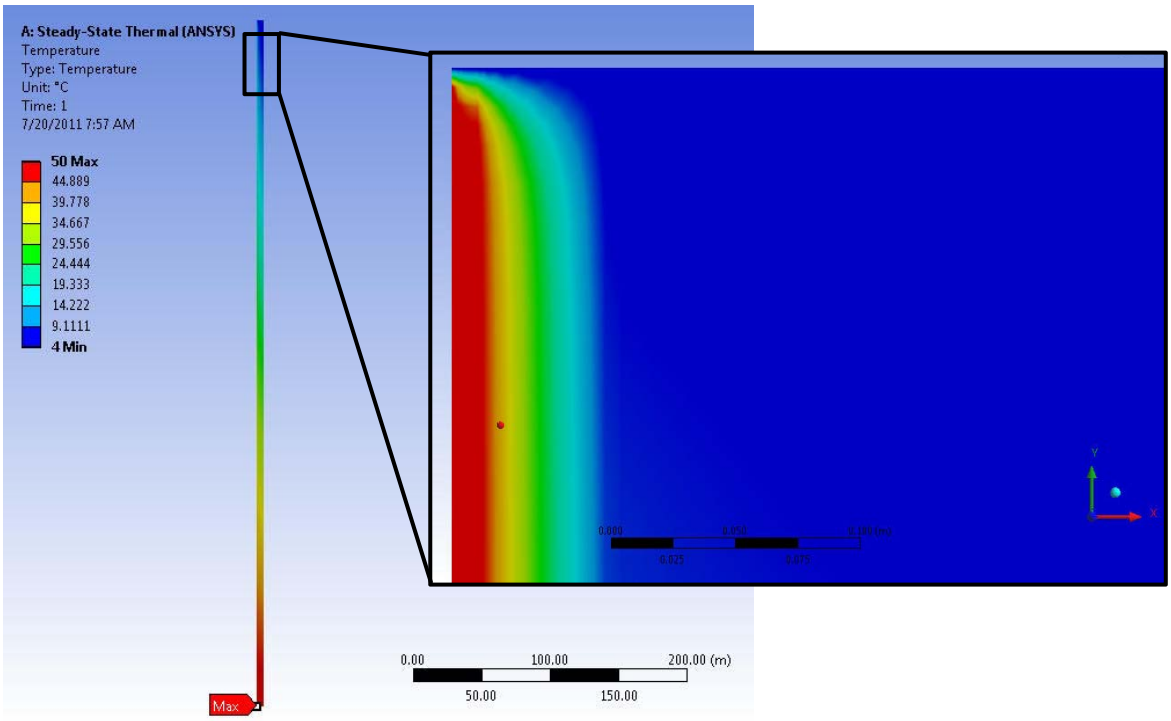

Figure C.2. Steady-State Thermal Model Temperature Contours
Results show a sharp drop in temperature near the top in comparison to the remaining region near the solid/fluid boundary.

C.2 Static Column Model

The next level of complexity added to the solution was to model a static column of oil in addition to the solid layers. The purpose of this model iteration was primarily to ensure that boundary effects were not influencing pressure results within the fluid region, and to act as a baseline case for comparison of varying well gas volume fractions (GVFs). Conjugate heat transfer between the solid-liquid phases was incorporated. Results from the steady-state thermal model were used as initial conditions for the solid regions, and the entire fluid region was initially set to 50˚C. This set of conditions mimics expected thermal profiles of a well that was running for a long period prior to shut-in.

The geometry of the current setup leads to unique spatial discretization challenges. While the domain is a total of 500 m long, it is only 5.146 m wide. Additionally, the thinnest layer is only 10.4 mm thick. Attempts to use the ANSYS automatic mesh generator to produce an unstructured mesh of the domain either failed or produced discretizations having an unfeasibly-large number of cells. Thus, it was decided to use a structured grid with mapped faces. In order to adequately resolve each layer, a minimum of three cells was specified to be used in the x-direction. This structure leads to a cell edge length minimum of 3.45 mm. Since using a uniform distribution would require 1,492 x-direction divisions, grid stretching was used as shown in Figure C.3.

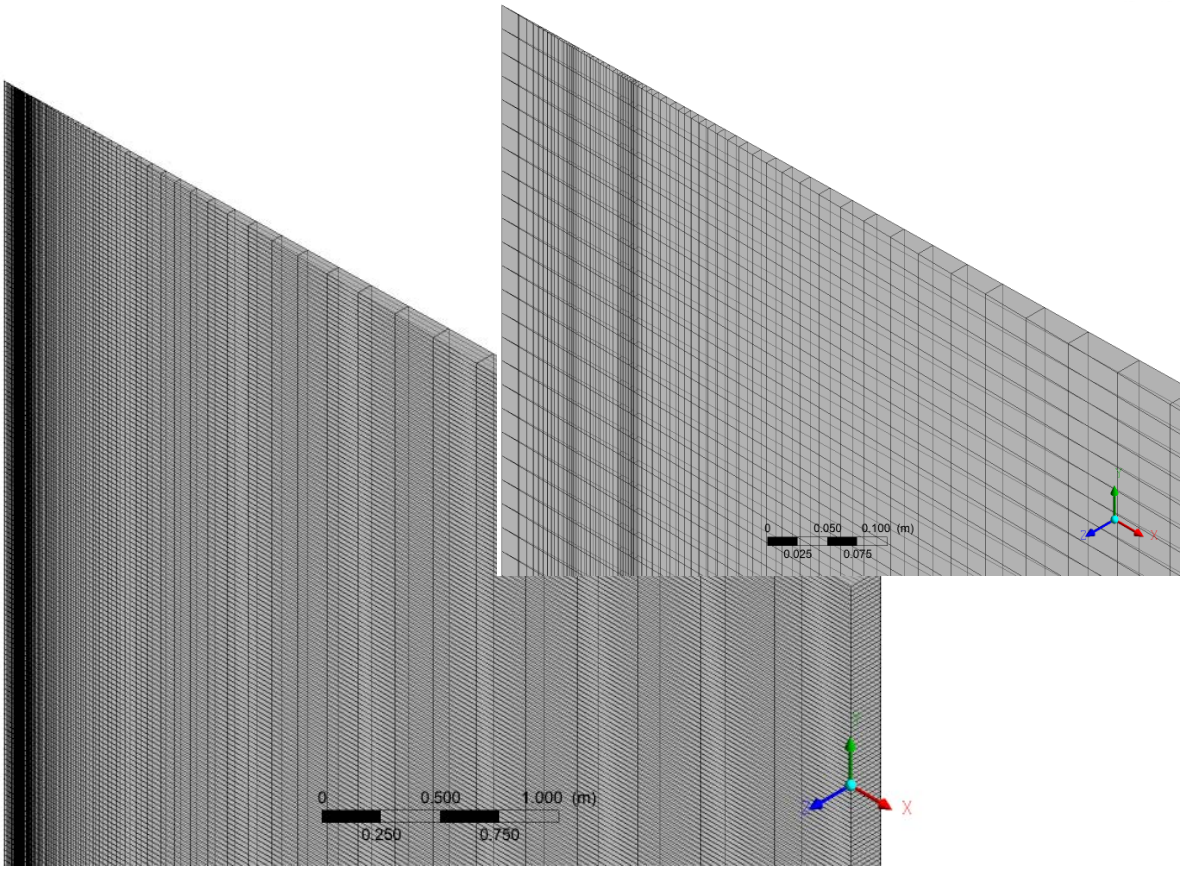

Figure C.3. Mesh at Top of Domain – Isocontour Views (Inset is Zoomed Version)
The mesh is stretched within each layer in the x-direction to provide adequate resolution, while minimizing the number of cells required.

Ideally, discretization in the y-direction would produce cells with aspect ratios close to one. Large aspect ratios can create convergence issues and lead to mesh-dependent solutions. However, specifying a low aspect ratio everywhere for the current problem would create a number of cells so high that obtaining a solution would become impractical. Therefore, stretching was used in the y-direction as well to keep aspect ratios relatively low near the top and bottom boundaries (see Figure C.4). Since gradients are low in regions with the highest aspect ratios, discretization errors are minimized while allowing for a significant reduction in the number of required computational cells. A resolution study increasing the grid density approximately 50% indicated that solutions were relatively grid-independent.

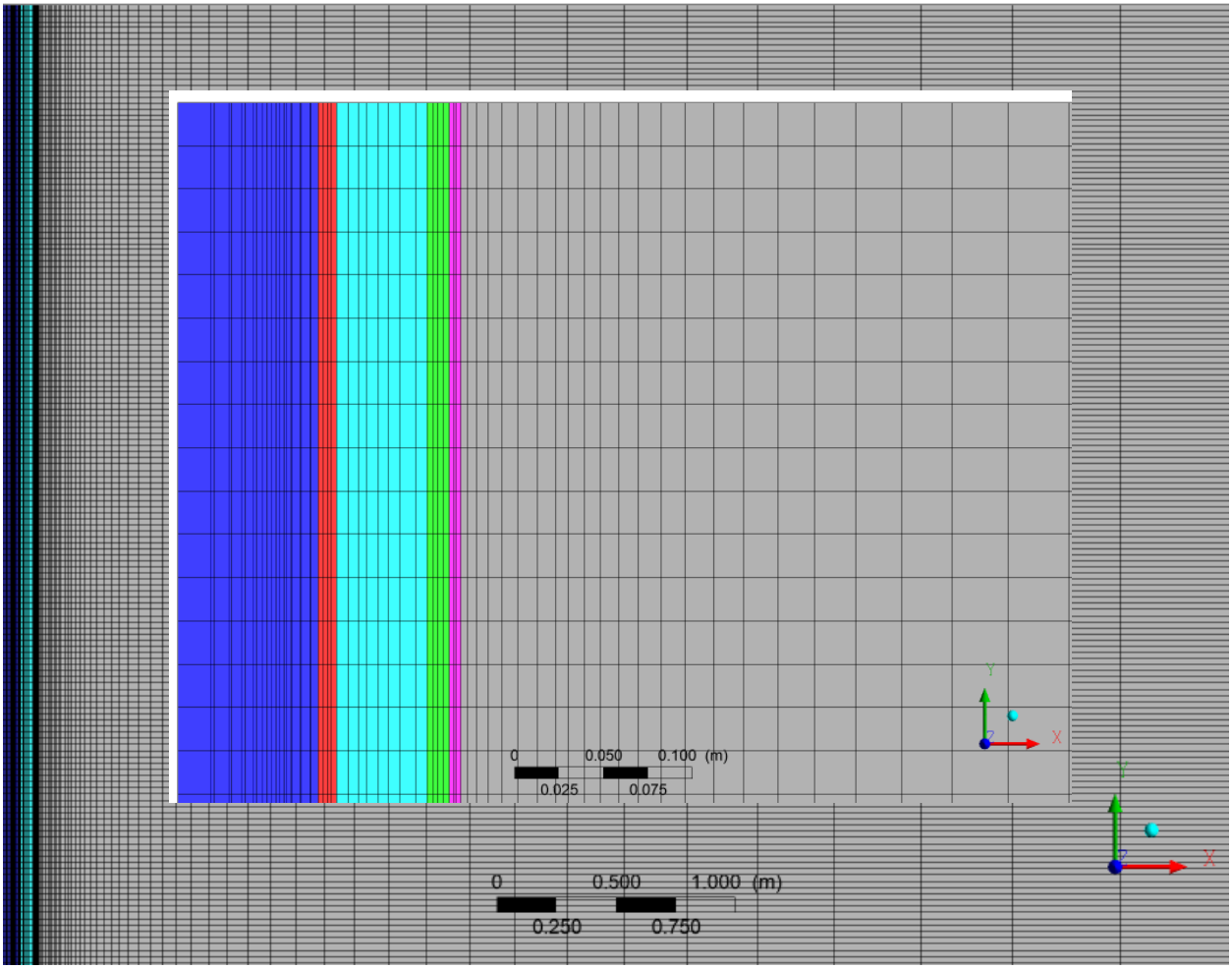

Figure C.4. Mesh at Top of Domain – Side Views with Color-Coded Layers (Inset is Zoomed Version)

Mesh stretching in both the x- and y-directions leads to localized regions of high aspect ratios. These are avoided in regions of expected high gradients.

Since the static column model has 100% oil in the fluid domain, no multiphase sub-models were needed for the simulation. However, a model for buoyancy was incorporated. The effect of shrinkage due to cooling was captured through the thermal expansion coefficient β. The absolute pressure is computed as the sum of the momentum equation contribution, any reference offset, and the hydrostatic pressure, i.e., $\{P_{abs} = P_{mom} + P_{ref} + \rho_{ref} g(z - z_{ref})\}$. The buoyancy influence comes through the momentum equation, to which is added the source term: $\{S_{M,buoy} = (\rho - \rho_{ref})g\}$. Since the liquid was treated as incompressible, the Boussinesq approximation was applied to treat the local gravitational body force through the fluid as a linear function of β and the local temperature difference, i.e., $\{S_{M,buoy} = (\rho - \rho_{ref})g = -\rho_{ref}\beta g(T - T_{ref})\}$. For this single-phase simulation, this is a reasonable assumption.

The static column model was initialized in the solid domain using the steady-state temperature profiles computed previously, while the fluid was set to 50˚C. The ANSYS CFX high-resolution advection scheme (Tannehill et al., 1997) was again employed for spatial

solutions, and a second-order backward Euler implicit transient scheme was used. An RMS residual target of 10^{-6} was specified for the steady-state convergence criteria, and a maximum of ten convergence loops was allowed at each time step. The temporal resolution was initially set for a constant time step, Δt=5 sec. This value was chosen based on the assumption that the simulation would be primarily conduction-dominated. An estimate based on explicit scheme stability of the 2-D heat equation (Tannehill et al., 1997) is $\Delta t \leq \frac{1}{2\alpha}\left[\frac{1}{(\Delta x)^2}+\frac{1}{(\Delta y)^2}\right]^{-1}$, where α is the thermal diffusivity $\alpha = \frac{k}{\rho c_p}$. Using the most conservative conditions of the smallest cell edge lengths and largest material thermal diffusivity, Δt ≤ 0.6 sec. Based on the smallest cell, Δt ranged from 0.6 sec to 94.3 sec, depending on the material. Since implicit schemes generally run at much higher time steps than explicit, it was felt that 5 sec was more than adequate for temporal resolution.

Calculations were carried out for a total simulation time of two hours based on the assumption that it would take one hour to complete the testing of the wellhead, and one subsequent hour for the SCSSV test. It was observed that during some time steps that the solution failed to reached the specified convergence criteria within the prescribed ten iterations. This indicated that the quality of the results might be poor. Temperature profile results after two hours are shown in Figure C.5(a), which confirm this assessment. One-dimensional temperature profiles taken approximately at the midpoint of the indicated layers are plotted over the entire height of the wellbore. Multiple unphysical inflection points in the profiles appear. It was hypothesized that the convergence issues could be due to temporal resolution if the time step was driven by changes in the local velocity field rather than being conduction-dominated. Thus, an adaptive time step allowing for Δt in the range from 0.1 sec to 5.0 sec was implemented, and the simulation was rerun. During the entire simulation, the time step remained close to 0.1 sec, and produced the temperature results shown in Figure C.5(b). Again, a high level of error is indicated by the unphysical inflection points in the data. Several other simulations that varied time step and/or mesh resolution were attempted with similar results.

(a)

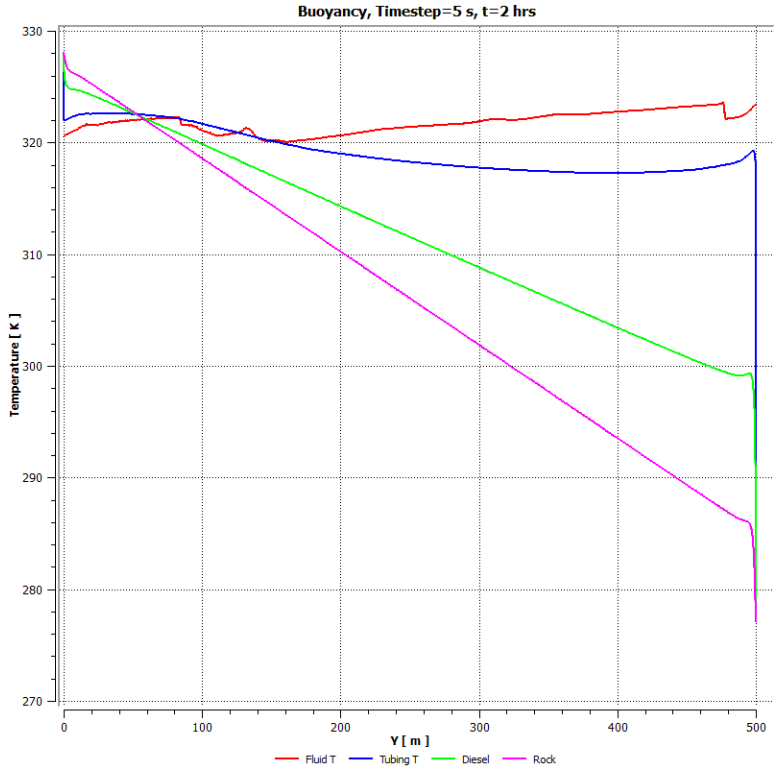

(b)

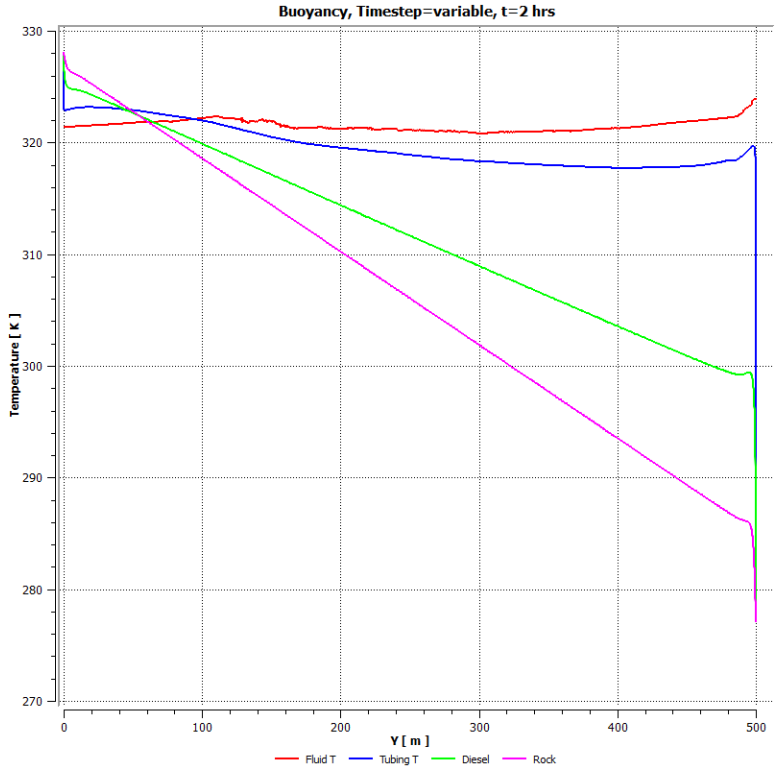

Figure C.5. 1-D Temperature Profiles of Static Column using Boussinesq Buoyancy Model
For cases using both a constant time step of 5 sec and a variable time step ranging from 0.1 sec to 5.0 sec, unphysical inflection points indicated unacceptable error in the solution.

Diagnostics of the static column model have been carried out to determine the cause of the errors in the numerical solution. It was found that removing the Boussinesq model, $\{S_{M,buoy} = 0\}$, produced expected temperature and pressure trends. One-dimensional temperature profiles for this computation are shown in Figure C.6. Essentially, the problem stemmed from the fact that the computer code could not handle the pressure response due to volume reduction in a closed domain. If the top wall that represents the wellhead is opened, the simulation runs without any convergence issues while the Boussinesq model is activated.

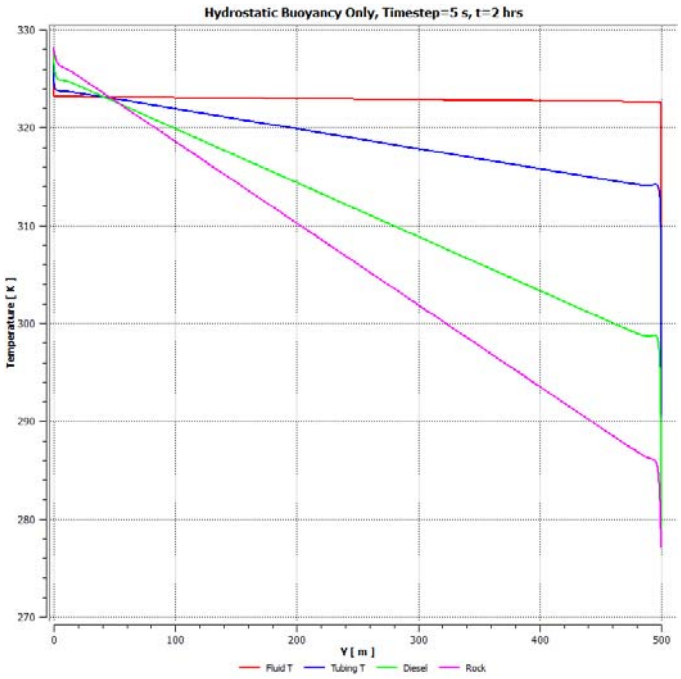

Figure C.6. 1-D Temperature Profiles of Static Column using Hydrostatic Buoyancy Only
Using the hydrostatic pressure contribution without the liquid shrinkage contribution produced expected pressure and temperature results.

Since the static column model consists entirely of oil that is assumed to be incompressible over the distance of the wellbore, results that consider only hydrostatic effects on pressure and ignore shrinkage were deemed acceptable. These results can be employed for comparison with multiphase wellbore cases. They have also been used to verify that the 5-m formation is sufficiently thick, such that the heat loss from the fluid does not influence the temperature profile near the right boundary after two hours. It should be noted, however, when advancing to the zero-leakage model, the buoyancy source term on the momentum equation cannot be neglected. To illustrate this point, assume a well contains oil and methane that uniformly drop 5°C:

- 70% GVF Case: Assuming a uniform ΔT=5 K drop in fluids, the pressure decrease in gas due to expansion-only from liquid shrinkage is 0.32 bar, while the cooling-only effect reduces the pressure 2.3 bar *(effect is 7.25 times larger)*.
- 5% GVF Case: Assuming a uniform ΔT=5 K drop in fluids, the pressure decrease in gas due to expansion-only from liquid shrinkage is 13 bar, while the cooling-only effect reduces the pressure 2.3 bar *(effect is 5.5 times smaller)*.

To summarize, this section has discussed the setup, challenges, and results associated with modeling a static column of oil with no leakage. Due to software limitations, it was not possible to incorporate liquid shrinkage effects in the computations. However, results of the case incorporating hydrostatic pressure behaved as expected. A brief resolution study carried out to a simulation time of ten minutes was used to check the mesh-independence of results. It was also verified that the thickness of the formation rock layer was sufficient to avoid any boundary influence. Providing a source of comparison for future multiphase results, along with verification of the rock thickness domain extents, were the achieved goals for this model.

C.3 Zero Leakage Model

The next model in the path of increasing complexity was the zero-leakage model. The purpose of this model was to serve as a benchmark for future cases that introduce leakage. The setup was similar to that of the static column model, except instead of an oil-only column of fluid there are both oil and methane gas present. Since it is assumed that the phases are segregated, the oil is initially specified at the bottom and gas at the top with a zero-thickness phase boundary. The mesh is stretched in the y-direction to provide higher resolution at the top, bottom, and at the phase boundary. Velocities were initialized to zero throughout the fluid domain, pressure at the top of the fluid domain was set to 100 bar, and temperature is set to 50˚C for both fluids.

Appendix D outlines early efforts to model the zero-leakage case in CFX, and later in FLUENT. The remainder of CFD efforts outlined in this section was executed utilizing FLUENT under fluid-specific models, 1) the oil utilized the Boussinesq buoyancy model and was specified as incompressible; 2) methane was modeled using the ideal gas equation of state. It is assumed that any fluid motion during the simulation is laminar; thus, no turbulence sub-model is specified. The volume-of-fluid (VOF) multiphase flow model was employed. In brief, the VOF method is based on solving a single set of momentum equations, and tracking the volume fraction of each of the fluids throughout the domain. Interface tracking was accomplished through the solution of a continuity equation for the volume fraction of the secondary phase (liquid in the present case).

The baseline case that will be used to compare leakage simulations was specified with the following conditions based on operator input: 20% gas volume fraction (GVF), a reservoir temperature of 50˚C, and a pressure directly below the PMV equal to 100 bar. The simulation was set up using the geo-reconstruct interface algorithm, while spatial and temporal resolution remained similar to that used for the previous subsection. Note that for this case though, axial grid stretching was set up to more highly resolve the gas-liquid interface, in addition to the boundaries. The simulation was carried out to two hours of simulation time, which required approximately seven days of wall clock time using eight processors and a constant time step of Δt=0.1 sec.

Temperature profiles are plotted versus axial distance in the graph of Figure C.7(a). Note that the fluid domain cut was taken radially halfway between the axisymmetric and tubing boundary. Likewise, cuts through solid material domains were also taken at radial halfway points. Subsequent plots in the report follow this system as well.

The temperature of the fluid in Figure C.7(a) shows a sudden drop between the liquid and gas interface at approximately 400 m. This behavior was expected due to the significant disparity of specific heat in the oil versus methane. With a viscosity about 42 times smaller than

that of oil, the methane cools much more quickly. As shown in Figure C.7(b), the phase interface remains sharp after two hours of simulation with the geo-reconstruct algorithm. It should also be noted that the phase interface drops approximately 0.4 m between the first and second hours of simulation. This behavior is due to shrinkage of the liquid column from cooling, modeled using the Boussinesq approximation.

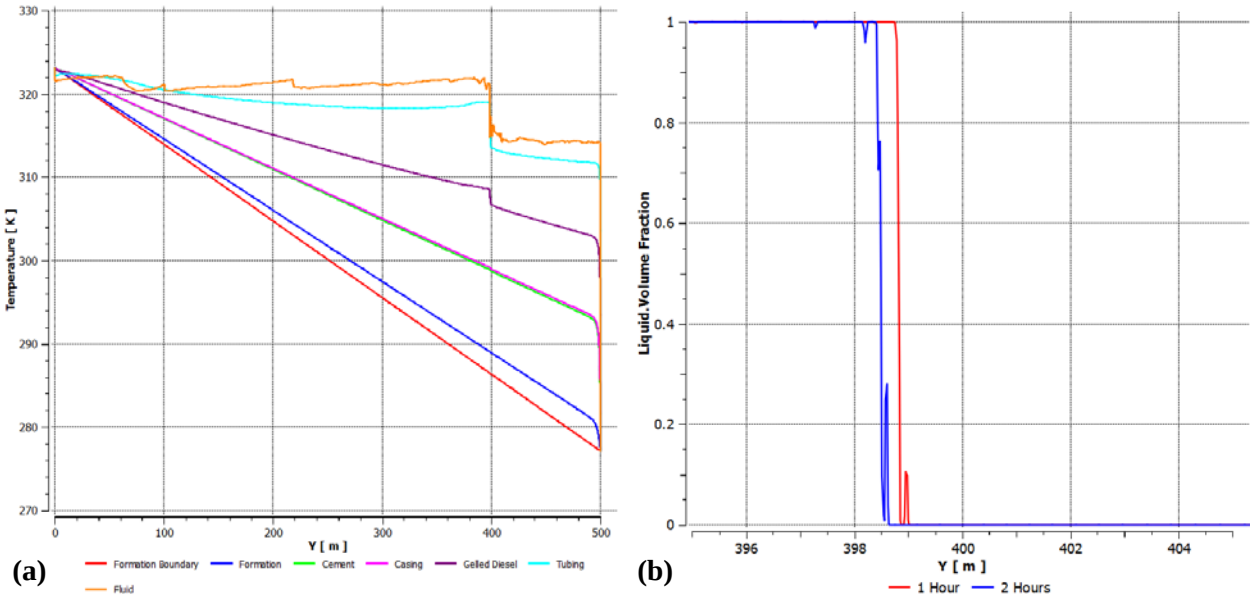

Figure C.7. Criteria Profiles for No-Leakage 20% GVF Case: (a) Temperature at Two Hours, (b) Liquid Volume Fraction at One Hour and Two Hours

Temperature in the fluid domain is shown to drop significantly at the phase interface around 400 m. The phase interface boundary remains sharp, dropping about 0.4 m during one hour of cooling.

Figure C.8 provides a comparison of various criteria at one-hour and two-hour time points in the simulation. From Figure C.7(a), it may be observed that there are some fluctuations in temperature throughout the liquid. A comparison of fluid temperature at one and two hours is offered in Figure C.8(a), which shows such fluctuations persist throughout the simulation. However, these are due to the fact that total/stagnation temperature is plotted, which includes both static and dynamic contributions. The total temperature is computed from the total enthalpy, defined as $h_o(T_o) = h(T) + \frac{1}{2}v^2$, where v represents the velocity of the fluid. Note from Figure C.8(b) that the fluctuation trends in temperature of the liquid approximately follow those of the velocity magnitude.

Figure C.8(c) presents the relative pressure profile through the fluid domain at one and two hours. The relative pressure linearly increases through the liquid section due to hydrostatic pressure. Height shrinkage from liquid contraction was approximately 0.4 m, leaving the liquid height at about 399.6 m. The expected hydrostatic gradient, $\Delta P = \rho g h$, was 33.3 bar for a liquid columnar height of 399.6 m. This result is fairly close to what is seen on the relative pressure profile, which is about 31 bar (a difference of approximately 7%).

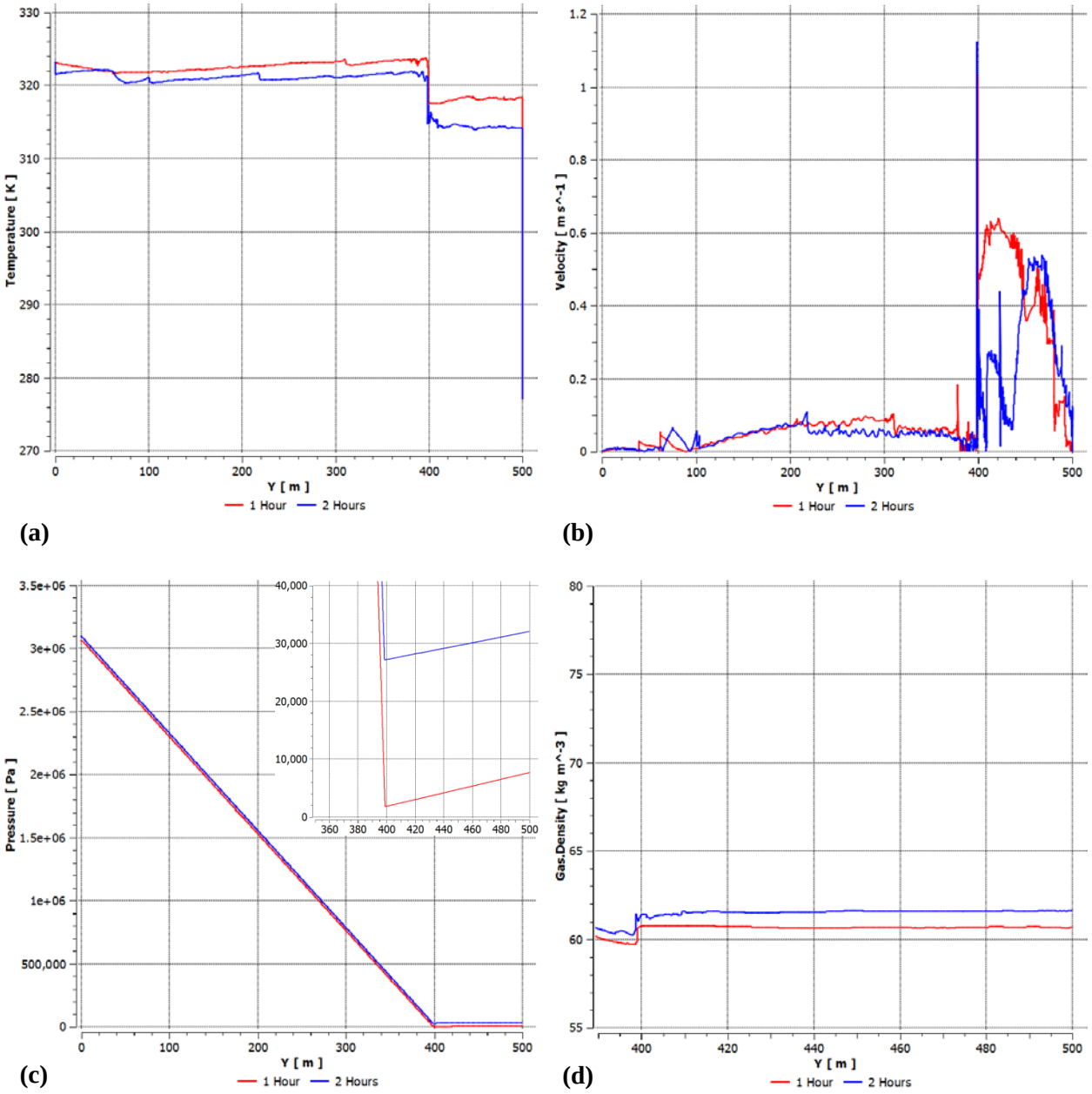

Figure C.8. Criteria Profiles for No-Leakage 20% GVF Case at One Hour and Two Hours: (a) Temperature, (b) Velocity Magnitude, (c) Relative Pressure, and (d) Gas Density

Total temperature of the liquid displays some localized fluctuations due to dynamic effects. Temperature and gas density remain relatively constant throughout the gas region. Pressure linearly increases with depth through the liquid due to hydrostatic forces. Pressure rise with time is due to "artificial mass" creation from solution of the continuity transport equation.

From Figures C.8(a) and (d), the density and temperature remain relatively constant throughout the gas section. The temperature drops significantly to seafloor temperature only near the boundary itself. Unlike the linearly decreasing profiles of the solid domains, mixing from natural convection in the gas keeps the temperature relatively constant. Zooming in on the gas section, it is observed that the relative pressure in Figure C.8(c) slightly increases spatially as it approaches the cooler region near the wellhead at the top of the domain (0.05 bar increase at

two hours). Since the temperature and density remain relatively constant, gas pressure would likewise be expected to be steady. It was found that if the gravity of the simulation was turned off, the gas pressure did not rise spatially. The slight spatial decrease in gas pressure may be an artifact of the calculation model and/or grid density. However, since the primary interest is in change from baseline conditions due to leakage, it was deemed impractical to make modifications that significantly increase computational time to remove this anomaly.

A second item to note from Figure C.8(c) is that the overall pressure increases with time through the gas, though the interface moves down to allow the total gas volume to expand from liquid contraction and the temperature of the gas cools by as much as 4˚C. According to the combined gas law for an ideal gas of fixed mass, $\left(\frac{PV}{T}\right)_1 = \left(\frac{PV}{T}\right)_2 = \text{constant}$. Thus, if the available volume for the gas increases while the temperature decreases, it would be expected that the pressure would decrease to compensate. The density also displays surprising behavior. Assuming the mass of the gas is fixed, due to the increase in available volume with time, it would be expected that the density would decrease. This result is not what is observed in Figure C.8(d).

Upon investigation, it was found that the counter-intuitive trends are due to residual levels in solution of the continuity transport equation allowing generation of "artificial mass" within the domain. Reducing the time step by an order of magnitude to 0.01 sec, while allowing up to 100 subiterations of the transport equations at each time step, reduced the scaled continuity residual by two additional orders of magnitude. This approach resulted in pressure and density dropping with time as the gas cooled, since "artificial mass" resulting from the solution procedure was produced with time at a significantly reduced rate. However, using eight processors, it was estimated that completion of the simulation out to two hours would require on the order of 100 wall clock days. Since obtaining the change in pressure between leakage and non-leakage cases is again the objective, it was deemed practical to allow the same rate of "artificial mass" generation for leakage cases and compare results after the same duration of simulation time. Though this scenario is not ideal, it was thought that such methods would still allow insight into leakage modeling while maintaining a reasonable timeframe.

C.4 Leakage Cases

Liquid Leakage

Two cases of oil leakage through the SCSSV are considered in this subsection. The first has a leakage rate of 400 cc/min, while the second is set to 800 cc/min. Note that in both cases, the leakage is simulated through specifying the bottom boundary with a mass inlet condition. For both simulations, the setup criteria for the cases include 20% GVF, 100-bar pressure (below the wellhead), and a reservoir temperature of 50˚C. The first hour of simulation is the same as that of the simulation in subsection 0, emulating the time taken to first check the PMV. Leakage then begins after the first hour, and continues out to two hours.

400-cc/min Leakage Rate

Since industry practices (API 14B) state 400 cc/min as the limit of allowed SCSSV leakage in-situ, this case is first evaluated. The leakage rate needs to be specified in terms of a mass inlet for the boundary condition, so the 400 cc/min is converted to "kg/s" units, and then divided by 360 (since only a 1˚ slice is being used). Multiplying by the specified 850 kg/m^3 density of oil, the mass flow into the bottom boundary may be written as 1.57e^{-5} kg/s.

Leakage of 400 cc/min over a one-hour duration, given the inner tubing ID of 6.184 inches, would be expected to give rise to an increase in liquid height of 1.2 m. Figure C.9 shows the vertical location of the phase interface between the: 1) zero-leakage case at two hours and 2) leakage case after the first hour. Comparing the leakage versus zero-leakage cases at two hours, it is seen that the phase interface rises by about 0.6 m. Since resolution is of the order of the absolute error (~ 0.3 m to 0.6 m), the quality of the results is deemed acceptable.

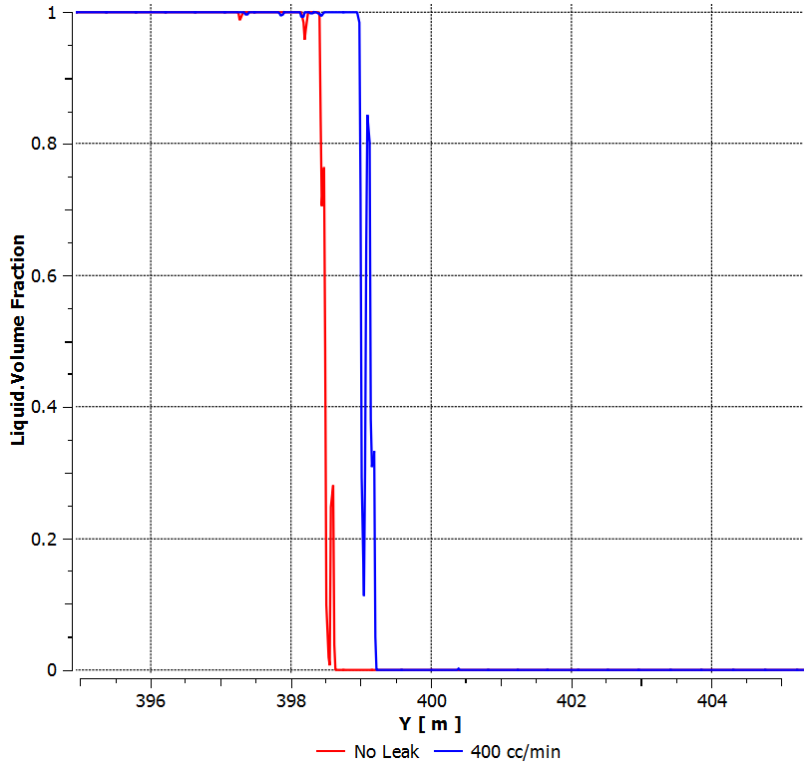

Figure C.9. Volume Fraction Profiles for 20% GVF Cases at Two Hours: No Leakage and 400-cc/min Leakage after the First Hour.
Phase interface location increases about 0.6 m comparing the leakage versus zero-leakage cases at two hours.

Figure C.10 indicates the change in relative pressure undergone as a result of leakage. As shown, the pressure rises approximately 0.76 bar at the phase interface in response to the leakage when compared to the case at two hours with zero leakage. Analytically, if the change in height of the gas phase due to liquid leakage were 0.6 m it would be expected that the change in gas pressure would be about 0.6 bar, assuming ideal gas and no change in temperature. This pressure may be computed from $\frac{P_1}{P_2} = \frac{V_2}{V_1} \rightarrow \frac{P_1}{P_1+\Delta P} = \frac{V_1+\Delta V}{V_1} = \frac{h_1+\Delta h}{h_1}$, where the change in height Δh is 0.6 m, the initial height of the gas column is 100 m, and the initial pressure of the gas is

100 bar. Since the idealization of no change in temperature is not strictly true, as shown by Figure C.11(a), the pressure rise of 0.76 bar indicated by Figure C.10 is not unreasonable. Figure C.12(c) also shows the result of liquid leakage on the density of the gas. With decreased volume for the gas mass to occupy, the density increases.

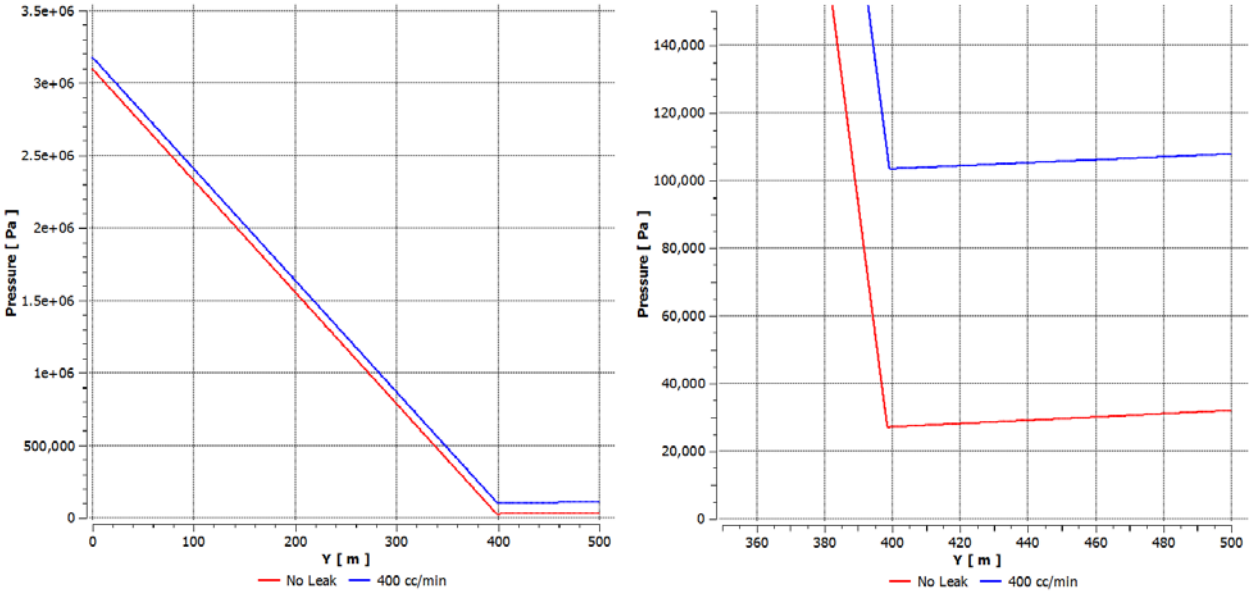

Figure C.10. Relative Pressure Profiles for 20% GVF Cases: No Leakage at One Hour, No Leakage at Two Hours, and 400-cc/min Leakage after the First Hour

Pressure increases about 0.76 bar in both liquid and gas sections as a result of leakage over one hour.

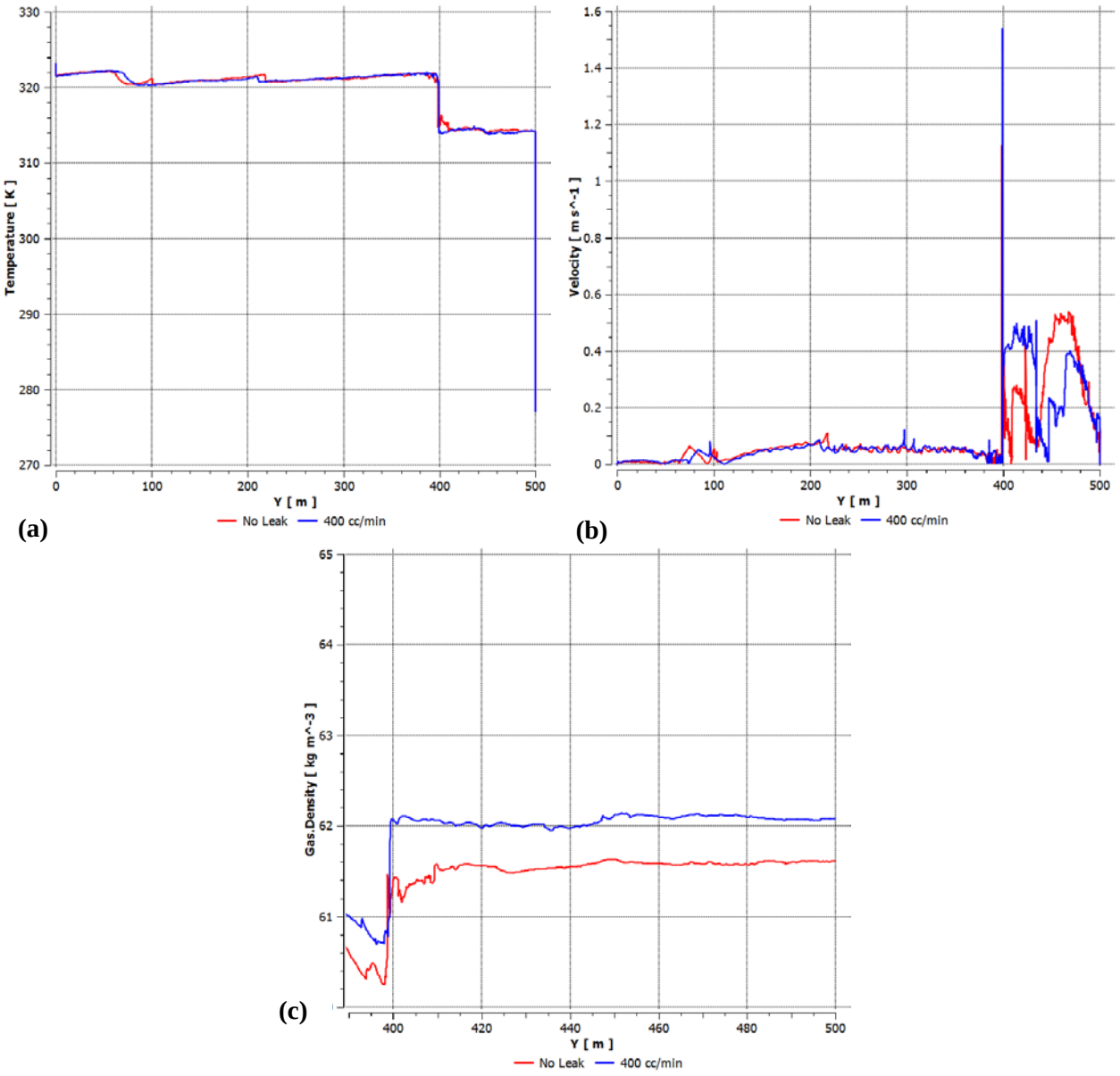

Figure C.11. Criteria Profiles for 20% GVF Cases at Two Hours: (a) Temperature, (b) Velocity Magnitude, and (c) Gas Density

Temperature profiles show leakage does not affect domain temperature substantially. Gas density profiles indicate a density increase with leakage resulting from volume reduction.

800-cc/min Leakage Rate

A case that doubles the liquid leakage rate to 800 cc/min was executed and compared at two hours to the 400-cc/min leakage and zero-leakage cases. As shown in Figure C.12, hydrostatic pressure increases due to the longer liquid column with increasing leakage rates. From zero leakage to 400 cc/min, the pressure increases at the phase interface about 0.8 bar, and from 400 cc/min to 800 cc/min, it increases about 0.8 bar.

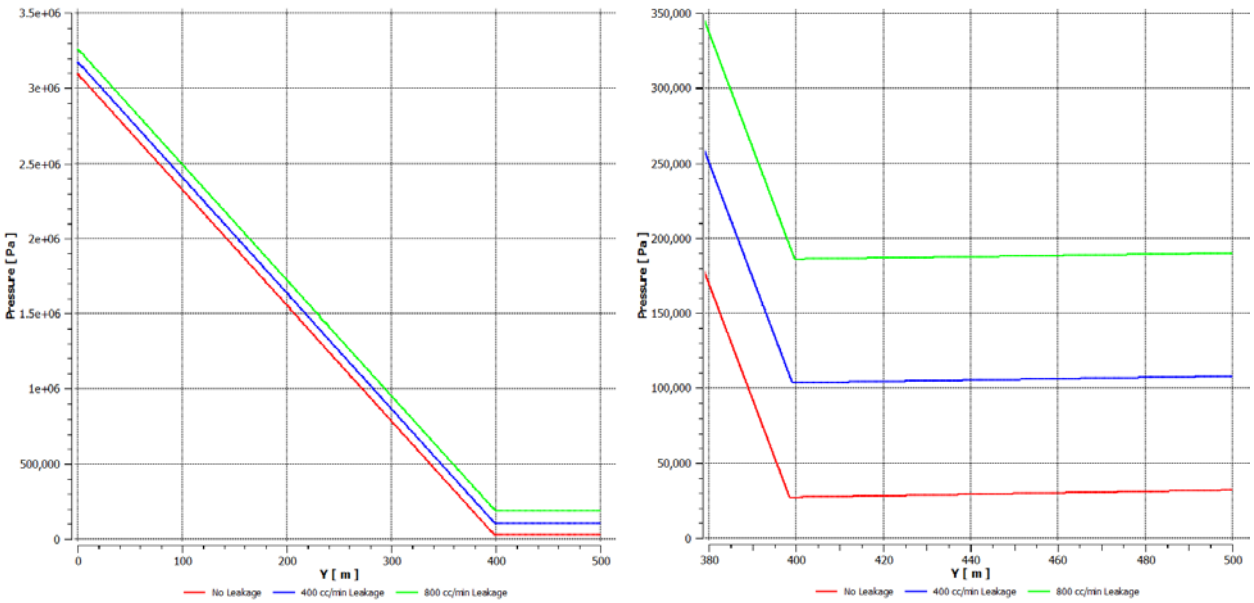

Figure C.12. Relative Pressure Profiles for 20% GVF Cases at Two Hours: No Leakage, 400 cc/min, and 800 cc/min

Pressure increases about 0.8 bar from 0 cc/min to 400 cc/min, and from 400 cc/min to 800 cc/min at the phase interface.

Figure C.13 shows expected results with respect to volume fraction and density. The liquid volume fraction increases as the leakage rate increases, and the density of the gas increases in response to a lower volume for the gas to occupy in the domain. The local fluctuations in temperature may be attributed to the fact that total temperature is being shown, which is dependent in part on dynamic effects. Local fluctuation trends in velocity at the same locations are demonstrated in Figure C.13(d).

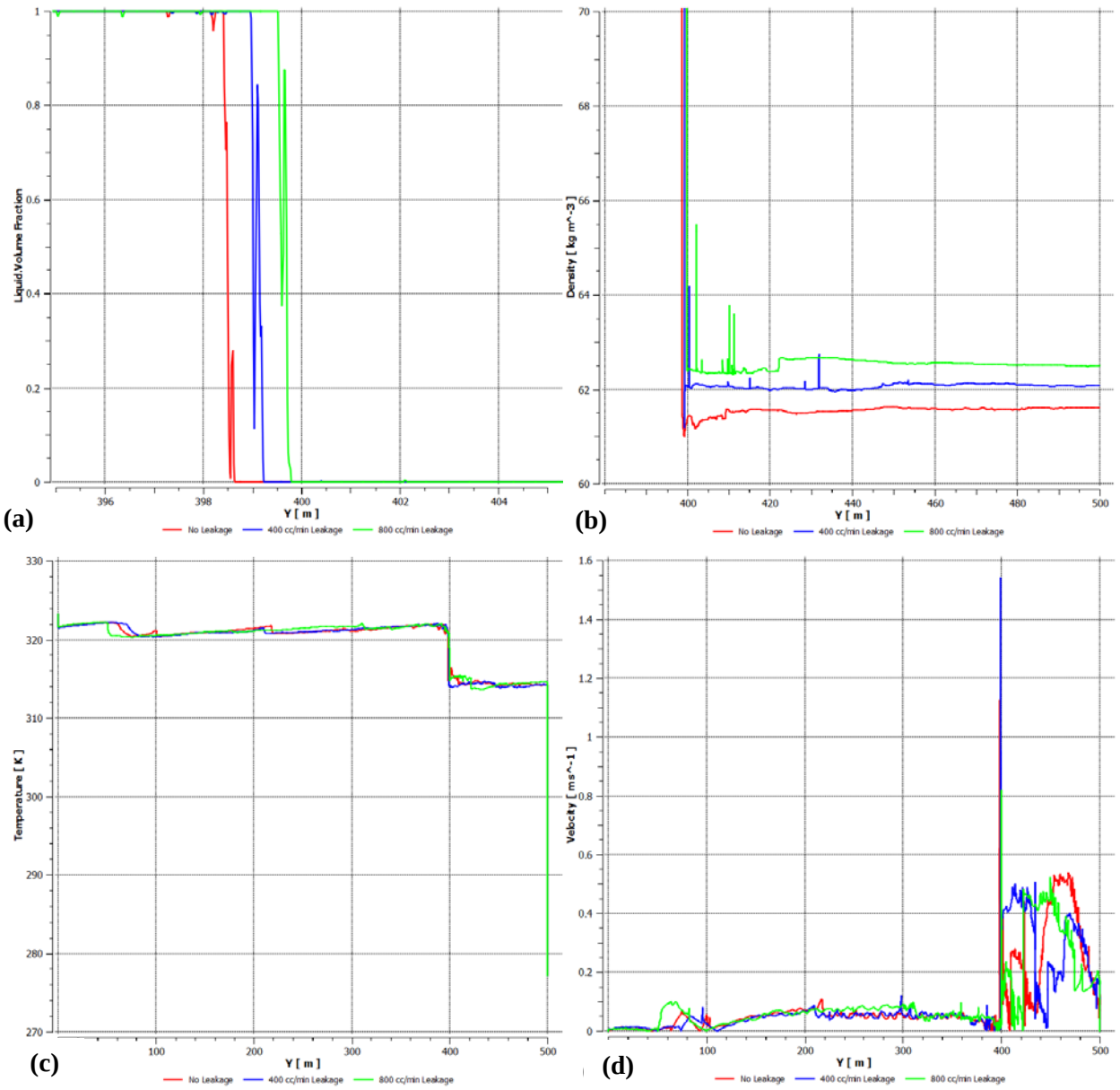

Figure C.13. Volume Fraction, Density, Temperature, and Velocity Profiles for 20% GVF Cases at Two Hours: No Leakage, 400 cc/min, and 800 cc/min.

Volume fraction of the liquid increases as leakage rates increase, and density increases as a result of less volume for the occupying gas. Temperature of the gas remains relatively unchanged.

Gas Leakage

Due to the coarse resolution of the fluid domain necessary because of computational and time constraints, it was decided that introducing the gas leakage through the bottom boundary would be impractical. Inaccuracies of tracking bubble phase interfaces up through the liquid would tend to make the solution undependable. Thus, it was decided to introduce the gas leakage near the phase interface.

The gas injection region was composed of a single row of cells extending radially across the fluid domain. The volume of the region was $4.48e^{-6}$ m^3. A leakage rate of 15 scfm was chosen since API practices (API 14B) state this as the limit of absolute gas pressure buildup in

lines during SCSSV testing. Using a density of 66.6 kg/m^3 (100 bar, 50˚C), the mass injection of gas for a 1˚ axisymmetric slice may be computed as 1.46e^{-3} kg/s. Modeling the injection required specifying momentum and energy sources, in addition to the mass source. The energy was computed as $\dot{Q} = \dot{m}c_pT = 1.46e^{-3}\left[\frac{kg}{s}\right] * 2865\left[\frac{J}{kg*K}\right] * 323.15\,[K] = 13.5\,[W]$. Dividing by the source cell volume, the energy source term then becomes 3.03e^6 W/m^3. Similarly, the momentum source term was represented as $M = \frac{\dot{m}v}{\forall}$, where v is velocity and $\forall$ is the volume of the injection region. Injection velocity was computed from the volumetric mass flow rate and the cross-sectional area of the axisymmetric slice, i.e., $v = \frac{Q_v}{A_c}$. The momentum source term for the injection was then calculated as 0.0133 N/m^3.

Relative pressure results are shown in Figure C.14 for the gas leakage case one hour into the simulation (prior to any leakage – accounts for wellhead test time), and at two hours (after one hour of SCSSV leakage). From the graphs, the pressure rises about 10.5 bar at the top of the domain (at 500 m) as a result of the leakage over one hour. Recall from Figure C.8(c) that pressure rose about 0.3 bar for the zero-leakage case at two hours due to artificial mass creation – as evidenced by continuity transport equation residuals. Thus, a pressure increase of 10.2 bar for the gas leakage case is taken from comparing the two simulations. Leakage of 15 scfm at 100 bar and 50˚C may be interpreted as 0.1682 acfm using the combined gas law. Assuming a methane density based on these conditions of 66.6 kg/m^3, the mass added can be computed as about 19 kg. If it is assumed that temperature and volume of the gas remained the same during the hour-long leakage, the pressure increase from the additional mass would then be 14.75 bar from the ideal gas law. Since temperature and volume of the gas do not truly remain unchanged during injection, a pressure rise of 10.2 bar is not unreasonable.

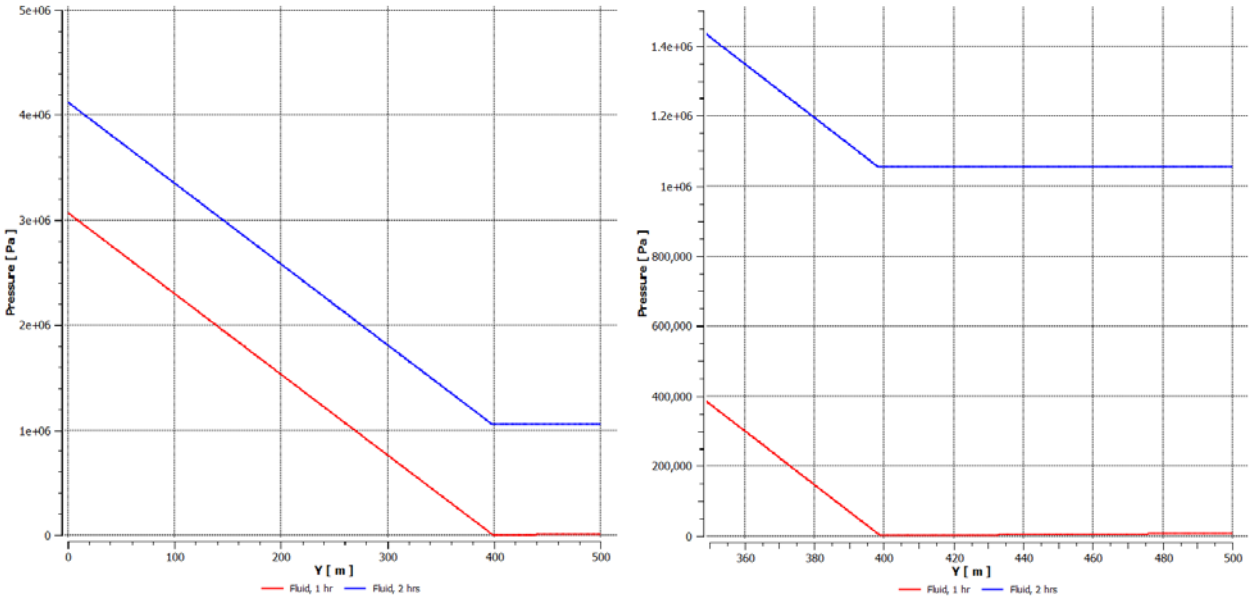

Figure C.14. Relative Pressure Profiles for 20% GVF Cases: No Leakage at One Hour, and 15-scfm Leakage after the First Hour

Pressure increases about 10.2 bar as a result of gas leakage over one hour compared to the zero-leakage case.

Comparing Figure C.15(b) with Figure C.7(b), it may be observed that the height of the phase interface does not change appreciably comparing the zero-leakage versus the gas leakage cases. The gas occupies the same volume, leading to a significant rise in density from the additional mass, as shown by Figure C.15(a).

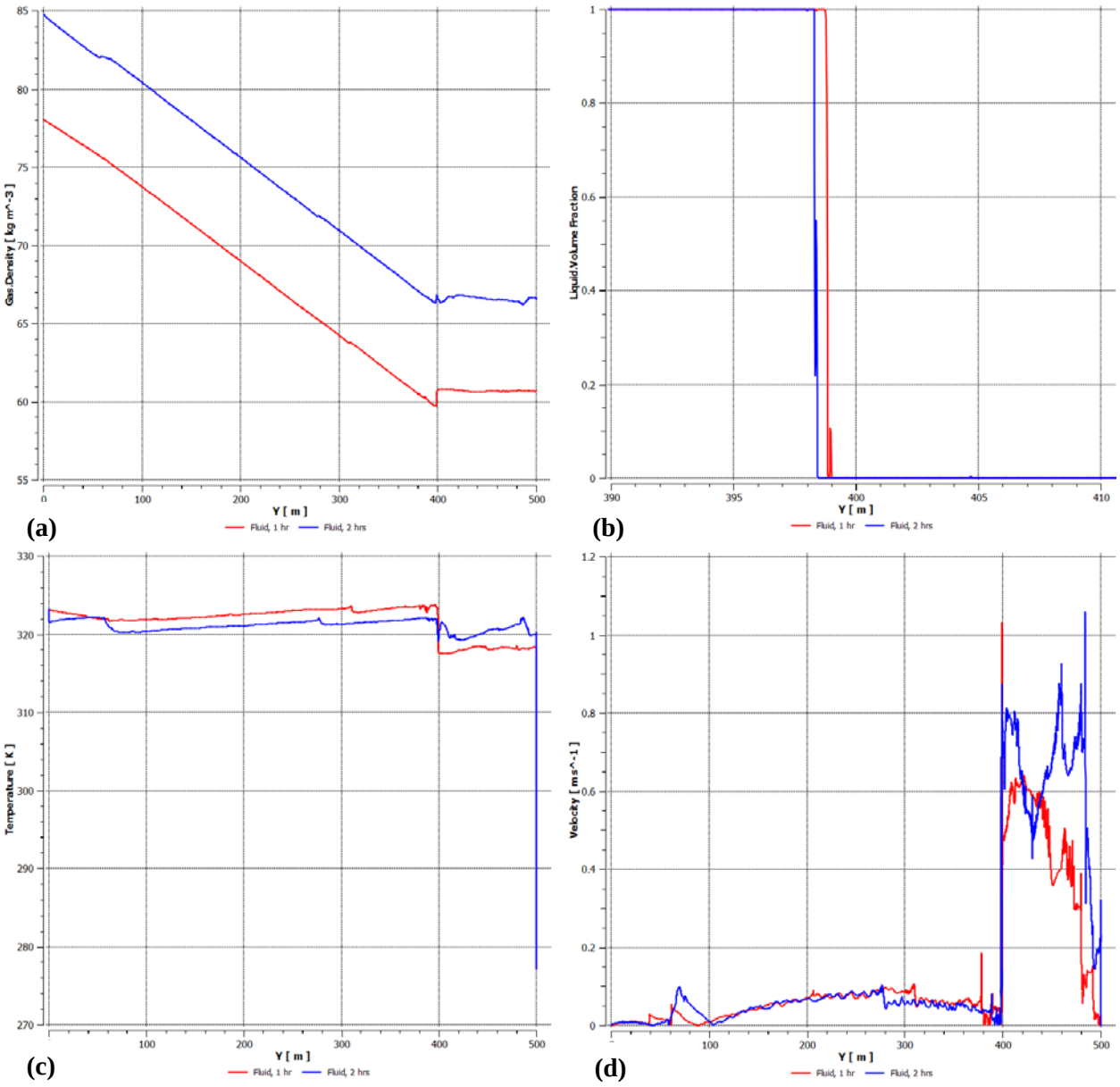

Figure C.15. Density, Volume Fraction, Temperature, and Velocity Magnitude Profiles for 20% GVF Cases: No Leakage at One Hour, and 15-scfm Leakage after the First Hour

Gas density increase is consistent with the addition of mass with only a small change in occupying volume. Overall temperature increase in gas is consistent with injection at the reservoir temperature, and a relatively high-level mixing – as indicated by velocity magnitude.

A drawback to the method of injecting gas at the phase interface, rather than at the bottom boundary, is that temperature may be somewhat overestimated. It is assumed that the gas comes into the domain at the reservoir temperature of 50˚C. In reality, the temperature would be somewhat lower after passing through the the liquid column. Since the liquid column

temperature remains within about 5˚C after two hours, this omission should not be significant. Note from Figure C.15(c) that the temperature rises after two hours of leakage rather than cooling. The effect of the hot leakage gas overcomes that of the formation cooling. Due to the low density of the gas, circulation of the hot injected fluid is much faster than was the case with the liquid leakage. This factor is noted in the velocity magnitude profile of Figure C.15(d).

C.5 CFD Summary

The zero-leakage model of Section C.2 first presented an overview of the model setup and submodel conditions. However, it was discovered during initial efforts that convergence of the solution using CFX was problematic. Various attempts were made to obtain a robust solution, as detailed in Appendix D. Investigations into an alternative software package indicated that it would be faster, and possibly more flexible. Therefore, licensing for FLUENT was obtained and the problem was set up again.

A 20% GVF benchmark case was successfully carried out for zero leakage. Temperature drop as a result of cooling was observed, as expected, as well as a downward shift in the phase interface due to liquid contraction. Counter-intuitive results for pressure behavior with time were evident, however. Density and pressure were seen to rise through the gas domain after one hour, while temperature fell. It was anticipated that the density would fall, given the increased volume for the gas to occupy due to liquid shrinkage. Lowered density, combined with falling temperature, would then be expected to lower the pressure. It was determined that artificial mass creation via solution of the continuity transport equation was the cause. Decreasing the time step by an order of magnitude and allowing a larger number of transport equation subiterations lowered continuity equation residuals by two orders of magnitude and produced expected pressure trends. However, computational and time requirements would be prohibitive to carry out such high temporally-resolved cases. Thus, since the change in pressure at the same time point for leakage versus non-leakage cases was the primary focus, the initial setup was retained for the remaining leakage cases.

Section C.3 presented results from cases introducing leakage of either gas or liquid into the domain. Liquid leakage was set up through the bottom boundary of the liquid domain. Total leakage rates of both 400 cc/min and 800 cc/min were modeled. A leakage rate of 15 scfm for the gas was carried out. The gas leakage was handled as an injection at the phase interface. This was due to concerns that the relatively coarse mesh would lead to volume fraction inaccuracies as the methane bubbled through the liquid. Table C.1 presents a summary of the relative pressure near the PMV at the top of the domain, as well as the phase interface height, for the non-leakage and leakage cases at two hours.

Table C.1. Summary of Relative Pressure and Interface Location for Leakage vs. Zero-Leakage Cases at Two Hours Total Simulation Time (One-Hour Leakage Duration)

Properties in the table were obtained from operator input.

LEAKAGE	RELATIVE PRESSURE @ 500 m	PHASE INTERFACE HEIGHT
none	0.3208 bar	398.5 m
400 cc/min, liquid	1.0795 bar	399.1 m
800 cc/min, liquid	1.9005 bar	399.7 m
15 scfm, gas	10.544 bar	398.4 m

Liquid leakage results have been compared to each other, as well as to the zero-leakage case. It was observed that the phase interface moves up as a result of the liquid leakage. A comparison of the theoretical rise to the computationally-predicted rise agreed reasonably well. The magnitude of the pressure rise as a result of leakage was also relatively close to analytical predictions. Temperatures did not change significantly as a result of leakage, which is not surprising given that liquid leakage occurred near the SCSSV where temperatures were near that of the reservoir.

The gas leakage case results also appeared consisted with expected trends. While the phase interface moved slightly downward as a result of liquid contraction, gas density still rose in the domain due to the significant increase in methane mass from the injection source. The temperature showed a minor increase due to the fact that 50˚C gas was injected directly at the phase interface, unlike the liquid leakage cases where it was introduced near the SCSSV. Pressure was seen to rise about 10.2 bar compared to the zero-leakage case. A check with analytical predictions agreed reasonably well, given that the theoretical solution assumed unchanging temperature and volume.

In conclusion, it was shown that it is possible to model wellbore response to relatively small leakage levels. Though the pressure response in time with the zero-leakage case did not behave as expected, using results at two hours as a benchmark to compare the pressure response of gas and liquid leakage cases showed relatively good agreement with theoretical results. Thus, correlation of leakage rate with experimental pressure could be accomplished as follows: 1) form a baseline case with zero leakage using CFD, 2) model several leakage rates to the same physical time point, and 3) interpolate experimental pressure rise to predict the actual leakage rate of the SCSSV into the shut-in well. Due to the amount of time required to carry out extensive CFD simulations for building up a leakage rate library though, the investigations into an analytical modeling method that could be used to replace CFD efforts were carried out, and are detailed in the body of the report.

APPENDIX D

CFD Modeling – Early Efforts

CFD MODELING – EARLY EFFORTS

Zero-leakage modeling was initially attempted using ANSYS CFX prior to switching to FLUENT. Convergence challenges and computational time limitations encountered during this phase are detailed in Section D.1 and Section D.2. After changing the software platform to FLUENT, the quality of initial results was assessed as shown in Section D.3.

Under fluid-specific models, 1) the oil utilized the Boussinesq buoyancy model and was specified as incompressible; and 2) methane used the direct density-difference buoyancy source term $\{S_{M,buoy} = (\rho - \rho_{ref})g\}$ and was modeled using the ideal gas equation of state. For heat transfer, the total energy that includes transport of enthalpy and kinetic effects was enabled. A homogeneous heat transfer submodel, which uses separate energy equations for each fluid but does not incorporate any interphase modeling terms, was specified. A homogeneous submodel where all fluids share a common velocity field was selected to account for multiphase conditions. It was assumed that any fluid motion during the simulation is laminar and, thus, no turbulence submodel was specified. A free-surface submodel was incorporated due to the distinct interface between the stratified layers. It should be noted that in simulations involving leakage of gas through the SCSSV, the free-surface model cannot be used for capturing bubble transients. The more computationally-expensive mixture model must be used for such scenarios.

D.1 CFX Convergence Limitations

Attempts to run the model described above in CFX were initially unsuccessful due to convergence failure. Reduction in time step down to 0.01 sec still did not allow for a reliable converging solution. At the recommendation of ANSYS support staff, the following diagnostic cases were carried out:

- Running the simulations without buoyancy activated.
- Using a constant thermal conductivity of the oil, as opposed to the expression given in subsection 3.2.2.
- Updating the software to version 13.0.
- Disabling the free-surface interface transfer.
- Ramping the temperature at top boundary down from 50˚C to 4˚C over 60 sec using a polynomial profile to avoid high gradients.
- Shrinking the domain vertically from 500 m to 5 m using the same number of cells and stretching coefficients in order to avoid high aspect ratios.

However, these approaches did not improve convergence. Further investigation into this issue revealed that the problem likely stemmed from the fact that high volume-fraction gradients were being aligned to parallel partition boundaries in the solver input file. Since the simulation had such a large number of cells, it was being run on a computing cluster using eight processors. Disabling the automatic domain partitioner and instead manually specifying partition boundaries to avoid the phase interface region allowed for solution convergence in as little as three iterations per time step.

D.2 CFX Computational Time Limitations

After altering the zero-leakage setup to obtain robust convergence, attention was turned toward reducing the required wall clock time needed for solutions. One way to reduce the physical time is to use more processors and assigning fewer spatial nodes to each in order to

speed up the overall simulation. Cases 1 to 3 shown in Table D.1 summarize a time study carried out with two, four, and eight processors. Note that due to licensing limitations, eight processers represent the maximum that could be used concurrently on a simulation. Doubling the processors from two to four reduced the projected time it would take to run the case out to two hours of simulation time by a factor of 3.75. Doubling again to eight processors reduced the time by another factor of approximately 3.6. However, the projected time for a single simulation was still too high (16.2 days) to consider performing the number of parametric studies needed to develop general SCSSV test correlations. This extended timeline would also make it unfeasible to utilize such an approach in the field. As the number of processors increases for a given mesh, at some point the global inter-communication between processors for boundary nodes overtakes any time saved by having fewer nodes handled locally. Thus, adding more processors would not necessarily solve the problem.

Decreasing the temporal and spatial discretizations in order to decrease the computational time was subsequently investigated. Case 4 gives the outcome of increasing the time step by a factor of 5 to $\Delta t=0.5$ sec. The projected time unexpectedly increases in comparison to Case 3. This behavior is due to the fact that significantly more subiterations become required at each time step to obtain convergence. Likewise, decreasing the number of nodes by a factor of three, in comparison to Case 3, results in a slight increase in the projected time for Case 5, because once again more subiterations are needed.

As a check on the computational effort required for the various submodels used to simulate physical processes, the complexity of the models was reduced. First, energy transport was changed from total energy to thermal energy. The thermal energy approximation transports enthalpy only and neglects mean flow kinetic energy. This model is intended primarily for low-speed flows where viscous effects are negligible and, thus, is a reasonable approximation for the setup of this project. However, from comparison of Cases 5 and 6 in Table D.1, it is clear that this does not lead to a significant speed-up in computational time. The final case turned off the buoyancy models for both the gas and oil, employed the thermal energy transport approximation, and turned off the free-surface multiphase model. Results of Case 7 indicate that the majority of the computational effort is due to the buoyancy and free-surface models. The entire two hours of simulation time is completed in 7.2 wall-clock hours using eight processors when these sub-models are eliminated. However, this finding was not directly of benefit to the current effort, since neglecting these models was not deemed appropriate for obtaining a high-accuracy solution.

Since it was found that the multiphase submodel is one of the most calculation-intensive aspects to the zero-leakage modeling, an approach was devised for eliminating this aspect of the problem. It was assumed that the gas and liquid phases are stratified at the beginning of the transient simulation. Thus, a method that numerically simulates the gas while analytically modeling the effect of the liquid could be used. In order to model the effect of the liquid, it is necessary to include the heat transfer effect, as well as the shrinkage effect.

Table D.1. Zero-Leakage Model Time Study using CFX

Results from time studies indicate that carrying out parametric studies of 10-15 wellbore cases would be impractical due to time constraints, unless necessary submodels were removed.

Case	Description	# of Processors	Simulation Time (min)	Wall-Clock Time (days)	Δt (sec)	Projected Wall-Clock Time for Two-Hour Simulation (days)
1	Two Processors	2	4	7.2	0.1	216
2	Four Processors	4	15	7.2	0.1	57.6
3	Eight Processors	8	23	3.1	0.1	16.2
4	Increased Time Step	8	27	5.0	0.5	22
5	Coarse Mesh	8	27	3.9	0.1	17.3
6	Coarse Mesh + Thermal Energy Only	8	48	6.9	0.1	17.25
7	Submodel Removal	8	120	0.3	0.1-5.0	0.3

From initial results of the static oil column case, it was observed that after two hours of cooling, the temperature of the liquid is still relatively homogeneous in the x-direction along the wellbore. Since the specific heat of the liquid is much larger than that of gas in the problem at hand, this arrangement will result in comparatively much greater gas cooling. Thus, it was felt that it may be reasonable to assume a linear heat flux profile through the liquid, $q" = -k\frac{dT}{dy}$, essentially treating the region as one-dimensional and ignoring heat loss to the formation. The bottom of the gas boundary can be implemented with a Neumann boundary condition as follows: $q"_{bottom} = -k_{liquid}\frac{T_{res}-T_{bottom}}{\Delta y}$, where T_{res} is the constant reservoir temperature, T_{bottom} is the average temperature of the face from the previous time step in the lowest row of cells of the gas domain, and Δy is the vertical distance of the liquid in the wellbore. This procedure accounts for heat transfer effects from the liquid to the gas.

To account for shrinkage effects, it is necessary to directly modify the pressure in the domain at each time step using an offset. An approximation for the change in volume of the liquid due to shrinkage was based on the thermal expansion coefficient: $\Delta V = V_i \beta \Delta T$, where V_i was the initial volume of liquid in the domain and ΔT is the change in bulk temperature of the fluid from t=0 s. Bulk temperature of the liquid may be approximated as the average between T_{res} and T_{bottom}. The decrease in liquid volume ΔV was equal to the consequent increase in gas volume, since the domain is fixed. It is assumed that the pressure offset is due to expansion of the gas only and does not affect the temperature directly, i.e., $T_{gas,i} = T_{gas,f}$ during the time step. Thus, using the ideal gas law, the change in pressure due to liquid shrinkage may be expressed as $\Delta P = \left(\frac{mRT}{\Delta V}\right)_{gas}$ at every time step. Leakage of liquid through the SCSSV was handled in a similar manner, artificially raising the pressure to model compression of the gas. Leakage of gas through the SCSSV could simply be modeled through a mass source term at the bottom boundary.

While setting up the single-phase model, it was discovered that CFX does not allow for defining global pressure offsets at each time step. While a transient problem can have a pressure

offset defined initially, this criterion cannot be changed during the simulation. Thus, this model would not be able to simulate shrinkage or leakage of the liquid. It was therefore necessary to abandon this approach for reducing the required computational time.

D.3 Preliminary FLUENT Modeling

Due to the high computational time costs associated with the solution of the SCSSV test during wellbore shut-in using CFX, it was decided to explore other software options. FLUENT has a wider variety of algorithms available for obtaining a transient solution. Thus, it was decided to do a side-by-side comparison of the two codes to see whether significant speed-up could be obtained using FLUENT. ANSYS technical support carried out this study. The results demonstrate that FLUENT was able to run an identical zero-leakage multiphase simulation over 15 times faster than CFX using the same number of processors and time steps. Therefore, it was decided to switch the numerical simulation platform to FLUENT.

A 70% GVF zero-leakage baseline case with the ideal gas equation turned on for the methane (in addition to the Boussinesq approximation in the oil that was included previously) was carried out initially. However, results indicated severe local temperature fluctuations beginning to occur throughout both the gas and liquid domains after about ten minutes of simulated time. Increasing the temporal resolution by halving the time step to Δt=0.05 sec did not improve results. Employing constant thermal conductivity in the oil and different solvers was not beneficial either. Mesh refinement was attempted next, quadrupling the total number of nodes to two million. Though this refinement removed the temperature fluctuations, the phase interface between the two fluids was diffuse, causing a local temperature jump near the gas-liquid boundary, as shown in Figure D.1.

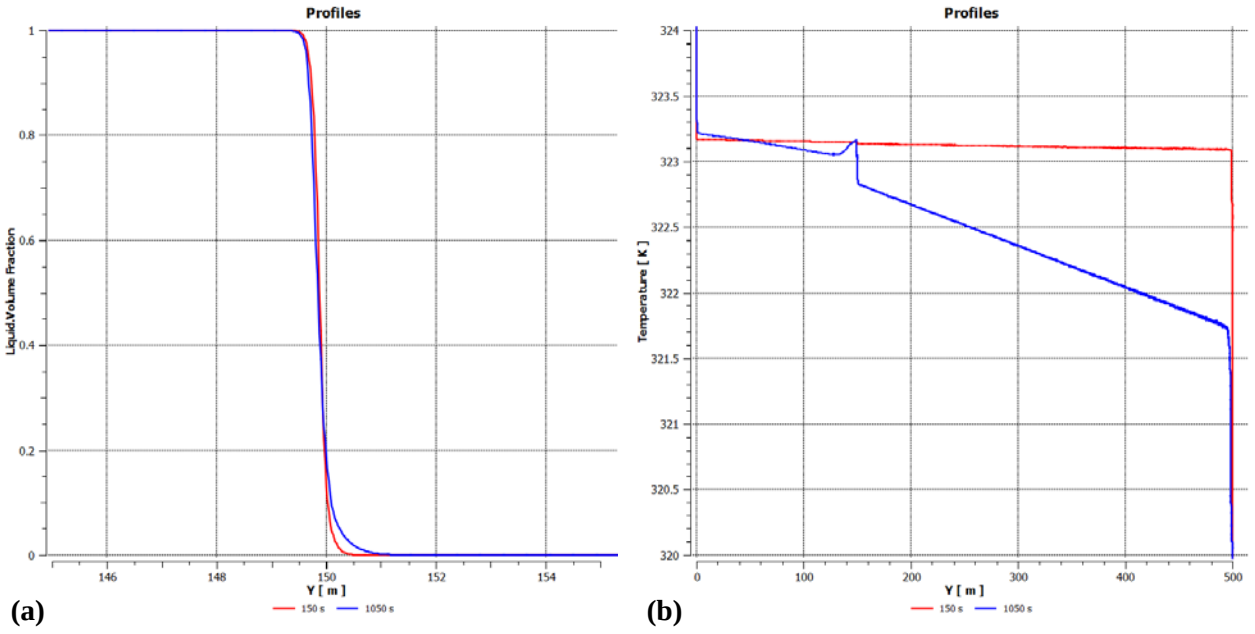

Figure D.1. Fluid Criteria Profiles with Refined Mesh at 150 sec and 1,050 sec: (a) Liquid Volume Fraction, and (b) Temperature

As time progresses, the phase interface becomes increasingly diffuse, leading to and unphysical jump in temperature profile.

An algorithm for solving the transient volume fraction equation was utilized to keep the interface sharp. This approach required explicit solution of the multiphase equation, and a geo-reconstruct scheme was chosen. Geo-reconstruct is a piecewise-linear algorithm for solution near interface cells. This approach assumes that the interface between the two fluids has a linear slope within each cell, and uses this linear shape for calculation of the advection of fluid through the cell faces. The combination of using a refined mesh and an explicit solver significantly raised the computational time requirements for achieving a one-hour simulation. Simulations took on the order of 7-10 days to complete using the new algorithm. A baseline 30% GVF zero-leakage case was run as a test case, and results at 2,300 sec (~ 38 min) are shown in Figure D.2 and Figure D.3. Note that the interface remains sharp, and no singular jump in temperature profile is observed. Due to these encouraging results, the geo-reconstruct scheme was used in subsequent FLUENT modeling efforts and is documented in Section 3 of this report.

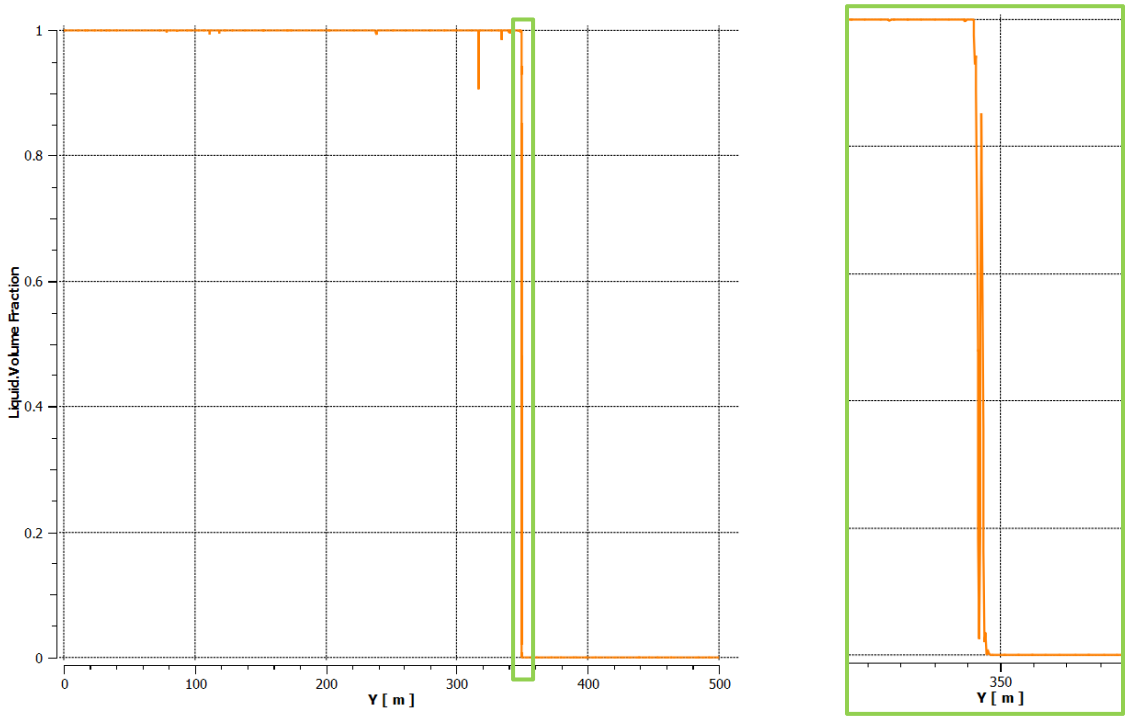

Figure D.2. Liquid Volume Fraction at 2,300 sec for Zero-Leakage Case using Geo-Reconstruct Interface Algorithm

The interface profile remains sharp, unlike diffuse cases using implicit volume fraction solvers.

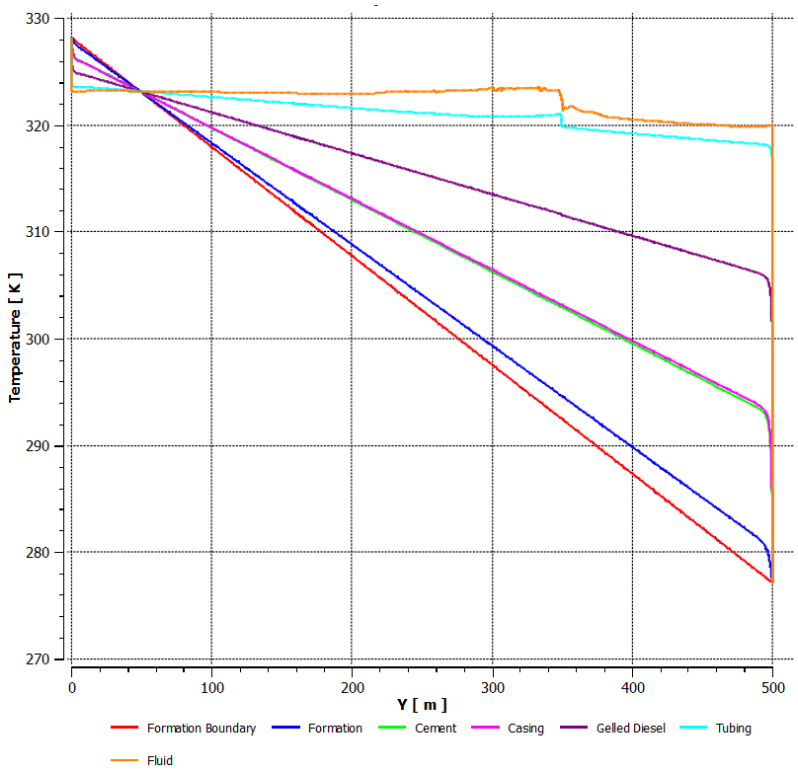

Figure D.3. Temperature at 2,300 sec for Zero-Leakage Case using Geo-Reconstruct Interface Algorithm

The temperature at the interface does not sharply jump, unlike cases using implicit volume fraction solvers.